

Department of  
Biotechnologies and Biosciences

PhD program in Chemical, Geological and Environmental Science Cycle XXXVII  
Curriculum in Chemistry

# **POLYSACCHARIDES DERIVED FROM BIOMASSES FOR THE DEVELOPMENT OF INNOVATIVE MATERIALS**

Surname Petroni Name Simona

Registration number 884053

Tutor: Giuseppe Zampella

Supervisor: Laura Francesca Cipolla

Coordinator: Marco Malusà

**ANNO ACCADEMICO / ACADEMIC YEAR 2023-2024**

*To my little sister so beautiful and so brave*

*God bless you for loving us so much*

## ACKNOWLEDGEMENTS

This research work has been an absolutely extraordinary experience that has allowed me to face the world of renewable resource chemistry and to discover the extraordinary value behind the resources that nature offers us for free. I thank infinitely for this my supervisor Professor Laura Cipolla for welcoming me into her laboratory and opening to me her inexhaustible knowledge, for her deep humanity and courage in the face of new challenges. I thank Massimiliano D'Arienzo for his listening and suggestions, for his extraordinary humility and friendship, they helped me a lot in difficult moments. I thank the Lord for choosing Hubert Hettegger as my supervisor during my research period in Austria, his knowledge of chemistry, his enthusiasm and his humanity deeply inspired me and allowed me to work with dedication despite missing my family so much. I also thank Hubert for allowing me to get to know Professor Antiej Potthast and Professor Thomas Rosenau, their knowledge of chemistry is so deep that in listening to their explanations I understood that molecules and reaction mechanisms were happening in front of their eyes. Despite this enormous knowledge Antie and Rosi are among the most humane and generous people I have ever met. And I am deeply grateful to Anna Lehrhofer for being my Puddy for always helping me without ever backing down, I will always carry her in my heart and thank her for giving me her wonderful recipes. I thank the wonderful Nawaros: Theo, Joanna, Jhon, Alaudin, Olga, Bara, Markus. I thank Markus and Giorgio for the many NMR spectra that gave great value and clarity to the results that were gradually coming in. I thank the young people I met in the Cipolla Lab: Sara, Federica, Federico, Andrea, Matilde and the whole BIOSTARPACK group; it was great to work in an atmosphere as festive as it was elevated.

I deeply thank my husband Nino and my sons Vincenzo and Antonio who never stopped supporting me despite the difficult times we went through, their love and optimism allowed me to go all the way. Finally, I thank my beloved family: my brothers and sister, my parents who always believed in study as the high road to be free and rise up. I thank God and Pope Francis for inspiring me to take this risk to try to change things. I am sure I have forgotten someone, but I am sure he will forgive me because I thank him anyway.



## TABLE OF CONTENTS

ABSTRACT .....	6
1. INTRODUCTION .....	7
1.1. Waste issue .....	7
1.2. New Plastic Economy .....	9
1.3. Sustainability .....	10
1.4. Bioeconomy (BE) paradigm .....	13
1.5. Biomass and renewable resources .....	16
2. OBJECTIVES .....	19
3. STARCH .....	20
3.1 Starch: literature review .....	20
3.2 Starch: Methods and Materials .....	24
3.3 Starch: Results and Discussion .....	30
4. CELLULOSE .....	60
4.1 Cellulose: Literature Review .....	60
4.2 Cellulose: Methods and Materials .....	69
4.3 Cellulose : Results and Discussion .....	77
<b>5 CONCLUSIONS.....</b>	<b>88</b>
<b>6 BIBLIOGRAPHY.....</b>	<b>90</b>



## ABSTRACT

The research project dealt with the transformation of polysaccharides derived from biomass into innovative raw materials for a responsible production and use of resources, in line with Goal 12 of the ONU Agenda 2030 and within the new bioeconomy paradigm (Adamowicz, 2017) for a sustainable development. The two polysaccharides under study were starch and cellulose, second and first most abundant biopolymer in the biosphere, respectively. Starch was assumed to originate from production waste of yuca manufacturing (Mirabella et al., 2014) and cellulose from agriculture and forestry waste (Sánchez et al., 2019).

Starch was studied at University of Milano Bicocca in the Department of Biotechnologies and Biosciences, with the aim to endow the polymer of photoresponsive moieties. The objective was pursued for on demand crosslinking and cleavage (Kaur et al., 2014) promoted with UV irradiation. Starch was successfully functionalized as cinnamyl ether and cinnamoyl ester. The ether showed the [2+2] cycloaddition as minor process and Z isomerization as major, while the ester showed a clue of photoinduced crosslinking even at very low degree of substitution (DS). The cellulose was studied at the University of Natural Resources and Life Science of Vienna; where the second polysaccharide was converted to phenyl carbamate in order to enhance its well-known ability to separate enantiomers (Okamoto et al., 1986a), and then grafted onto pre-functionalized silica gel by Cu(I) catalysed alkyne-azide click chemistry. Anchoring to silica increases the lifetime of the resulting High Pressure Liquid Chromatography (HPLC) column, even in a range of suitable eluents including THF, chloroform, acetone, which are not normally suitable for the coated cellulose stationary phase (Bezhitashvili et al., 2018).

# 1. INTRODUCTION

## 1.1. Waste issue

The use of disposal packaging for every kind of good in modern life is determining a steady growth of waste produced per capita. A recent Eurostat's report measures and compares the production of packaging waste in the countries of the European Union ("Packaging waste statistics"); the analysis shows that the production of waste per inhabitant never stops to rise from 2010 to 2021. In the 2021 the average packaging waste per person produced was 188.7 Kg, with a large variability across European countries from the 73.8 Kg of Croatia to 246.1 Kg of Ireland. The most used material for packaging is represented by paper and cardboard and plastic is the second. The main contribution to waste production comes in the order from Germany, Ireland and Italy.

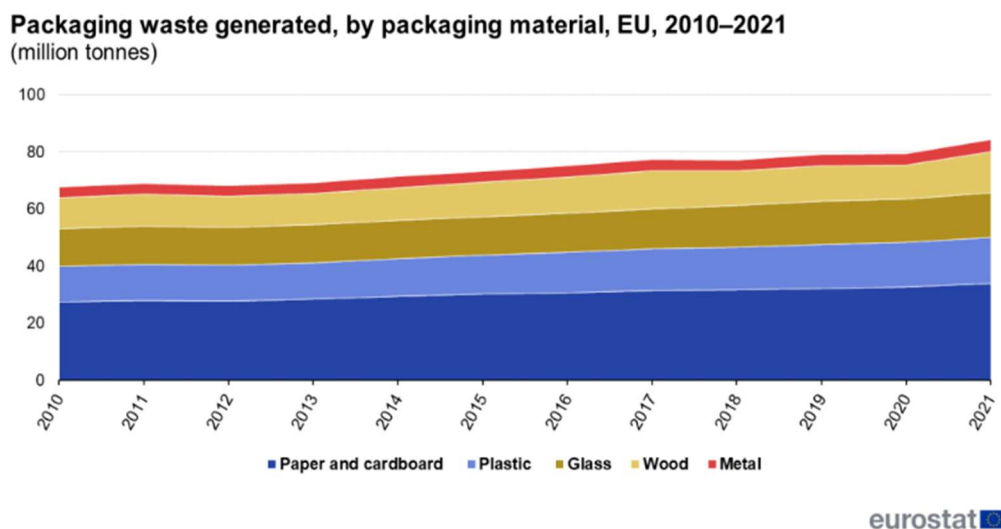


Figure 1 Packaging waste generated by packaging materials in the EU from 2010 to 2021 ([https://doi.org/10.2908/ENV\\_WASPAC](https://doi.org/10.2908/ENV_WASPAC)).

Although several countries are tackling the problem by improving recycling or by exploiting smart incineration; it is sad to observe that the trend never changed, and it is expected to double in 20 years. The data are more alarming for the future of our planet, if it is considered that about 32% of the plastic waste escapes from the collecting systems and enters in the oceans and in the anthropic infrastructures polluting them. Geyer et al (Geyer et al., 2017) estimated in 2015 a production of 8300 million metric tons (Mt) of plastic; whose largest part, 6300 Mt ( 79 %), after a short usage is wasted; of this waste the 9 % is recycled, the 12% incinerated and 79% disposed



of in the landfill or in the natural environment. By assuming a growing production as observed until 2015; by 2050 the amount in landfill will be roughly 12,000 Mt.

Historically the use of plastic for packaging started in 1977 with the introduction in the shops of plastic bags, since then the disposal package became widespread as the workhorse of progress. From then the scientists highlighted the rising pollution levels reporting the presence in the oceans of small particles of plastic, called by Thomson in 2004 microplastics (MPs) (Law and Thompson, 2014), they were considered as a consequence of the inadequate disposal. However in the last decades the presence of MPs in fresh water and soil showed that other sources of this pollutant had not been considered and their presence in the biosphere is today out of control (Richardson et al., 2023). In the soil, for example, initially the presence was ascribed totally to the widespread application of mulch in crops, in a second time it was discovered that the use of sewage sludge as fertiliser was the source of MPs in the soil (J. Wang et al., 2019). Indeed Wang et al. documented that the plastic present in the sludge had assumed a fibre shape with a composition of polyester (67%) and acrylic (17%) very similar to the percentages of the textile materials, this pointed out a second main source of pollution: the textile materials. The synthetic fibres observed in the soil were from the sludge used as fertiliser coming from wastewater treatment plants; in this wastewater is included the one coming from the washing machines. The textile industry is the fourth cause of environmental crisis, for raw materials demand, water consumption and waste production, after food, housing and transportation (“A new Circular Economy Action Plan”; COM 2020/98/final).

The ageing of plastic in the environment, converts plastic in microplastics, small particles with size less than 5 mm, which represents nowadays a problem even worst of the bulky plastic; MPs are detected in the soil, in fresh water and recently have been detected in the clouds, featuring a further threat for the climate change (Wang et al., 2023) as a contribution to the greenhouse effect. Due to this ubiquitous presence in the environment MPs represent today a serious problem for the ecosystems, of which mankind is a part, because they are entering in food chain of living organisms and their presence was detected in the living tissues and the effects on the health is not yet well understood (Amato-Lourenço et al., 2021) (Yang et al., 2023).

## 1.2. New Plastic Economy

With the green deal (“The European Green Deal”) Europe took the leadership of the ecological transition, and within this frame the European Union presented a proposal on the 30<sup>th</sup> of November 2022 to stop the wasteful package, boosting reuse and recycling. The document claims Eurostat data, mentioned above, about the waste averagely produced by a European citizen; the document points out this waste will increase by about 20% in the 2030 if no action will be taken. With the proposal n. 677 EU aims at regulating the package production and waste through three pillars: first prevent the generation of waste by eliminating unnecessary packages and promoting packaging to reuse and to refill. Second, to create a closed loop in the EU of packaging done with recyclable materials through an economically viable way. Third, create an efficient market of recycled resources to deplete the use of primary resources.

The proposal of regulation COM (2022) 677 has been approved in EU Parliament, however on the 17<sup>th</sup> of December 2023, during the Council with the Ministers of the Environment of European countries, Italy was the only country to not approve the proposal. The Italian Minister manifested his concern about the economic loss due to reuse and refill for Italian SME (Avvenire “Il regolamento. Sugli imballaggi l’Italia resta isolata,” 2023).

Moreover on 23<sup>th</sup> of May 2024 an infringement procedure was opened against Italy because did not implemented correctly the EU directive 2019/904 that limits the use of Single Use Plastic (SUP) in many unnecessary cases and encouraging reuse and recycle as primary choice for companies (“Infrazioni, aggiornamento del 23 Maggio 2024,”).

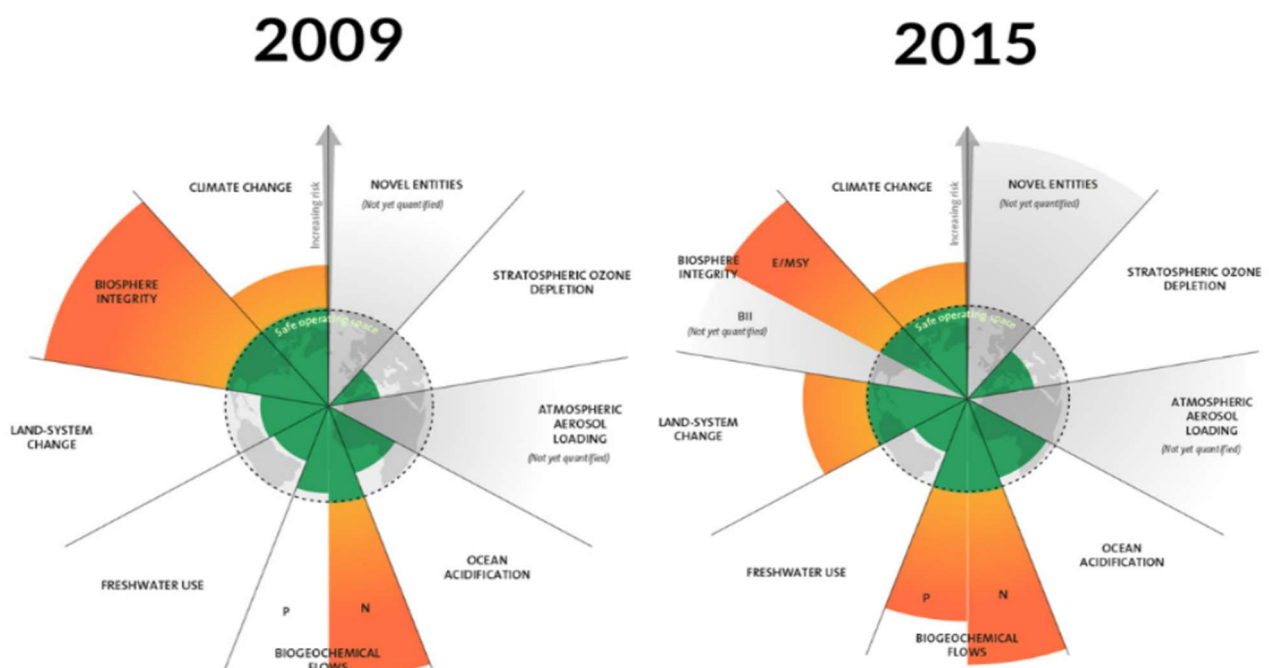
The slowness of Italy is not justified; beyond the environmental crisis, the plastic’s problem is highlighted also by the markets; for packaging the use of primary sources is 40% for plastic and 50% for paper, and it results in economic losses that are well described by the document of Ellen MacArthur foundation “New Plastic Economy”. The data reported show the economic losses related to the actual plastic economy, in particular on packaging; after a short usage the value of plastic is lost by 95%, and its absolute value corresponds to 80-120 billion dollars. The second important data is that 32% of this material escapes from collecting systems and it goes into the environment or it clogs anthropic infrastructures with a cost in terms of natural productivity and externalities of about 40 billions dollars, exceeding the plastic pool profit. The Ellen MacArthur foundation proposes a scenario in which this crisis is turned into a business opportunity by rethinking the plastic market: “The New Plastic Economy: Rethinking the Future of Plastics”.

The Foundation is deeply involved in the promotion and the dissemination of the circular economy model (<https://www.ellenmacarthurfoundation.org/>), and the European Union embraced this new model and most of the documents disclosed by the EU have numerous references to the foundation by Ellen MacArthur. An example is the COM 2020/98 “A new Circular Economy Action Plan for a cleaner and more competitive Europe”.

The EU with the Green Deal is pursuing the objectives of reducing, reusing and recycling in order of priority, with minimum energy and chemicals by keeping the material in the business as long as possible. The question we wish to answer is: which materials are sustainable alternatives to make the transition from fossil resources?

### 1.3.Sustainability

Nowadays the consensus on the urgency of the “ecological transition” is global ( ONU Italia La nuova Agenda 2030 per lo Sviluppo Sostenibile)( Laudato si' (24 maggio 2015) | Francesco ) and the problem of microplastic is only one of the planet’s threats. Several studies assess the irreversible decline of the planet and in this regard a study started in 2009 from the Resilience Center of Stockholm by Joan Rockstrom (Rockström et al., 2009a) is very effective to describe in a comprehensive way the earth perturbed by human activity. This study represents the planet as a framework (Rockström et al., 2009a) characterised by 9 key processes (Fig. 2), that are in equilibrium within boundaries that define the “safe operating space” for mankind.



2023

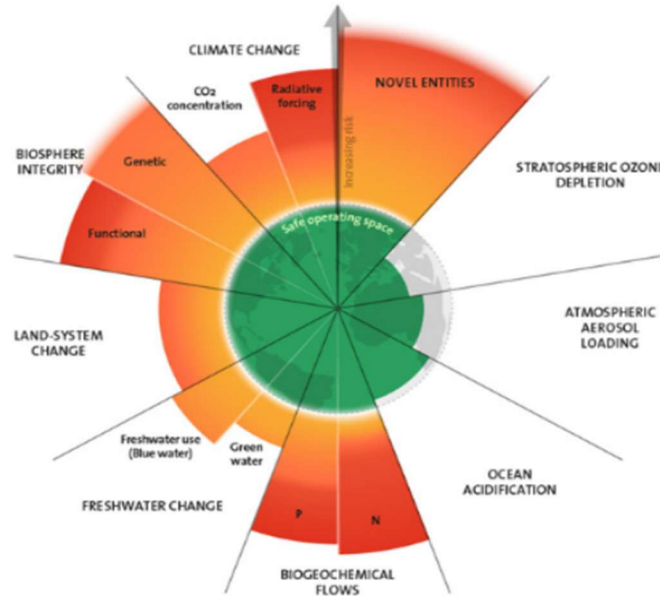


Figure 2. Planetary boundaries of the safe operating space for humanity crossed from 2009 to 2023 ([Planetary boundaries - Stockholm Resilience Centre](#)).

The framework is shown in Fig. 2 for three subsequent years, and it describes the rapid escalation of nine planetary boundaries; climate change (CO<sub>2</sub> concentration and radiative forcing), biosphere integrity (functional and genetic), land-system change, freshwater change (blue water and green water), biogeochemical flows (nitrogen and phosphorous) and novel entities.

The group of scientists reported about an Earth system stable for 10.000 years; this period known to geologists as Holocene interglacial age had characteristics conducive to mankind life, (Rockström et al., 2009b), the models predicted a persistence of 7.000 years without catastrophic interference. Unfortunately, the Holocene Era started to be perturbed in the latter part of the eighteenth century with an increase of CO<sub>2</sub> concentration detected through the air trapped in the polar ice; this year coincides with the design of the steam engine by James Watt in 1784. Afterwards the activities related to industrial revolution produced rapid modifications; since then the planet entered in the Anthropocene age (Crutzen, 2002). A more recent paper from Rockstrom group (Richardson et al., 2023) presents the Holocene state as the benchmark to strive for preserving the resilience of the earth system, in this modelling human activity is the new

forcing functional component called “anthroposphere”. The interaction between biosphere, anthroposphere and geosphere is studied as the planetary system.

Looking at the literature concerning the planetary boundaries model, it is interesting the recent work enriched by the qualification of the planetary boundary: “Novel Entities”. In this regard, defining the boundary was quite tough due to the lack of tracking type and amount of chemicals in many circumstances (Persson et al., 2022). Novel entities are considered: any synthetic chemical and substances (e.g. microplastics, endocrine disruptors, and organic pollutants), any anthropogenically mobilised radioactive materials, including nuclear waste and nuclear weapon (Richardson et al., 2023). The novel entities' safety hazards and their impact on the earth system as single substances or in combination with others or even in specific environmental conditions are unstudied for most of them. Persson (Persson et al., 2022) proposes to consider the amount of novel entities that can be released with adequate safety assessment and tracking as a control variable of the boundary; as long as the synthetic substance is not demonstrated to be safe for the biosphere the boundary is set to zero. An interesting reference in this regard is the phase out of the chlorofluorocarbons as ozone depleting substances (ODS), whose release in the environment was successfully regulated by the Montreal Protocol (1987). And the insecticide DDT phased out thanks to the devoted work of Rachel Carson (“Silent Spring | Rachel Carson’s Environmental Classic | Britannica,” 2024). The problem is huge, to have an idea we have to consider that one of the most regulated systems; the European REACH (Registration Evaluation Authorisation and Restriction of Chemicals) has 80 % of entities, in use for more than 10 years, not yet safety certified. According to the aforementioned definitions of the “Novel Entities” planetary boundary has been definitely crossed, and also in this case it is alarming that the production never stops to rise (Fig. 3). The growth speed overpasses the global capacity of monitoring and assessing, and again among novel entities of special concern plastic are major.

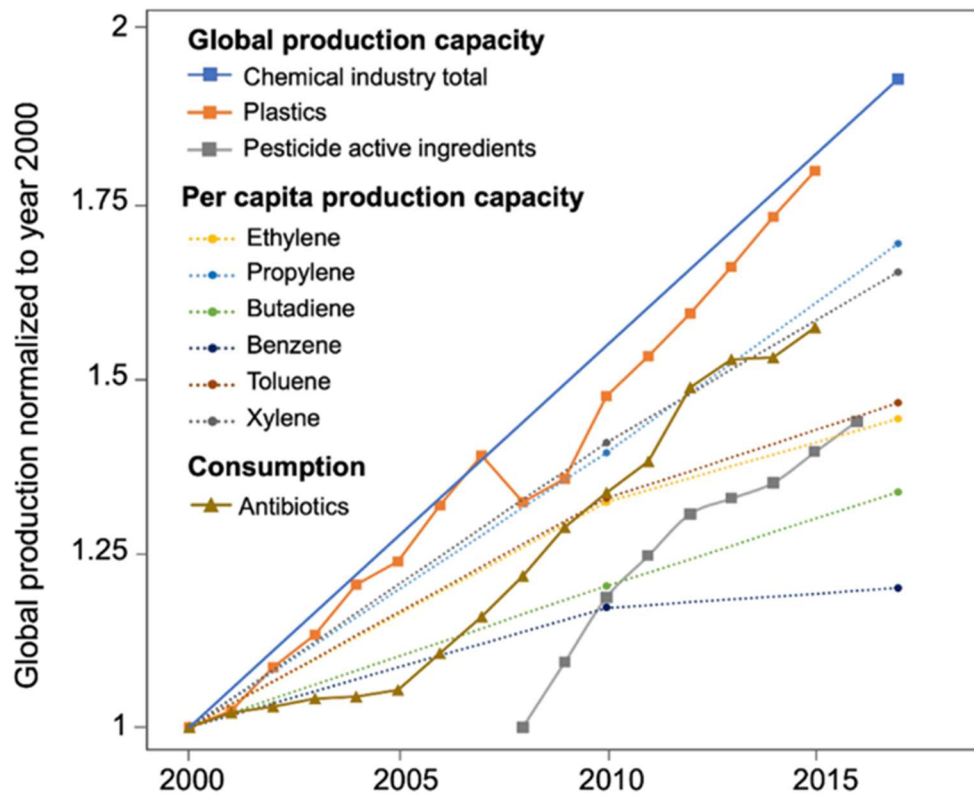


Figure 3. Novel entities global production (Persson et al., 2022).

### 1.4. Bioeconomy (BE) paradigm

The positive news in this discouraging scenario is that the EU took the leadership of the ecological transition and of the sustainable development invoked by ONU Agenda 2030. In particular the objectives 12, 13, 14 and 15: sustainable production, contrasting climate change, preserving life under water and on the earth respectively (Steffen et al., 2015) have been pursued by theoretically dismantling the bankruptcy paradigm of *linear economy: take, use and waste* to refund the old bioeconomy in the perspective of sustainability. The first step in this direction was the transition from fossil-based to bio-based economy, that involves for the largest part the energy needs with sun, wind and water as primary sources in the next future. In addition the phase out of petroleum extraction will be accomplished replacing also the 4% of petroleum used for fine and bulk chemicals (Okkerse and Bekkum, 1999).

The debate on the feasibility of fully supplying fine and bulk chemicals, including plastics, with renewable resource feedstock is still ongoing, however just to mention the Friday for Future movement's slogan "there is no plan B" and the change must begin.

Raw materials will be gathered from renewable resources and exploiting innovative biotechnologies. The families of biotechnologies endowed for different purposes have been identified; the white biotechnology, will be in charge for fine and bulk chemicals; the red biotechnology suited for medicine and the green biotechnology for crops (Soetaert and Vandamme, 2006).

As operating centres of these technologies biorefineries are nowadays intensively studied to supply the feedstock materials, bulk and fine chemicals. Even though the technological maturity of biorefineries is not at the same level of the petroleum refineries, the efforts to reduce this technology gap are multiplying both in academia and industry (*The Role of Bioenergy in the Bioeconomy*, 2019).

In this regard the European Union provided a visionary strategic plan to ecological transition exposed in the Bioeconomy strategy (Directorate-General for Research and Innovation, 2018).

The bioeconomy (BE) paradigm is a global priority to support the rescue from planet decline, even though its definition is still evolving; in 2009 the Organization for Economic Cooperation and Development (OECD, 2009) defined bioeconomy as the development of biological processes and products. In 2013 McCormick and Kautto (McCormick and Kautto, 2013) defined BE the economy of materials, products and fuels that are derived from renewable bioresources.

In 2012 the European Union encouraged the member states to pursue BE, intended as "the production of renewable biological resources and the conversion of these resources and waste streams into value-added products, as food, feed, bio-based products as well as bio-energy". The EU strategy provides five objectives and an action plan:

- to ensure food security
- to manage natural resources in a sustainable way
- to reduce dependence from non-renewable resources
- to mitigate and adapt climate change
- to create jobs and maintain competitiveness



An interesting dissertation on the definition of Bioeconomy is also provided by Adamowicz (Adamowicz, 2017) which emphasises that the bioeconomy is not a new theory, but rather a concept for analysing and understanding today's challenges such as sustainable development.

Bioeconomy concept is also a strategic field in which smart actions are promoted in research and in human capital on multidisciplinary planes, by recovering the existing concept of agribusiness and expanding it to sectors such as forestry, fisheries, energy generation and use of waste, that are suffering under the stress of the linear economy.

The science and technology growth particularly in genetic, molecular biology and biotechnologies is pushing the transition towards bioeconomy, indeed biotechnologies increased significantly the number of goods affordable through renewable resources, even from waste. This change of paradigm was firstly gathered by the EU institutions devoted to managing and programming the development of the EU Union and the Member States; it promotes the development of suburbs and countrysides through the valorization of specific agriculture production; considered marginal contributors to growth and development until now.

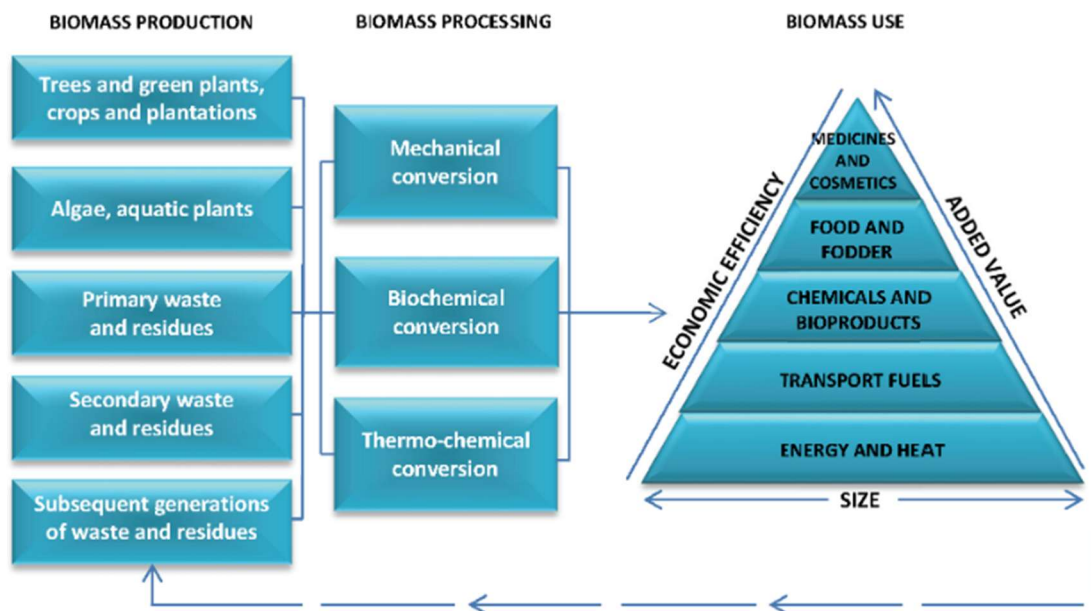


Figure 4. Biomass-based economy (Adamowicz, 2017).

The importance of the bioeconomy paradigm became evident in 2015 during the SCAR (Standing Committee on Agricultural Research) conference. The final report (Kovacs, 2015) produced by SCAR Commission concluded that bioeconomy has the potential to solve the major problems of the Anthropocene Era such as: food security, sustainable resources management,



lower dependence on non-renewable resources, limiting adverse climate change, job creation and maintaining competitiveness. The steps towards efficient management of the resources starts from the perception of natural resources as valuable from the beginning to the end of life in the so-called “cradle to grave” approach.

## **1.5. Biomass and renewable resources**

In the 2016 the EU Commission updated the COM 2012/60 on bioeconomy with including the actions needed for this more comprehensive approach:

- to develop environmental standards for tracking secondary raw materials and promote their usage in single market
- to implement a close-loop for plastic to cover recycling, biodegradability, presence of hazardous and immission in marine environment
- to reduce food waste
- to change the characteristics of fertiliser emphasising the biological solutions

The final targets from these actions were ambitious; recycling of municipal waste of 65% by 2030 and in the case of packaging 75%, to allow a reduction of waste to landfill to 10% of the total mass of waste by 2030. Biomass managed as a valuable resource thanks to the advancement in biotechnology and science will allow to achieve these targets with a strategy based on cascading approach, circularity and diversity.

Cascading approach: biomass is a renewable resource and must be used multiple times in order to add value to the chain and in the end will be an energy source to mitigate GHG greenhouse gas emissions. Cascading does not solve the problem of waste generation, since waste is produced when the cost of reuse and recycling is higher than the value of good, in this regard is important circularity.

Circularity must be based on three pillars: 1) waste is not generated if the good is designed for reuse and for disassembling to refurbish. 2) consumables, after a sequential use, must return to the environment contributing to its restoration without harm, while durables are designed to maximise the use and eventual upgrade 3) the process must be feed with renewable energy.

Diversity has to be promoted in bioeconomy; different scales, products and natural species are important for the resilience of the planet.

In 2011, 11.4 billion t (t) of dry matter (dm) biomass have been obtained from agriculture, grazing and forestry, 58% have been used for feeding, 16% for bioenergy (heat and electricity), 14% for plant-based food, 10% for material use and 1% for biofuels worldwide. In 2015 the biofuels might have reached 2 %. The amount of biomass used for materials and chemicals in 2011 was 1.26 billion TDM. The most important application areas were construction and furniture with 522 million TDM, mainly lignocellulose; 444 million TDM for animal bedding, mainly by-products from agriculture and forest (lignocellulose). Pulp and paper with 201 million TDM, mainly cellulose, hemicellulose and starch. Chemical-technical industry (including polymers) with 59 million TDM, mainly plant oils, starch and sugar and rubber. Textile fibres with 35 million TDM, mainly cotton and man-made cellulose fibres (Piotrowski et al., 2015).

**Global biomass supply 2011 by sources,  
Total: 11.4 bn t dry matter**

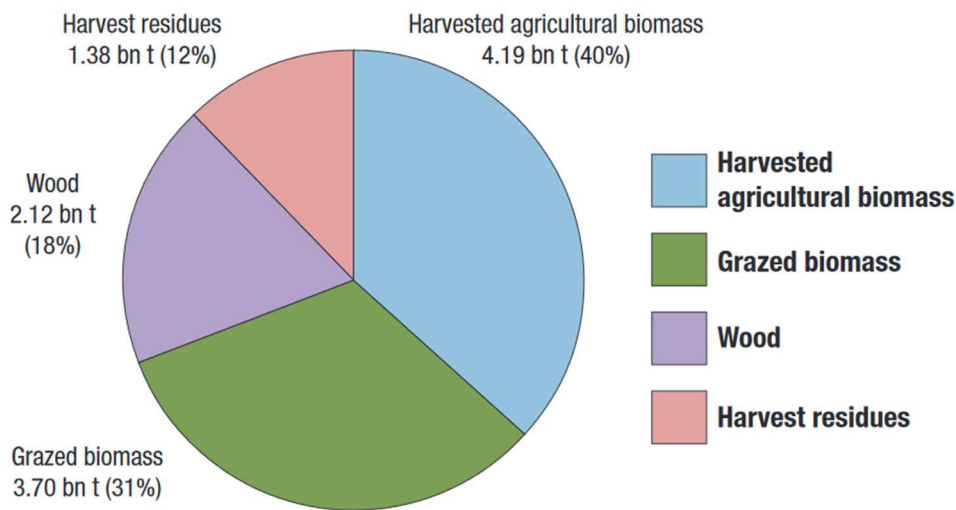


Figure 5. Sources of global production of biomass in 2011 (Piotrowski et al., 2015).

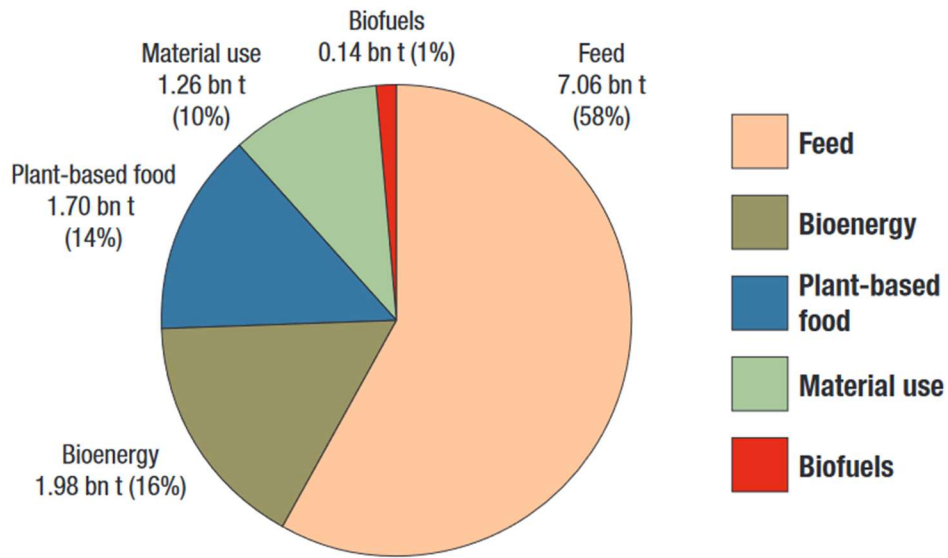


Figure 6. Global biomass demand by business sectors in 2011 (Piotrowski et al., 2015).

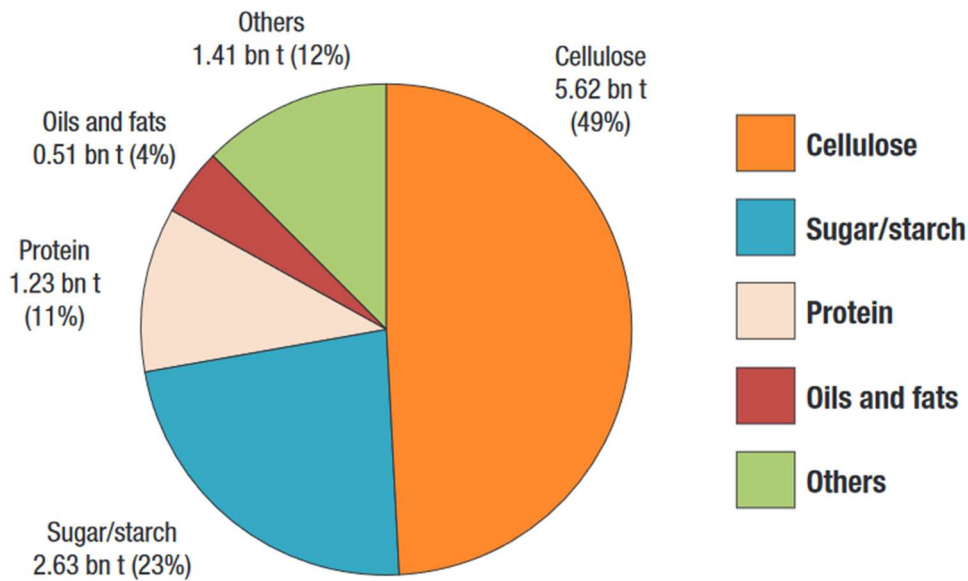


Figure 7. Amount of raw resources obtained from global biomass in 2011 (Piotrowski et al., 2015).

The data reported above are obtained from a study of Nova Institute in 2015 (Piotrowski et al., 2015) that points out an excess of demand with respect to the supply of only 6%, hence it can be managed, and surprisingly the demand for materials is ten times higher than the one for biofuels. Notably the biomass is composed mainly by Cellulose and Starch/Sugars (Fig. 7), which are the protagonists of the present work. The work is indeed focused on the modification of cellulose and starch in order to produce innovative materials.

## 2. OBJECTIVES

The research wishes to respond to the demand of materials based on renewable resources even from waste; with the ambition to realise low value goods, such as packaging and high value goods such as high-tech materials, starting from bare starch and cellulose.

In the production of pure starch from Yuca (*Manihot Esculenta Crantz*) is produced 10-15% of pulp; this secondary waste is rich in starch by 50-60% on dry mass. The pulp is usually exploited as low value feed for animals, however also in this case it represents a concern for disposal, since being rich in moisture, it degrades rapidly in warm environments with proliferation of microorganisms. The use of residual starch obtained from the waste through biotechnological processes, as proposed by Sriroth et al., is an opportunity to solve a disposal issue and to generate value. To the case of yuca waste studied by Sriroth et al. (Sriroth et al., 2000) a second step was envisaged that is the topic of the present work; the conversion through a chemical process into a smart plastic having a photoresponsive crosslinking. The photoresponsivity, designed a priori, is intended to improve the mechanical properties of starch by cross-linking. The field of application is biodegradable plastic bags, characterised by weakness to mechanical stress, and when used for compostable waste disposal submitted to a quick biodegradation, which is a property actually thought for a compostable behaviour. By crosslinking starch with UV exposure the bag will be improved in mechanical strength; the property will be eliminated at the end of use through the reverse reaction of crosslinking, at low energy cost (Cohen and Schmidt, 1964). By introducing cinnamyl ether or ester groups into starch, a new type of bio-based polymer was developed. The results of the research open perspectives for innovative materials in different fields of application: packaging, sensing and actuation.

In the case of cellulose the application as chiral selector for the separation of enantiomers is known (Sánchez et al., 2019), and to this aim cellulose was converted by chemical processes to phenyl carbamate (Okamoto et al., 1986b) that enhances the separation performances. The application of cellulose as a chiral selector adds very high value to the resource; indeed the use of sophisticated organic chemistry generates a material very expensive compared to the starting cellulose.

## 3. STARCH

### 3.1 Starch: literature review

Research is fostering the development of starch-based innovative products, to be applied in the expanding fields of biomaterials, regenerative medicine and therapeutic areas (e.g., hydrogels, aerogels and biofoams) (Falua et al., 2022).

The richness of hydroxyl groups present in the glucopyranose units makes starch easy to modify in terms of structure and functional properties exploiting chemical or enzymatic methods (Santayanan and Wootthikanokkhan, 2003a).

Starch represents the energy storage of metabolism; it is abundant in cereals, tubers, rhizomes and seeds (Bertoft, 2017). Starch is biosynthesised by at least 4 enzymes: ADP-glucose pyrophosphorylase (AGPase), starch synthase (SS), branching enzyme (BE) and debranching enzyme (DEB). Among these enzymes, granule-bound starch synthase I (GBSSI) is in charge for the amylose biosynthesis (Kato et al., 2020). Starch is usually present in the form of granules in the parenchyma cells and the form of the granules is typical of the vegetable kind (Do et al., 2020). Granules occur with all shape and size, as ellipsoids, spheres, tubules, platelets and the size is in the range from 0.1  $\mu\text{m}$  to 200  $\mu\text{m}$  (Spinozzi et al., 2020). In the starch's granules two glucans are present: amylose, whose primary structure is the linear repetition of D-glucose unit by  $\alpha$ -1,4-linkages and few branches  $\alpha$ -1,6 and amylopectin characterised by many branches  $\alpha$ -1,6 and lateral chains with shorter length (Fig. 8). The granules are characterised by a semi crystalline structure with a low degree of crystallinity in a range of 15-45%, they are densely packed with a density of 1,5  $\text{g}/\text{cm}^3$  (Pérez and Bertoft, 2010a). Usually the crystalline pattern is A-type for cereal, while tubers and rhizomes have B-type pattern and C-type occurs in legumes (Pérez and Bertoft, 2010b).

The crystallinity of starch was widely studied, even though there are still unpredicted behaviours coming from nature (Spinozzi et al., 2020), the double helices left handed of the amylopectin branches show the arrangement that determines the crystal nanodomains (Fig. 8).

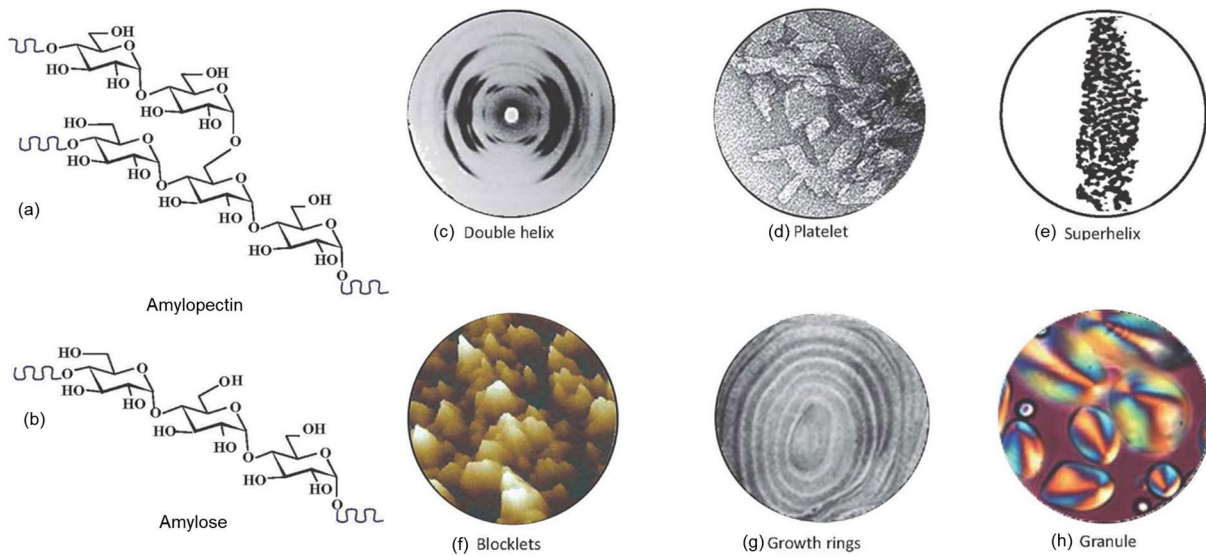


Figure 8. Starch hierarchical structure (Spinozzi et al. 2020).

The levels of starch's hierarchical structure are shown in Fig. 8, they start with the components amylopectin (a) and amylose (b); follow with the double helices shown by X-ray fibre diffraction pattern (c), Transmission Electron Micrograph of crystalline platelets obtained from starch's hydrolysis(d), TEM crystalline granules' fragment (e); AFM image of blocklets obtained by iodine vapour exposure (f); rings of alternating semi-crystalline and amorphous structure starting from the central point hilum (g). Maltese cross observed under polarised light of starch granules (h).

Despite its interesting structure, starch finds little room in the widespread use of polymers for materials application, the moisture sensitivity and the brittleness still represent issues to be overtaken. In this regard, acetylation (Santayanon and Wootthikanokkhan, 2003b), blending with synthetic polymers (e.g. PE, PVA or SBR latex), incorporation of nanometric bio-fillers (Bugnotti et al., 2023), and modification with cross-linking units which induces network formation (Garavand et al., 2017) (Delville et al., 2002) have been employed to improve the tensile strength and the hydrophobicity of starch. However, poor compatibility among starch, filler and synthetic polymers, non-biodegradability or even toxicity of some incorporated compounds raise concerns about the application of these materials in specific fields, such as food packaging (Yudhistira et al., 2024). In this scenario, the use of naturally occurring crosslinking agents has recently attracted increased attention as a promising route to tackle environmental and health concerns, along with economic issues.

From Nature richness, cinnamic acid, an aromatic carboxylic acid naturally enclosed in all green plants and also in the reproductive organs of flowering plants (Krauze-Baranowska, 2002), can be fished out as a promising option. Cinnamic acid has a low toxicity and a broad spectrum of biological activities. It plays key physiological roles in plant growth, development, reproduction, and disease resistance and it has also been used by medicinal chemists to alter the potency, permeability, solubility, or other parameters of selected drugs or pharmacophores. Many cinnamyl derivatives are well-known antioxidants and are supposed to have several health benefits due to their strong free radical scavenging properties. It has been reported also about their antibacterial, antiviral and antifungal properties (Guzman, 2014).

In addition, the well-known ability of cinnamyl derivatives to undergo a reversible [2 + 2] cycloaddition under UV light at a specific wavelength (Cohen and Schmidt, 1964) (Schmidt, 1971) has been extensively exploited for the production of several photo-cross-linkable polymers, such as poly(vinyl cinnamate) applied in liquid crystal display stack for a light controlled molecular orientation (Adams et al., 2014) (Egerton et al., 1981a) (Egerton et al., 1981b).

Recently, cinnamyl units have been also employed in the so-called “smart materials”, whose molecular structure and subsequent properties can be changed in response to external stimuli such as light, heat, and pH, imparting them interesting and programmable properties for advanced applications (Sepehrifar et al., 2017) (Abdallh et al., 2019). In these systems, such as shape memory polymers, cinnamyl derivatives have been introduced as pendant groups or directly included in the polymer backbone, allowing to replace toxic and non-sustainable adducts such as anthracene, thiols, or azo compounds (Bazin et al., 2022) (Du et al., 2020) (Hu et al., 2021). Furthermore, the photoactivated crosslinking polymerization represents an eco-friendly procedure as it does not require neither heating nor solvents (Sangermano et al., 2014) (Sangermano et al., 2018) (Bongiovanni et al., 2021).

Very few studies in the literature report on the exploitation of cinnamyl derivatives in combination or grafted to starch for the production of photo-cross-linkable bio-polymers. The grafting of cinnamyl moieties is normally achieved through esterification processes which result in esters where the vicinal double bond and the  $sp^2$  carbon of the carbonyl group are arranged in a planar rigid structure which, in principle, may hinder the photo-cross-linking reaction. Moreover, evidence of cinnamyl photodimerization is typically limited to the precursors rather



than the final complex materials, and generally assessed only by UV–vis spectroscopy (R. Zhang et al., 2020) (Li et al., 2021) (Z. Wang et al., 2019).

Stimulated by this background, the present study proposes an innovative synthetic protocol to obtain a new starch-based polymer bearing cinnamyl functionalities to confer photo-cross-linkable properties. In detail the etherification approach has been adopted and compared to the esterification approach, providing more insight on the role of chromophore configuration and structure in [2+2] cycloaddition. In fact, the ether linkage with the allylic carbon hybridised  $sp^3$  allows the free rotation of the C-C bond, thus providing greater flexibility to the two double bonds undergoing photodimerization, for comparison the ester linkage has a planar  $sp^2$  configuration with a more conjugated  $\pi$  orbitals (Kaur et al., 2014) but less flexibility.

Yuca (or cassava) *Manihot Esculenta* Cratz was selected as the starch source, since this cultivation is very sustainable; it has high starch content in the tubers that are also perennial (Fig. 9A). Moreover, yuca survives in a climate characterised by drought and it does not require demanding agricultural practices (Tabaglio et al., 2023). Despite the crop being so sustainable, the peel and pulp coming from manufacturing represent a big concern (Fig. 9B), due to the high level of moisture and residual starch (50-60% on dry bases) the microorganisms proliferation is quick, making the disposal a threat for the environment (Sriroth et al., 2000). Considering the huge amount of waste produced by the yuca market and the value loss highlighted by starch content, recently the valorisation of this resource captured the attention of scientific community (Weligama Thuppahige et al., 2023)





Figure 9. A) The tuber of Yuca is one of the richest nutrition in starch. B) A small-scale production of starch from yuca in Nigeria ([Obasanjo Farms commissions new cassava plantlets tech in Ogun – Daily Trust](#)).

In this research primarily a comprehensive characterization of the pristine starch coming from yuca was performed and then the structure and the functionalized starch cinnamyl ether were carefully studied by X-ray diffraction (XRD), attenuated total reflection Fourier transform infrared (ATR-FTIR) spectroscopy, liquid and solid-state nuclear magnetic resonance (NMR), and thermogravimetric analysis (TGA).

To prove the efficacy of the proposed synthetic strategies in supplying a photo-cross-linkable material, the photochemical properties of the starch cinnamyl ether have been carefully checked by UV-Vis, and by NMR and only by NMR for cinnamoyl due to the model molecule availability. Finally, considering the high demand of transparent biodegradable materials in the frame of packaging products (Guillard et al., 2018), a proof of concept of the potential applicability of the novel bio-based polyether in the preparation of transparent and homogeneous films is reported.

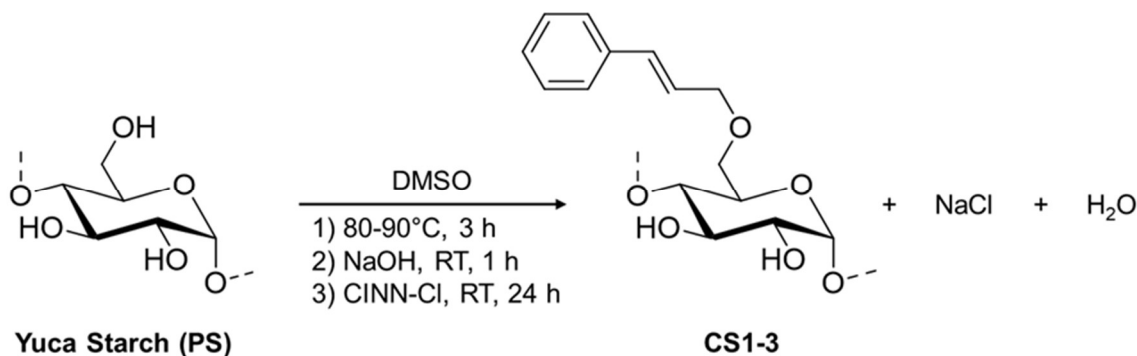
## 3.2 Starch: Methods and Materials

### 3.2.1 Materials

Before use, yuca (or cassava) starch powder originated from Colombia (almidon de yuca dulce produced by Cimpa s.a.s.) was dried in a static oven for 48 h at 65 °C; the average weight loss resulted between 9 % and 11 %. Cinnamyl chloride (3-chloropropenyl)benzene (CINN-Cl, CAS 2687-12-9, purity 95 %), Cinnamyl bromide (3-bromopropenyl)benzene (CINN-Br, CAS 4392-

24-9, purity 97 %), [AMIM]Cl (1-allyl-3-methylimidazolium chloride, CAS 65039-10-3, purity  $\geq 97$  %), pyridine (CAS 110-86-1, purity 99.8 %) and benzoyl chloride (PhCOCl, CAS 98-88-4, purity 99%), anhydrous NaOH (pellets, purity grade  $\geq 98$ %), tetrahydrofuran (THF, inhibitor-free, HPLC grade  $\geq 99.9$ %) were purchased from Sigma-Aldrich and used without any further purification. Acetone (CAS 67-64-1, 96.6 % purity grade), and analytical grade ethanol (EtOH, CAS 64-17-5) were purchased from Thermo Fisher Scientific. Anhydrous dimethyl sulfoxide (DMSO, CAS 67-68-5, analytical grade) was purchased from VWR International. Ultrapure water was obtained by the Milli-Q® system with residual conductivity of 13  $\mu$ S/cm. DMSO- $d_6$  (CAS 2206-27-1, 99.5 atom % D) and trifluoroacetic acid-d (TFA-d, CAS 599-00-8, 99.5 atom % D) for NMR spectroscopy were purchased from Acros Organics. Thin layer chromatography (TLC) was performed on silica gel 60 F254 coated glass plates (Merck), using a 10:0.5 CHCl<sub>3</sub>: EtOH mixture as the eluent and visualised by an UV lamp at 254 nm wavelength.

### 3.2.2 General procedure for the synthesis of starch cinnamyl ether derivatives.



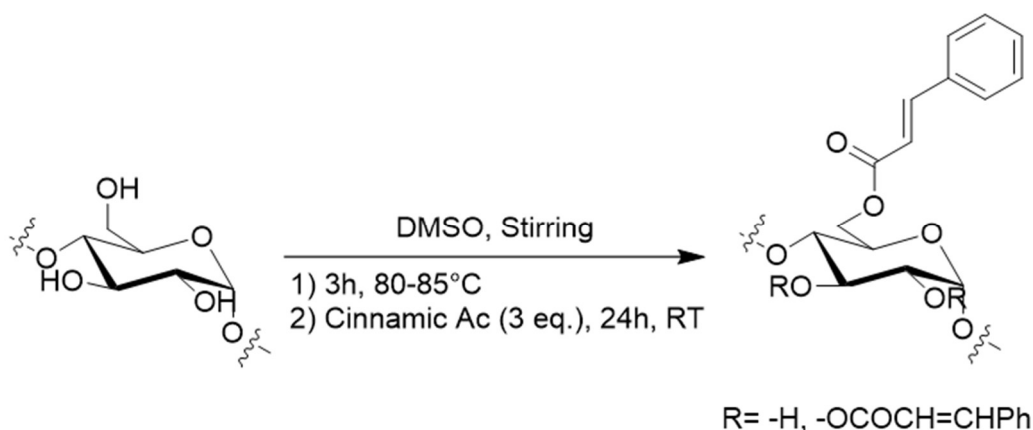
*Scheme 1. Synthesis of Starch cinnamyl ether.*

Different starch/NaOH/cinnamyl halide ratios were used in order to obtain different substitution degrees (DS). The ratios are calculated on the mmol of anhydroglucose units (AGU, MW = 162.14 g/mol).

Typically, 1 g (6.16 mmol AGU) of dried yuca starch is suspended in 16 mL of dry DMSO (c = 62.5 g/L) in a round-bottom flask and heated to 90 °C with an oil bath under magnetic stirring till dissolution (3 h). The solution is then cooled to room temperature and powdered NaOH, previously suspended in 2 mL of the reaction mixture, is added (6.16 mmol or 18.48, Table 4). The mixture is homogenised for 1 hour. Cinnamyl chloride (CINN-Cl) (1.23 mmol, 6.16 mmol, or 27.72 mmol) is added, and the reaction is kept under stirring for 24 hours at room temperature.

The solution is transferred into a plastic centrifuge tube, cold acetone (30 mL) is added and gently mixed. After 10 min the crude product precipitates, the suspension is centrifuged (5000 rpm, 20 °C, 10 min), the solvents carefully removed and the solids (white powder) washed under magnetic stirring for 10 min with a mixture of 30 mL of acetone and 5 mL of deionized water in order to remove residual organics (cinnamyl halide or by products derived thereof) and inorganics (NaOH and NaCl); the suspension is centrifuged (5000 rpm, 20 °C, 10 min), the solvents carefully removed and the washing is repeated once more with fresh acetone : water mixture, followed by a final washing with pure acetone (30 mL). The collected solids are dried under vacuum in a desiccator. TLC of mother liquors was used to monitor washing effectiveness from organic by-products.

### 3.2.3 Procedure for the synthesis of starch cinnamoyl ester derivatives.



*Scheme 2. Synthesis of Starch cinnamoyl ester.*

1 g (6.16 mmol AGU) of dried yuca starch is suspended in 16 mL of dry DMSO ( $c = 62.5$  g/L) in a round-bottom flask and heated to 90 °C with an oil bath under magnetic stirring till dissolution (3 h). The solution is then cooled to room temperature and Cinnamic Acid powder is added to the round bottom flask under stirring (18.5 mmol 3 molar equiv.). The reaction mixture is kept under stirring for 24 hours at room temperature. The product's isolation and purification have been carried out according to the procedure reported above for starch ether derivatives.

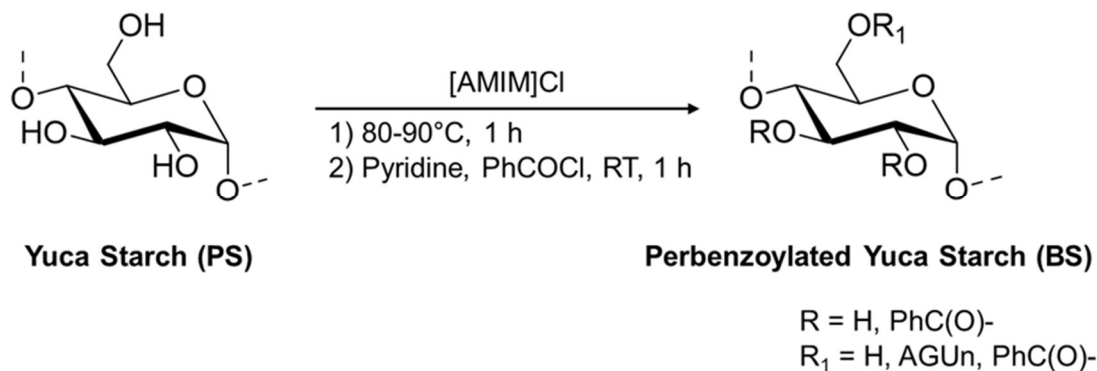
### 3.2.3 Starch cinnamyl ether film preparation

450 mg of cinnamyl-starch ether (DS 0.09, CS1) are dissolved in 10 mL of deionized water at 90 °C under magnetic stirring for 1 hour. After complete dissolution, 2 mL of the solution are

casted at room temperature on a petri dish of low-density polyethylene. The film is peeled-off, and dried at room temperature in air for 3 days.

### 3.2.4 Yuca starch Gel Permeation Chromatography (GPC)

GPC analysis was performed on perbenzoylated starch samples, prepared as follows: 32 mg (0.196 mmol AGU) of dried yuca starch were dissolved in 1 g of [AMIM]Cl in a glass flask by stirring at 90 °C for about 1 hour. After complete dissolution, the mixture is cooled to room temperature. Subsequently 200  $\mu$ L of pyridine (2.48 mmol), and 200  $\mu$ L of benzoyl chloride PhCOCl (1.72 mmol) were added. The mixture was vortexed for 10 min and stirred at room temperature for 1 hour in order to afford a homogeneous solution. The crude product was precipitated by adding 10 mL of a 7:3 EtOH: H<sub>2</sub>O mixture. The solids were recovered by centrifugation (3000 rpm, 15 min), after removal of the supernatant. In order to fully remove the ionic liquid, pyridine salts and the excess of reagents, the precipitate was vortexed in a 7:3 fresh mixture of EtOH: H<sub>2</sub>O (10 mL, 10 min) followed by centrifugation (3000 rpm, 15 min). These steps were repeated twice.



*Scheme 3. Benzoylation procedure of pristine starch PS*

The white solid was dried under reduced pressure. 1 mg of perbenzoylated starch was dissolved in THF and filtered with a GHP 0.45  $\mu$ m Acrodisc syringe filter for the GPC analysis (Salanti et al., 2012). The analyses were performed with a HP1100 series liquid chromatography connected to a HP 1040 UV photodetector at a wavelength of 240 nm. The injector had a Rheodyne loop valve with a loop capacity of 20  $\mu$ L. The GP-column system was composed as follows (according to the solvent flow direction): Agilent PLgel 5  $\mu$ m (500 Å), Agilent PLgel 5  $\mu$ m (1000 Å) and Agilent PLgel 5  $\mu$ m (10000 Å). THF at a flow rate of 1 mL/min was flushed. PL Polymer Standards of Polystyrene from Polymer Laboratories were used for calibration. The evaluation

of the number-average molecular weight ( $M_n$ ) and the weight-average molecular weight ( $M_w$ ) of the samples was performed. Moreover, the ratio  $I = M_w/M_n$ , defined as the Dispersity Index was also calculated. The reported  $M_n$  and  $M_w$  values are the average of three analyses (standard error  $M_w$ : 500 g/mol;  $M_n$ : 100 g/mol).

### 3.2.5 ATR-FTIR

Fourier transform infrared spectra were acquired in the attenuated total reflectance mode at room temperature in the range of 4000-550  $\text{cm}^{-1}$  with a ThermoFisher Nicolet iS20 instrument (spectral resolution of 4  $\text{cm}^{-1}$  and 64 scans). The ATR-FTIR spectra are analysed by OMNIC software and reported after background subtraction and baseline correction.

### 3.2.6 Solution $^1\text{H}$ and $^{13}\text{C}$ -NMR

The solution NMR spectra were recorded with a Bruker Avance 400 WB spectrometer operating at a proton frequency of 400.13 MHz for  $^1\text{H}$ -NMR and at a carbon frequency of 100.61 MHz for the  $^{13}\text{C}$ -NMR. The analyte was prepared by dissolving about 30 mg of starch samples in 750  $\mu\text{L}$  of DMSO- $d_6$  (2 h, 70-90  $^\circ\text{C}$ , under stirring). The solution was then transferred in a NMR test tube at room temperature, and 50  $\mu\text{L}$  of deuterated trifluoroacetic acid (Tizzotti et al., 2011) were added in order to quench residual hydroxyl group signals, for an accurate determination of the substitution degree (DS) and the degree of branching (DB).

### 3.2.7 Determination of the degree of substitution (DS) and degree of branching (% DB)

The DS is defined as the number of substituents per anhydrous glucose unit (AGU); the value may vary between 0 and 3, for the hydroxyl groups on carbon 2, 3 and 6; the maximum value (3) can be obtained only in case the 6-OH is not involved in  $\alpha(1,6)$ -linkages. Since starch contains  $\alpha(1,6)$ -branched amylopectin, the DS cannot reach the maximum value.

The DS is determined by the ratio between the normalised integration area of the aromatic protons ( $A_{Ph}/5$ ) and the integration areas of the anomeric protons  $A_{\alpha(1,4)} + A_{\alpha(1,6)}$ , following equation (1).

$$DS = \frac{A_{Ph}}{5 \cdot (A_{\alpha(1,4)} + A_{\alpha(1,6)})}$$

*Equation 1*



The % DB is estimated through the percent ratio between the peak area of the anomeric proton involved in the  $\alpha(1,6)$  linkage (4.77 ppm) and the integration areas of the anomeric protons  $A_{\alpha(1,4)} + A_{\alpha(1,6)}$ .

$$DB(\%) = \frac{A_{\alpha(1,6)}}{A_{\alpha(1,4)} + A_{\alpha(1,6)}} \cdot 100$$

*Equation 2*

### 3.2.8 SS-NMR

Solid state NMR spectra were recorded with a Bruker (Billerica, MA, USA) 400WB spectrometer operating at a proton frequency of 400.13 MHz under the following conditions for cross polarisation magic angle spinning (CPMAS) experiments:  $^{13}\text{C}$  frequency 100.48 MHz, contact time 3 ms, decoupling length 5.6  $\mu\text{s}$ , recycle delay 10 s, 2 k scans. For cross polarisation with polarisation inversion (CPPI) experiment (Wu and Zilm, 1993) CP and PI times were 50  $\mu\text{s}$  and 43  $\mu\text{s}$ , respectively. In all the spectra, adamantane was used as an external secondary reference.

Samples were packed in zirconia rotors and spun at 11.2 kHz to avoid signal overlapping with spinning sidebands.

### 3.2.9 UV-Vis Spectroscopy

UV-vis analyses were performed with an UV-vis Cary 60 spectrophotometer in a 5 mm quartz cuvette, with samples  $10^{-4}$  M for cinnamyl functional group concentration in water. The samples were irradiated with a UVLS-24 Fisher UV-lamp equipped with 35 W lamp emitting at wavelengths centred at 365 and with a Helios UV low pressure Hg Lamp with emission peak at 254 nm. To avoid overheating effects, the samples were cooled with an ice-cold water bath during irradiation.

### 3.2.10 UV-DRS

Diffuse reflectance spectroscopy was performed using a PerkinElmer, precisely, Lambda 1050+ UV/vis/NIR spectrophotometer. The powders were dispersed in EtOH and drop-casted on a quartz slide.

### 3.2.11 TGA

The TGA analysis was performed with a Mettler Toledo TGA/DSC1 STARe system. The thermograms span from 30 °C to 1000 °C, with a heating rate of 10 °C/min, and a constant 50 mL/min N<sub>2</sub> flow.

### 3.2.12 XRD

XRD patterns of the powder samples were recorded on a Rigaku (Tokyo, Japan) DMAX III diffractometer in Bragg–Brentano geometry, equipped with a Cu source ( $\lambda = 1.54056 \text{ \AA}$ ) in the following conditions:  $2\theta$  range from 2 to 45, steps of 0.05 ° and 3 s counting time.

## 3.3 Starch: Results and Discussion

### 3.3.1 Characterization of yuca starch

Starch is a natural polymer characterised by two components, the linear  $\alpha(1,4)$ -polysaccharide amylose, and the branched  $\alpha(1,6)$ -polysaccharide amylopectin. Charoenkul et al. (Charoenkul et al., 2006) reported for yuca starch a 17 % amylose content in and 83 % amylopectin. Since the extent of substitution with the cinnamyl moieties will be influenced by starch composition, a preliminary characterization of yuca starch was performed. Pristine yuca starch was characterised in terms of its number-average molecular weight, weight-average molecular weight, and dispersity index by GPC analysis, together with its degree of branching by solution <sup>1</sup>H-NMR.

The determination of the average molecular weight of the two components is usually performed through GPC chromatography after derivatization (Zoia et al., 2011). Thus, a preliminary benzylation of the analyte both for the complete solubilization in the chromatographic solvent and for the UV detection was performed (Section 3.2.4), using the ionic liquid [AMIM]Cl as the solvent, in dark conditions.

GPC analysis (Fig. 10 and Table 1) allowed the determination of the number-average molecular weight ( $M_n$ ), the weight-average molecular weight ( $M_w$ ) and the peak molecular weight ( $M_p$ ), which is defined as the molecular weight at the maximum absorbance, along with the polydispersity index (I).

The GPC profile (Fig. 10) displayed a polymodal distribution, thus the curve was deconvoluted by a Gaussian distribution, affording three different contributions (profiles 1, 2, 3, Fig. 10); the area (%) for each contribution is reported in Table 1.

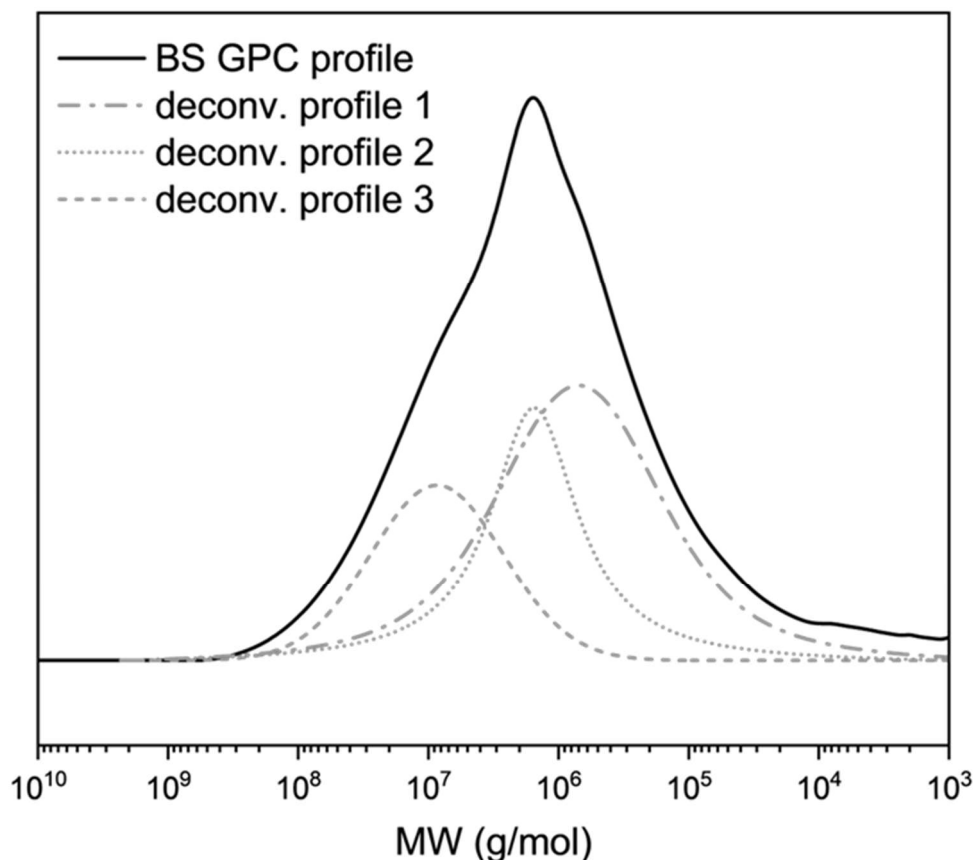


Figure 10. GPC chromatogram of yuca starch and the corresponding peak deconvolution.

The deconvoluted peaks 1, 2, and 3 correspond to molecular weight (Mw) of  $1.1 \cdot 10^6$ ,  $1.8 \cdot 10^6$  and  $6.3 \cdot 10^7$  g/mol, respectively. The higher Mw peak (profile 3) was related to the amylopectin component, in agreement with literature data, reporting values between  $10^7$  and  $10^9$  g/mol (Zhou et al., 2010) (Hoover, 2001) (Tester et al., 2004a). Amylose has a relatively lower Mw compared with amylopectin, ranging from  $10^5$  to  $10^6$  g/mol. Accordingly, the profile 2 was mainly (but not uniquely) attributed to higher Mw amylose, whereas profile 1 was considered to comprise mostly (but not entirely) lower Mw amylose (Shi et al., 1998).

Table 1. Contribution of the various Mw fractions (1-3) in yuca starch components as estimated by the deconvolution of the GPC profile. The area (%) for each contribution is also reported.



	yuca starch profile	1	2	3
Area (%)	—	47	33	20
$M_p$	$1.4 \cdot 10^6$	$6.8 \cdot 10^5$	$1.5 \cdot 10^6$	$8.5 \cdot 10^6$
$M_n$	$4.8 \cdot 10^6$	$8.7 \cdot 10^5$	$1.6 \cdot 10^6$	$1.45 \cdot 10^7$
$M_w$	$6.1 \cdot 10^7$	$1.1 \cdot 10^6$	$1.8 \cdot 10^6$	$6.3 \cdot 10^7$
I	12.8	1.3	1.2	4.3

The yuca starch degree of branching calculated in respect to the anhydroglucose unit was determined by solution  $^1\text{H-NMR}$  as described in the Materials and Methods section and resulted in 3.7 %; as a consequence, a maximum degree of substitution of 2.96 can be expected.

### 3.3.2 Starch synthesis: parameters optimization.

The synthetic routes identified for starch functionalization were etherification and esterification. The general requirement to provide a suitable photo-crosslinking degree was to have one moiety each of 10 anhydro glucose units (AGU) and a distance between two double bonds of 4 Å (Schmidt, 1971). To determine the number of moieties introduced the Degree of Substitution (DS) was adopted. DS is the average number of substituents on AGU; theoretical DS varies from 0 to 3 and can be determined by quantitative protonic Nuclear Magnetic Resonance Spectroscopy ( $^1\text{H-NMR}$ ) (Chi et al., 2008).

#### 3.3.2.1 Esterification

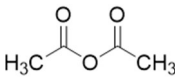
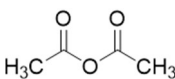
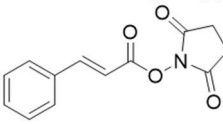
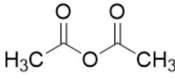
In order to set up the best reaction conditions for the introduction of photo cross-linkable moieties, a model acylation reaction was first studied: reaction medium, starch concentration, and temperature were main parameters to be considered.

##### *Acetylation as model acylation reaction*

A model reaction was employed to study the reaction's conditions between starch and acetic anhydride. The model reaction was based on a low cost and commercially available acylating agent (i.e. acetic anhydride) and robust literature background. The choice of reaction medium passed through the test of Pyridine, as solvent and additive, (Garg and Jana, 2011) (Santayanan and Wootthikanokkhan, 2003) and DMSO (Dona et al., 2007).

The different reaction conditions tested are resumed in Table 2.

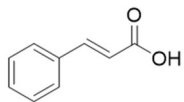
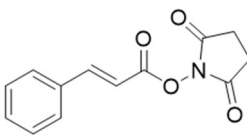
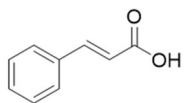
Table 2. Experimental conditions to maximise DS tested on model reaction and target.

<i>Type</i>	<i>Medium</i>	<i>Reagent</i>	<i>Temp.</i>	<i>time</i>	<i>DS</i>
Model	Pyridine (heterogeneous)	 acetic anhydride (10 eq.)	RT	22 h	0
Model	Pyridine (heterogeneous)	 acetic anhydride (10 eq.)	75°C	22 h	0.7
Target	Pyridine (heterogeneous)	NHS ester (1 eq.) 	75°C	22 h	0
Model	DMSO (homogeneous)	 acetic anhydride (10 eq.)	75 °C	22 h	>1

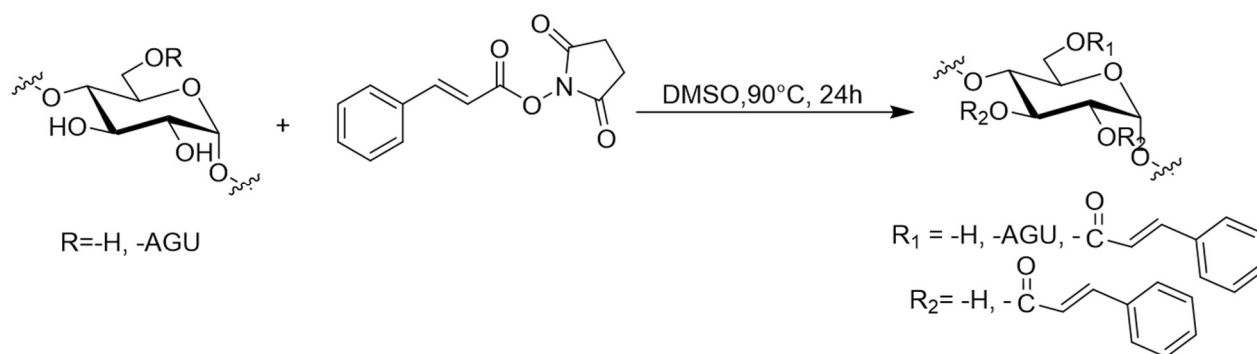
The best results were achieved in dimethyl sulfoxide (DMSO) at a concentration of 26,7 g/L of starch and a temperature of 70-90°C. DMSO allows a homogeneous phase that results crucial for effective acylation. A DS>1 was determined by <sup>1</sup>H-NMR after a careful dissolution of the NMR sample (Schmitz et al., 2009).

The photoreactive moiety of choice, the cinnamoyl group, should be introduced with a suitable acylation reaction. Since the only commercially available reagent was cinnamic acid, activation of the carboxyl group to acyl nucleophilic substitution was needed. Based on the best conditions determined as reported above concerning reaction parameters. The reaction was carried out with different acylating derivatives, as reported in Table 3.

Table 3. Tests on experimental conditions of Starch esterification.

Type	Medium	Reagent	Temp.	time	DS
Target	DMSO	 5.5 eq (0.3 % H <sub>2</sub> SO <sub>4</sub> )	85 °C	22 h	0.01
Target	DMSO	 1 eq.	85 °C	22 h	0.09
Target	DMSO	 3 eq.	RT	24 h	0.01

The reaction of transesterification with 1 eq of NHS ester, a cinnamyl active ester (Scheme 4), affords a DS=0.09 (determined by <sup>1</sup>H-NMR) which almost matches the requirement for the subsequent photo-crosslinking. However, the isolation and purification of the product was unsuccessful, as shown in <sup>1</sup>H-NMR spectra in Fig. 11 (solid red).



Scheme 4. Starch cinnamyl transesterification.

The Fisher esterification with 0.3% of sulfuric acid H<sub>2</sub>SO<sub>4</sub> as catalyst and cinnamic acid afforded a DS of 0.01, however some fragmentation occurred as shown by the splitting in multiple peaks of anomeric proton signal (5.2-4.9 ppm) in <sup>1</sup>H-NMR of Fig. 11.

On the other hand the simple autocatalytic Fisher esterification with cinnamic acid provided cinnamoyl ester without any fragmentation, and represented a possible green pathway for modification.

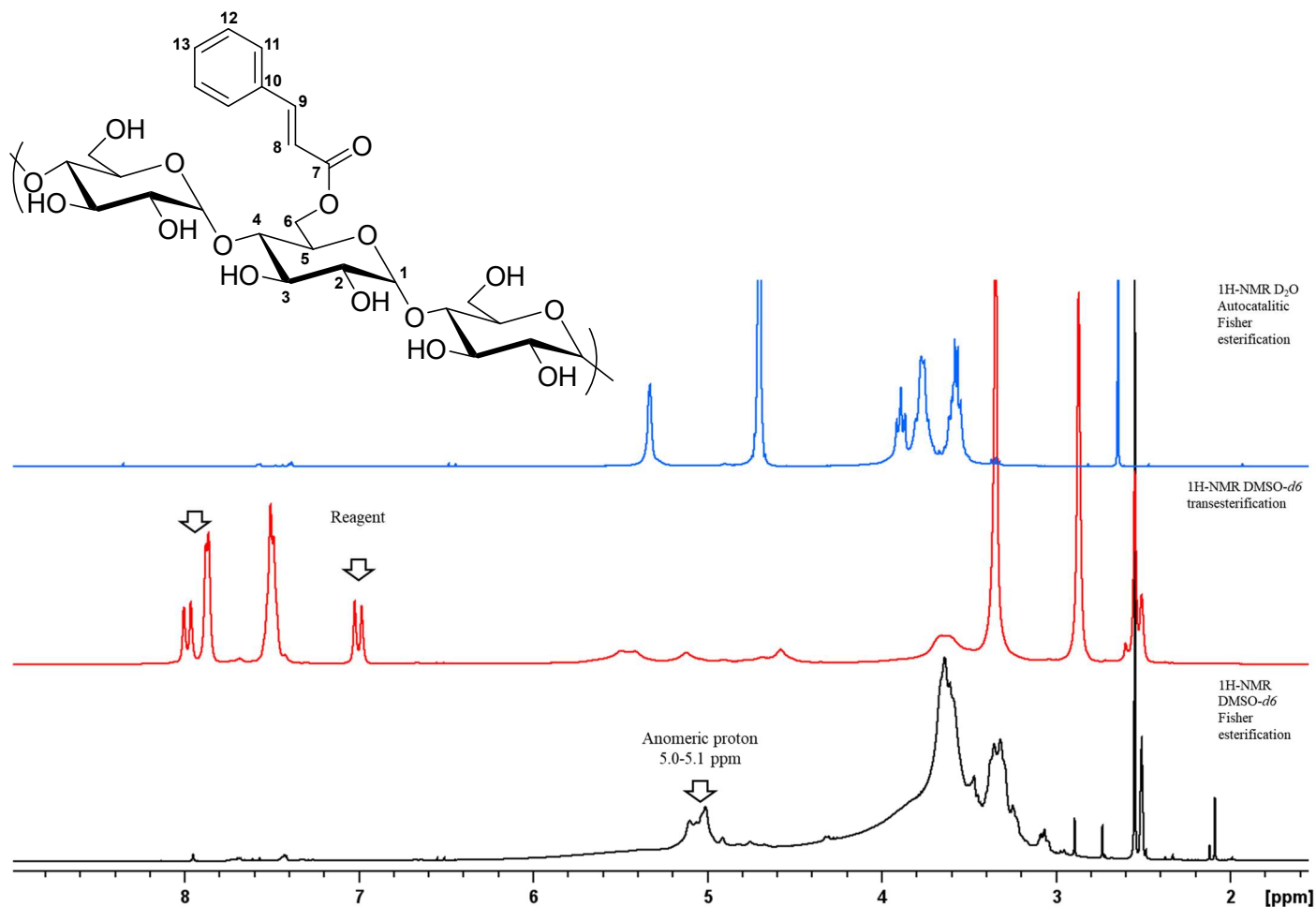


Figure 11  $^1\text{H-NMR}$  Spectra of starch cinnamoyl derivatives (solid blue) autocatalytic Fisher esterification (solid red) transesterification with NHS (solid black) Fisher esterification by  $\text{H}_2\text{SO}_4$  catalysis.

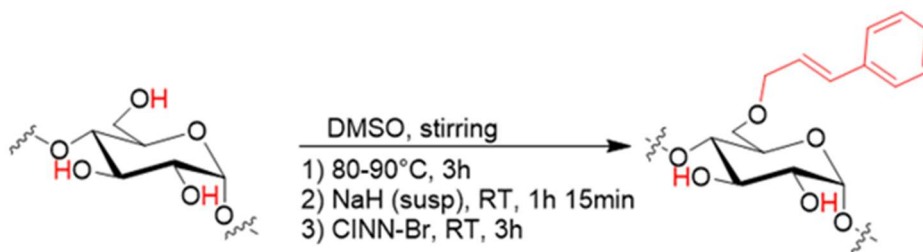
$^1\text{H-NMR}$  (solid black) [ $\text{DMSO-d}_6$ ]:  $\delta$  (ppm) = 7.95 (s), 7.68 (m, H-11, 11'), 7.58 (d,  $J=16.02$  Hz, H-9), 7.46-7.40 (m, H-12, 12' H-13), 6.66 (dd), 6.52 (d,  $J=16.02$  Hz, H-8), 5.2-4.9 (bm, H-1  $\alpha$ -1,4), 4.9 (bs, H-1  $\alpha$ -1,4 reducing end), 4.75 (bs, H-1  $\alpha$ -1,6), 4.67 (bs), 4.3 (m), 4.26 (d), 3.63 (bm, H-3, 5, 6, 6'), 3.37-3.20 (bm, H-2, 4), 3.0 (m, H-4 end group). Sample name: SPC-80-16.

$^1\text{H-NMR}$  (solid red) [ $\text{DMSO-d}_6$ ]:  $\delta$  (ppm) = 7.98 (d, 1 H,  $J=16.04$  Hz, H-vinyl reagent), 7.87 (m, 2 H, H Ar reagent), 7.49 (m, 3 H, H-Ar reagent), 5.49 (bs, -OH-3), 5.41 (bs, -OH-2), 5.11 (bs, H-1  $\alpha$ -1,4), 4.9 (bs, H-1  $\alpha$ -1,4 reducing end), 4.68 (bs), 4.57 (bs, -OH-6), 3.65 (bm, H-3, 5, 6, 6'), 3.3 (water), 2.86 (s, 4 H, H-Aliphatic reagent), 2.50 (DMSO). Sample name: SPC-80-17.

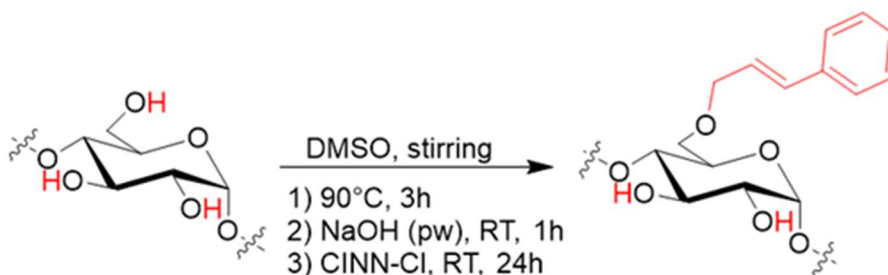
$^1\text{H-NMR}$  (solid blue) [ $\text{D}_2\text{O}$ ]:  $\delta$  (ppm) = 8.35 (s), 7.58-7.56 (m, 2 H, H-11, 11' substituent), 7.46 (d, 1 H,  $J=16.08$  Hz, H-9), 7.40-7.38 (m, 3 H, H-12, 12' H-13 substituent), 6.46 (d, 1 H,  $J=16.02$  Hz, H-8), 5.33 (bs, H-1  $\alpha$ -1,4), 4.73 (water), 3.89 (t, H-3), 3.80-3.73 (m, H-6, 6', H-5), 3.63-3.49 (m, H-4, H-2), 3.34 (t, H-4 end group), 2.64 (s, Acetone ), 1.09 (t, EtOH ) (Ishizuca et al. 2004).  
Sample name: SPC-80-123.

### 3.3.2.2 Etherification

In order to study the behaviour of cinnamyl moieties grafted through the ether bond a reaction of nucleophilic substitution  $\text{S}_{\text{N}}$  with cinnamyl bromide was set up, that received a further optimization thanks to the information of the paper "Synthesis of epoxides from alkyl bromides and alcohols with in situ generation of dimethyl sulfonium ylide in DMSO oxidations"(Z.-W. Zhang et al., 2020), which highlights a role of cinnamyl bromide, DMSO and NaOH in the competitive synthesis of epoxides. In order to refute this work, two tests were carried out: synthesis of starch cinnamyl ethers with NaH as a deprotonating agent (scheme 5) and cinnamyl chloride as alkylating agent (scheme 6).



*Scheme 5. Starch cinnamyl transesterification.*



*Scheme 6. Starch transesterification.*

Both reactions afforded a high degree of substitution confirming the thesis of Zhang's paper; moreover, in the case of cinnamyl chloride the DS is one order of magnitude higher than cinnamyl bromide. Hence the optimised synthesis of starch cinnamyl ethers embraced the reaction parameters of scheme 6.

### 3.3.3 Starch Cinnamyl Ether synthesis and characterization

Starch-cinnamyl ether with different DS (namely low, medium and high) were synthesised, in order to tune the physico-chemical properties, and to check the readiness to undergo the photodimerization reaction. The availability of starch-cinnamyl ether with different DS was considered as an opportunity to address several aspects: i) the identification of diagnostic signals, robustness and sensitivity of the analytical techniques explored for the detailed characterization, such as solution and solid state NMR, UV-Vis, ATR-FTIR spectroscopies, ii) solubility, thermal stability and optical behaviour, being key issues for the design of sustainable material processing and features (i.e. the balance between water solubility for sustainable processing and hydrophobicity as a water vapour barrier is crucial for food packaging (Bergel et al., 2018)) iii) the identification of the best DS for the subsequent photocrosslinking reaction.

The synthesis of the cinnamyl-starch derivatives required first the complete dissolution of starch in DMSO at 80-90 °C; afterward the solution was reacted with powdered NaOH at room temperature for 1 h, and finally cinnamyl halide was added.

Three different molar equivalents of NaOH and cinnamyl chloride were used, affording products CS1-CS3 with different degrees of substitution.

In order to tune the substitution degree, different molar equivalents of NaOH and cinnamyl chloride in respect to the molar equivalents of AGU were tested (Table 4). Assuming that the maximum DS is very close to 3, reagent amounts correspond to CINN-Cl/AGU of 0.2, 1.0, 4.5 molar ratios, respectively.

*Table 4. Reagent amounts used for the etherification reaction (starch is dissolved in DMSO, concentration ~ 60 g/L).*

Sample name	Starch (g) and AGU (mmol) amounts	NaOH/AGU molar ratio	CINN-Cl /AGU molar ratio	DS*
CS1	1.00 g, 6.16 mmol	1	0.2	0.09
CS2	1.00 g, 6.16 mmol	1	1	0.33
CS3	1.00 g, 6.16 mmol	3	4.5	1.24

\*determined by NMR.

The effectiveness of the starch derivatization with the cinnamyl moieties was first assessed by FTIR-ATR spectroscopy (Fig. 12).

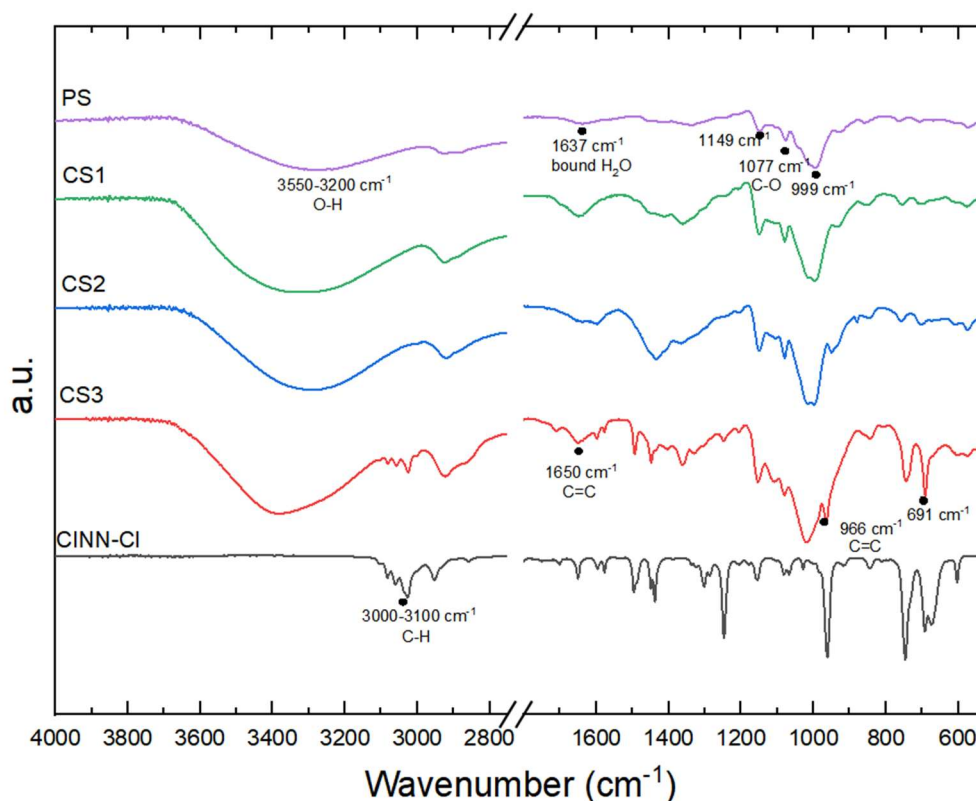


Figure 12. FTIR-ATR of pristine yuca starch (PS), cinnamyl chloride (CINN-Cl), and cinnamyl starch samples CS1-3.

The 1200-800 cm<sup>-1</sup> region shows the characteristic band due to C-O vibrations in the COH and COC groups of starch. The spectrum is modified by the presence of cinnamyl moieties, in particular the appearance of the peaks at 691 cm<sup>-1</sup>, 966 cm<sup>-1</sup> and 1650 cm<sup>-1</sup> could be attributed to the double bond stretching (C=C) of the disubstituted alkene, and the peaks at 3000-3100 cm<sup>-1</sup> to the C-H stretching of the alkene. The diagnostic signals of the cinnamyl units are well visible



in CS<sub>3</sub>, with signal intensities as a function of the amount of reagents used, qualitatively indicating the presence of cinnamyl moieties in the starch derivatives.

Given the effectiveness of the etherification process as determined by FTIR, solution <sup>1</sup>H-NMR was used for further confirming the etherification reaction, and for the DS determination of the samples (Table 4). The spectra were recorded in the presence of deuterated trifluoroacetic acid, since it quickly exchanges the protons of the unsubstituted OH groups with deuterium atoms, thus eliminating disturbing signals overlapping with the proton peaks of the starch backbone, needed for an accurate DS quantification. The non-deuterated trifluoroacetic acid resulting from this equilibrium gives rise to a broad signal centred at around 7.5 ppm, out of the diagnostic region of interest.

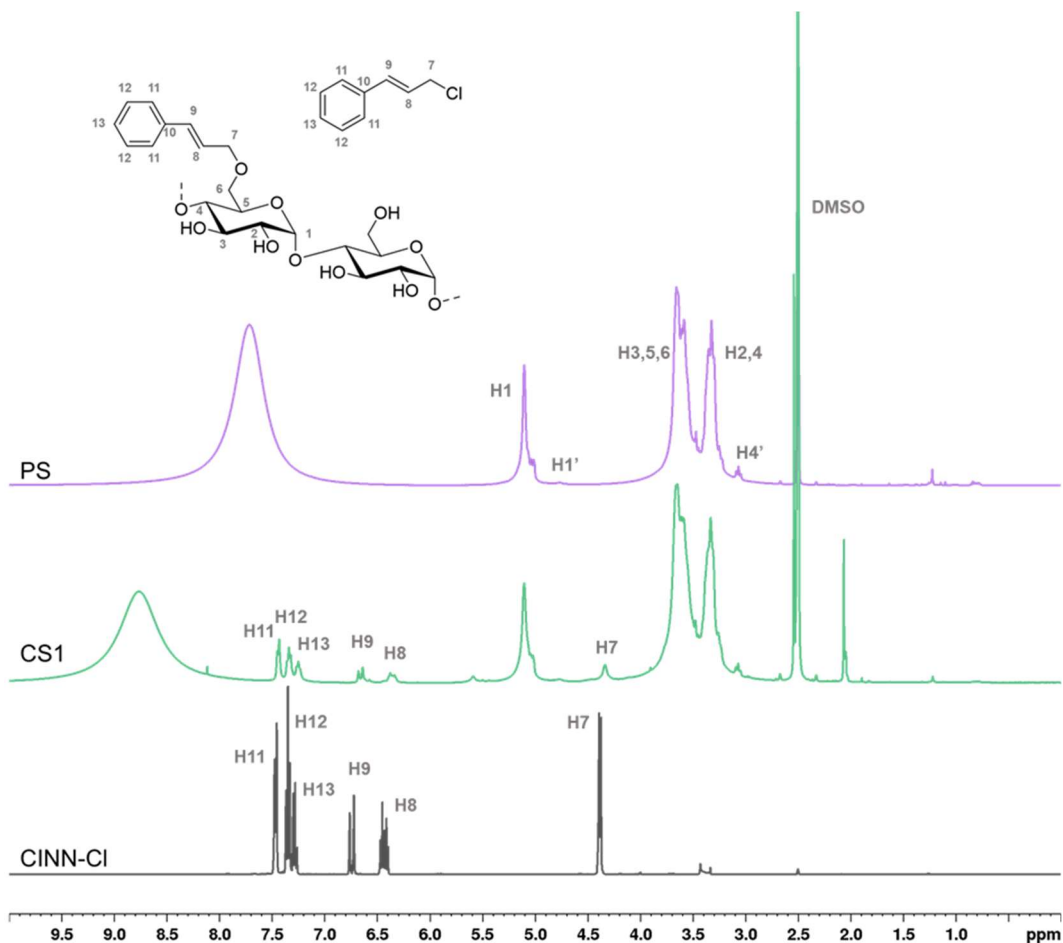


Figure 13. Comparison of <sup>1</sup>H-NMR in DMSO-d<sub>6</sub> of pristine starch (PS), CS1 (green) and cinnamyl chloride (black). For sake of clarity, numbering of the cinnamyl moiety in cinnamyl chloride and in the starch derivatives has been arbitrarily assigned (not compliant with IUPAC nomenclature); H1 refers to the anomeric protons involved in the (1,4) glycosidic linkage; H1' refers to the anomeric protons involved in the (1,6) glycosidic linkage; H4' refers to the non-reducing terminal glucose units.

The appearance of the peaks related to the cinnamyl moieties can be observed even for the low substitution sample CS1. The aromatic protons (H-11 - H-13) resonate in the range 7.5 – 7.2 ppm, while the vinyl protons are detected at 6.65 ppm (H-9) and at 6.35 ppm (H-8). The allyl methylene protons (H-7) resonating at 4.34 ppm in the cinnamyl chloride are shifted to slightly higher fields (4.26 ppm) in the corresponding starch-cinnamyl ethers.

In addition, the broadening of the signals of the cinnamyl substituent in the functionalized samples if compared to the pure CINN-Cl is a consequence of the positional distribution of the group within the AGU moiety (C-2, C-3, and C-6), and of the three different starch components observed by GPC. The anomeric protons  $\alpha$  (1,4) and  $\alpha$ (1,6) resonate at 5.10 ppm and 4.77 ppm, respectively; the integrals of these peaks in  $^1\text{H-NMR}$  spectra allowed them to quantitatively determine the DS (Table 2).

$^{13}\text{C}$  NMR spectrum for the starch-cinnamyl ether (CS1) is reported in (Fig. 14). In Table 5 the assignment of carbon and protons was performed with the correlation of HSQC NMR.

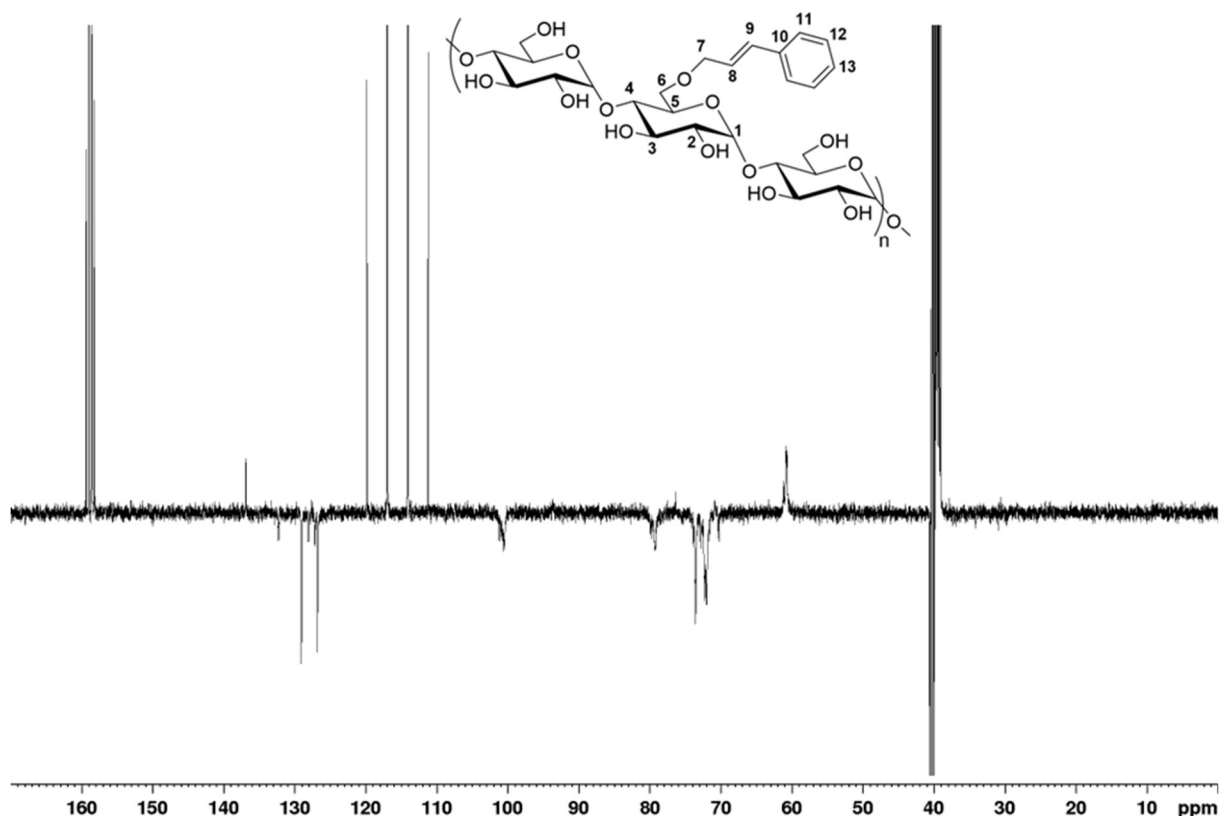


Figure 14.  $^{13}\text{C-NMR}$  APT (Attached Proton Test) in  $\text{DMSO-d}_6$  and  $\text{TFA-d}_1$  of CS1.

$^{13}\text{C-NMR}$  APT [101 MHz,  $\text{DMSO-d}_6 + \text{TFA-d}_1$ ]:  $\delta$  (ppm) = 158.88 (C=O TFA), 136.91(C-10), 132.34 (C-9), 129.10 (C-12, 12'), 128.13 (C-13), 127.25 (C-8), 126.8 (C-11, 11'), 115.53 ( $\text{CF}_3$ )

TFA), 100.63 (C-1), 79.27 (C-4), 73.62 (C-3), 72.30 (C-2), 72.09 (C-5), 70.38 (C-4 end group), 60.87 (C-6, 6'), 39.64 (DMSO). Sample name: SPC-80-16.

Table 5. Chemical shift assignments  $^1\text{H}$  and  $^{13}\text{C}$ -NMR of starch ether.

$^1\text{H}$ -NMR assignment	$^1\text{H}$ Chemical shift (ppm)	$^{13}\text{C}$ -NMR assignment	$^{13}\text{C}$ Chemical shift (ppm)
<i>H-1</i>	5.08	<i>C-1</i>	100.5
<i>H-1s</i>	5.6	<i>C-1s</i>	96.6
<i>H-2</i>	3.33	<i>C-2</i>	72.30
<i>H-3</i>	3.67	<i>C-3</i>	73.62
<i>H-4</i>	3.36	<i>C-4</i>	79,27
<i>H-4 (end group)</i>	3.08	<i>C-4 (end group)</i>	70.38
<i>H-5</i>	3.60	<i>C-5</i>	72.09
<i>H-6,6'</i>	3.63	<i>C-6,6'</i>	60.87
<i>H-6,6's</i>	3.62	<i>C-6,6's</i>	69.5
<i>H-7</i>	4.33	<i>C-7</i>	70.9
<i>H-8</i>	6.35	<i>C-8</i>	127.1
<i>H-9</i>	6.65	<i>C-9</i>	132.3
-	-	<i>C-10</i>	136.8
<i>H-11</i>	7.40	<i>C-11</i>	126.8
<i>H-12</i>	7.34	<i>C-12</i>	129.0
<i>H-13</i>	7.24	<i>C-13</i>	128.13

Solid state  $^{13}\text{C}$  CPMAS NMR spectra were also recorded in order to further characterise all of the cinnamyl-starch derivatives. Spectra of starch-cinnamyl ethers with 0.33 DS (CS2), pristine starch (PS), and cinnamyl chloride (CINN-Cl) are reported in Fig. 15. The resonances of starch carbons are found in the region 94 - 105 ppm for C-1, 80-84 ppm for C-4, 68-77 ppm for C-2, C-3, C-5 and 58-65 ppm for C-6.

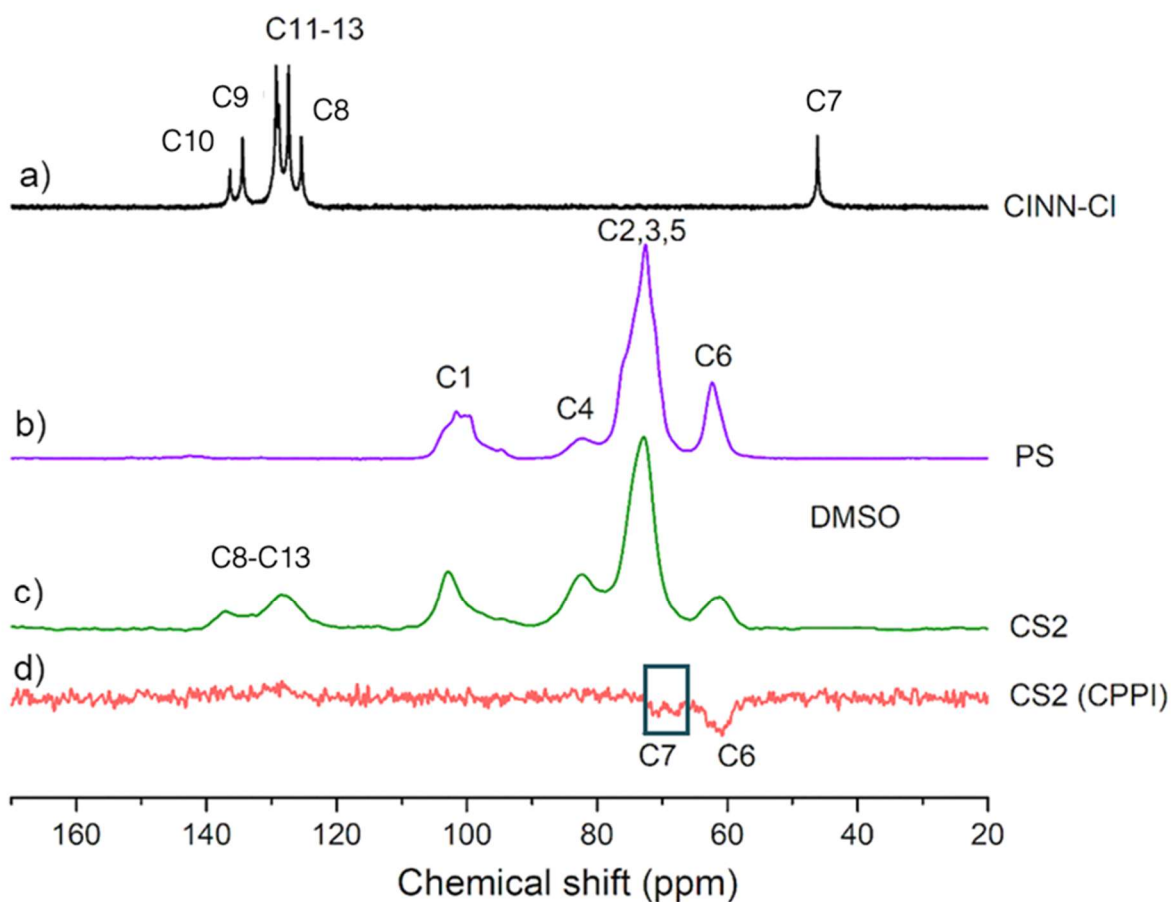


Figure 15.  $^{13}\text{C}$  CPMAS NMR of a) CINN-Cl, b) pristine yuca starch (PS), c) cinnamyl starch CS2, and d)  $^{13}\text{C}$  CPPI NMR spectra of CS2 sample (cinnamyl methylene carbons involved in the ether linkage are highlighted).

The vinyl carbons of CINN-Cl resonate at 134 and 125 ppm (C-9 and C-8, respectively, Figure 13), while the phenyl ring resonances are located in the range 125 - 130 ppm (C11-13) and 136 ppm (C10). The presence of the corresponding peaks, despite broader, in the substituted starch CS2 further confirms the presence of the cinnamyl moiety. The allylic carbon C-7 in the cinnamyl chloride resonates at 46 ppm (Fig. 15a), while it is not detected in the cinnamyl-starch samples (Fig. 15, and Fig. 14). In agreement with literature data on cinnamyl ethers (Kasashima

et al., 2010) the occurrence of the etherification reaction is expected to cause a shift of the allylic carbon C-7 to about 70 ppm, in the same spectral region of starch carbon atoms. In order to try to identify the C-7 signal and to definitely ascertain the formation of the covalent bond between starch and the cinnamyl moieties, a Cross Polarisation with Polarisation Inversion (CPPI) pulse sequence was applied to the solid-state NMR analysis of sample CS2. The parameters were optimised in order to obtain  $^{13}\text{C}$  spectra with CH<sub>2</sub> resonances as negative peaks and suppressing all the other carbons resonances (e.g.: CH<sub>3</sub>, CH and quaternary) (Wu and Zilm, 1993). The  $^{13}\text{C}$  CPPI NMR spectrum of CS2 (Figure 15d) shows three signals. The first centred at 61 ppm is due to the C-6 carbon of the glucose units. The other two located at about 68 and 71 ppm represent the cinnamyl allylic CH<sub>2</sub> involved in the ether linkages (C-7), in agreement with literature (Kasashima et al., 2010). The presence of two peaks may be due to different sites of grafting onto starch chains. Nevertheless, these signals, together with the absence of the peak at 46 ppm related to the allyl chloride, definitely prove the successful covalent grafting of cinnamyl moieties on yuca starch.

It is worth mentioning that the C-1 carbon signal is sensitive to starch crystalline conformations (Bugnotti et al., 2023). As a matter of fact, the signal shape of C-1 resonance of yuca starch is typical of crystalline starches, while the C-1 line shape of derivatized samples (CS1-3) indicates the amorphization as a result of the processing, in agreement with XRD analyses (Fig. 16). In the X-Ray (Fig.16) analysis the A-type pattern of yuca granules is shown, even though normally granules from tubers and rhizomes have B-type crystal pattern.

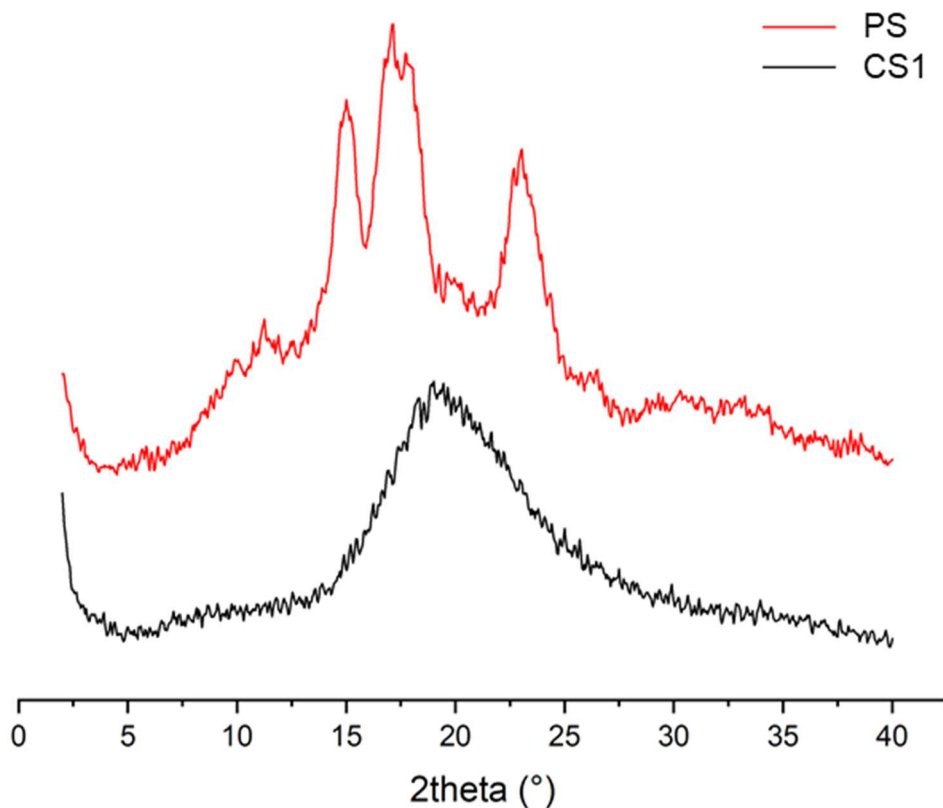


Figure 16. XRD patterns of yuca starch (PS) and functionalized starch (CS1), as representative.

Taken together, the complementary ATR-FTIR, solution and solid-state NMR spectroscopy techniques definitively confirm the covalent ether bond of yuca starch with the cinnamyl moiety. Solubility behaviour was studied on starch cinnamyl ethers CS1-3. Low substituted CS1 (DS = 0.09) resulted soluble in demineralized water. CS2 (DS = 0.33) was soluble in ethanol after a long mixing time at room temperature but not in water, whereas the CS3 derivative (DS > 1), was insoluble in polar solvents as water, ethanol and acetone both at r.t. and under reflux, while it could be dissolved in toluene at 90 °C.

The optical properties of the starch-cinnamyl derivatives were investigated (Fig. 17).

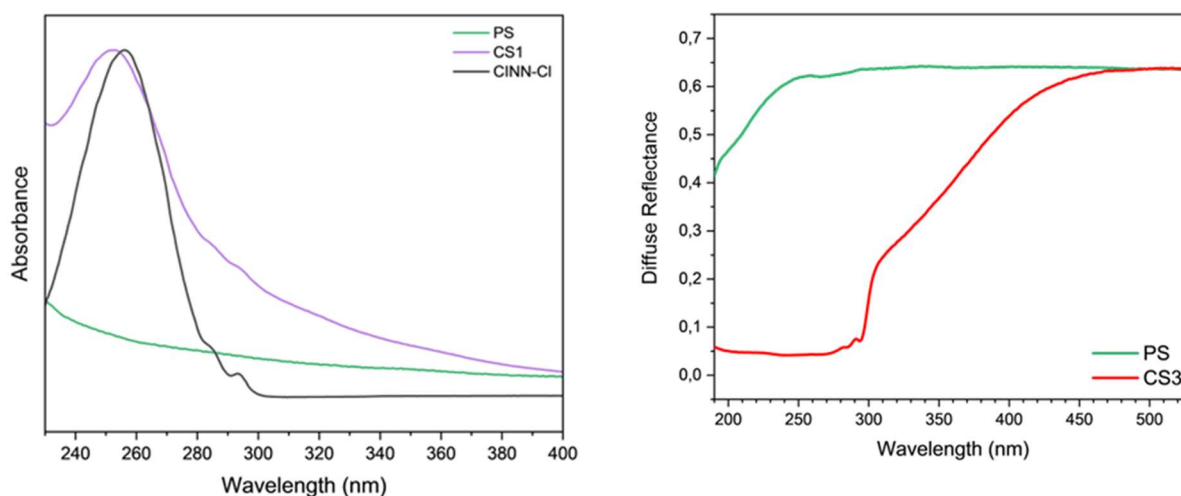


Figure 17. a) Solution-phase UV-Vis normalised spectra of native yuca starch (green line), starch cinnamyl ether (sample CS1, violet line) and CINN-Cl precursor (black line); b) UV-DRS spectra of pristine starch material (green curve) and starch cinnamyl ether with the highest DS (sample CS3, red line).

Due to solubility issues in water, the UV-Vis study was performed exclusively on the low substitution sample, namely CS1, and compared with cinnamyl chloride and pristine starch (Fig. 17a). As expected, pristine yuca starch does not display any absorption; maximum absorption of CINN-Cl and CS1 was detected at 257 and 252 nm wavelength, respectively. The low hypsochromic shift in the absorption band for cinnamyl-starch may be reasonably related to the substitution of the allyl chloride with the ethereal oxygen, further confirming the occurrence of the etherification reaction, even in the low substitute sample. The optical properties of substituted derivative CS3, resulting insoluble in water, were inspected by UV-DRS (Fig. 17b). The diffuse reflectance spectrum of the CS3 powders revealed a remarkable depletion of the reflectance intensity, that is, an increase of the absorption ability, when compared to pristine starch; the observed behaviour is as an additional evidence of the cinnamyl chromophores grafting. The thermal stability of substituted starch samples was investigated by TGA analyses and compared to pristine yuca starch (Fig. 18).



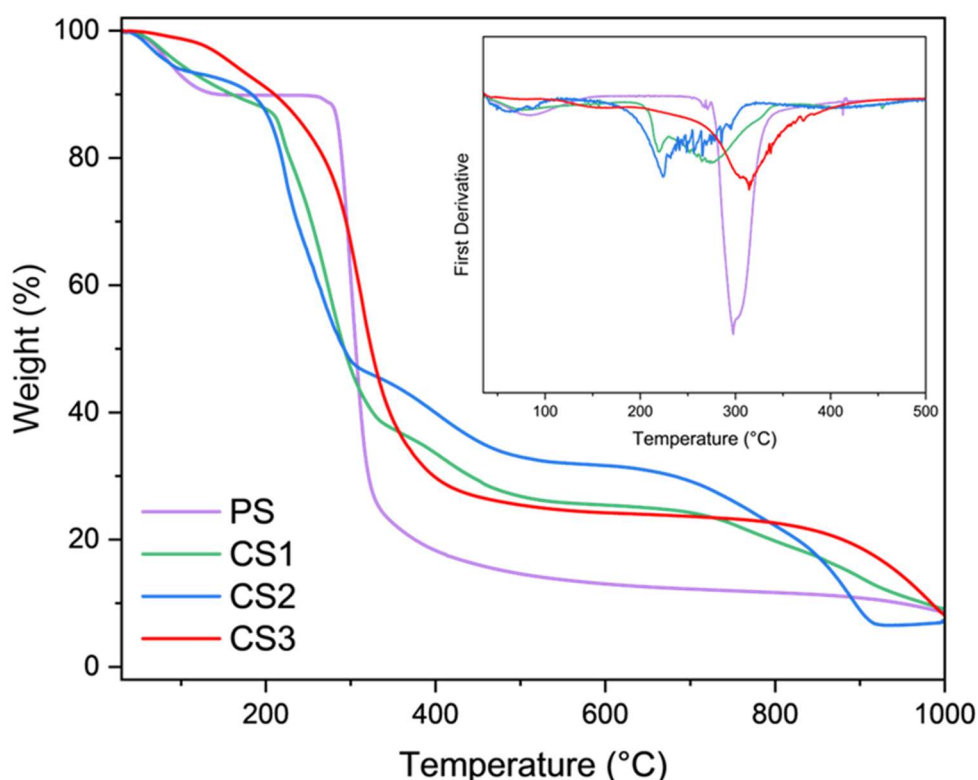
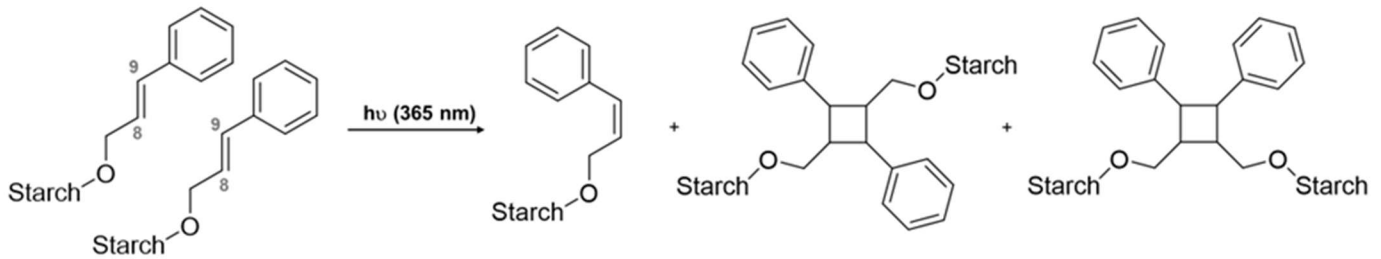


Figure 18. TGA of pristine yuca starch (PS), compared to starch cinnamyl ethers CS1 ( $DS=0.09$ ), CS2 ( $DS=0.33$ ) and CS3 ( $DS=1.24$ ).

The thermal degradation of pristine starch (PS) in a nitrogen atmosphere resulted in a two-step process, starting with a dehydration step between 35 °C and 144 °C corresponding to a weight loss of about 10 %, followed by the decomposition of the polysaccharide initiating at 270 °C with a maximum weight loss at 297 °C. In the case of starch ethers, a multi-step decomposition was observed and these thermograms can be explained as a combination of non-functionalized and functionalized fractions of the polymer (Tester et al., 2004b). As long as the substitution degree increases (i.e. CS3 sample), a single step profile is detected as well as a slight enhancement of the thermal stability (Fig. 18, inset).

### 3.3.6 Starch Cinnamyl Ether photodimerization

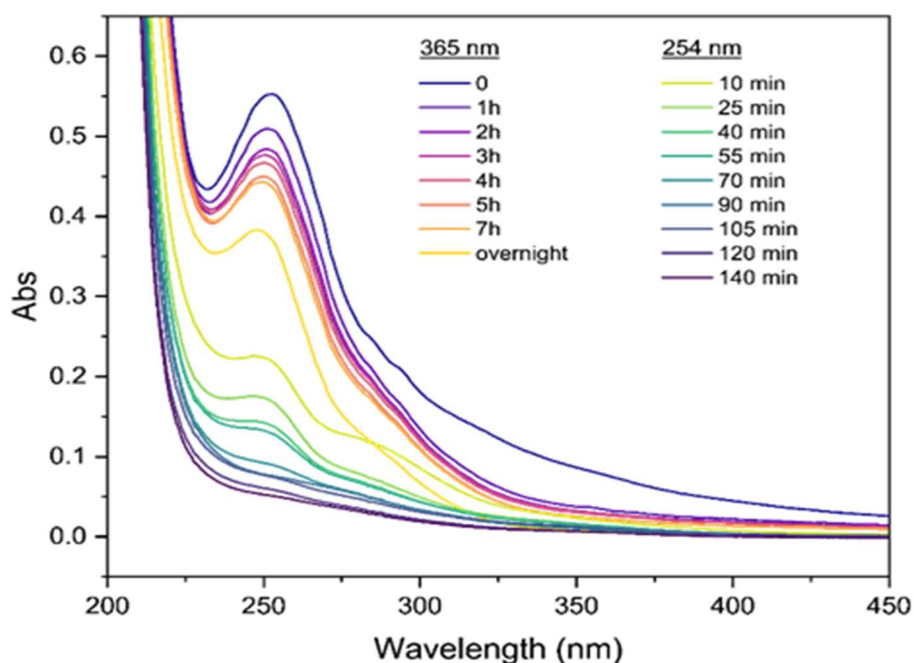
The starch-cinnamyl ethers were submitted to photoinduced dimerization by exposure at 365 nm (Scheme 7).



*Scheme 7. Photoinduced reaction of cinnamyl-starch derivatives.*

The evaluation of the absorbance in the UV range is a commonly used method to monitor cycloaddition reactions in cinnamyl derivatives. Thus, a proof of concept of the photo-cross-linking ability of the cinnamyl-substituted starch was pursued by evaluating the changes in the UV-Vis spectra after irradiation at  $\lambda \sim 365$  nm and, subsequently, at  $\lambda = 254$  nm (Fig. 17). The wavelength selection was based on the UV-Vis spectrum, showing a maximum absorption at  $\sim 250$  nm, featured with an extended tail terminating at  $\sim 370$  nm. The study was performed exclusively on the low substitution sample, namely CS1: as previously reported, CS1 was soluble in water.

**a**



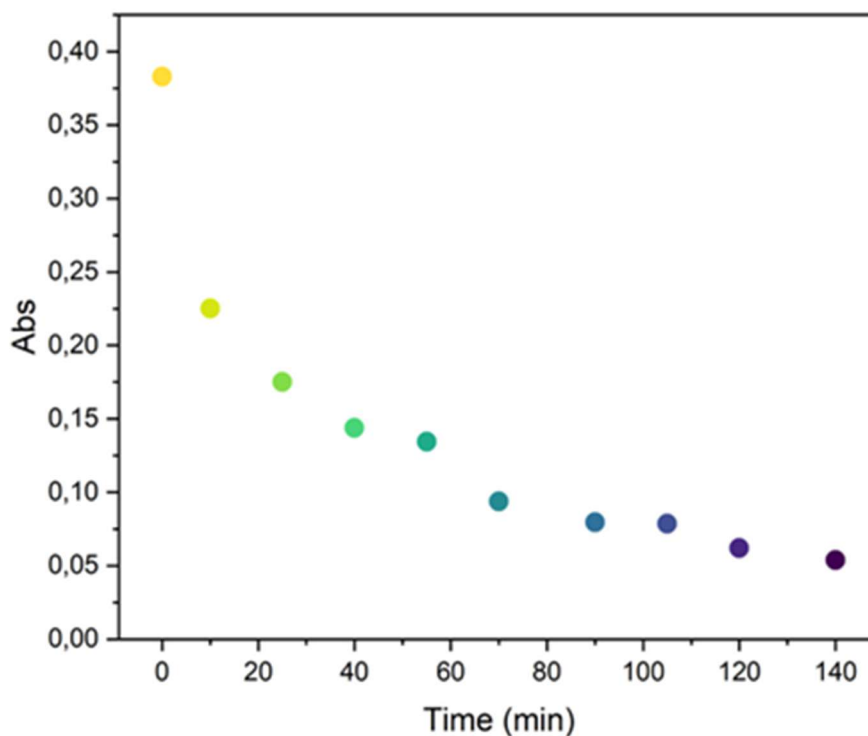
**b**

Figure 19 a) UV-Vis spectra of CS1 sample after exposure at  $\lambda \sim 365$  nm and, subsequently, at  $\lambda = 254$  nm; b) maximum absorption plotted against UV irradiation time at  $\lambda = 254$  nm.

A progressive decrease of the absorption band at  $\sim 250$  nm was detected, especially upon irradiation at  $\lambda = 254$  nm; this observation can be ascribed to the double bonds conversion into the saturated cyclobutane ring, thus losing the p-conjugation with the benzene ring (Fig. 19a) (Egerton et al., 1981b). The variation of the maximum absorbance ( $\sim 250$  nm) plotted against the irradiation time (Figure 19b), showed an exponential decay until a plateau was reached at 140 min of irradiation. These preliminary results confirm that, in aqueous solution, the cinnamyl-functionalized starch can undergo photodimerization in the liquid state.

The photodimerization of starch ether derivatives was further studied through  $^1\text{H-NMR}$  analysis and HSQC Fig. 20 and Fig. 21 respectively; the CS2 sample was dissolved in  $\text{DMSO-}d_6$  and irradiated at  $\lambda \sim 365$  nm for 24 h. The cyclobutane signals, resonating between 3 ppm and 4.5 ppm, are usually considered a proof of the photodimerization reaction (Adams et al., 2014) (Amjaour et al., 2019) (Fonseca et al., 2008). However, these diagnostic peaks are expected in the crowded region of the starch signals. Upon UV exposure, NMR spectra showed changes in

the aromatic and vinyl signals (shaded areas) and new peaks (\*) at ~ 5.9 and ~ 6.9 ppm (Fig. 20). The new signals at ~ 5.9 and ~ 6.9 ppm can be ascribed to H-8 and H-9 in a Z configuration, as a result of a photoinduced isomerization. Indeed, in the Z configuration, vinyl hydrogens resonate slightly more upfield. Even so, the decrease of the integral value of vinyl protons in respect to the aromatic H11-H13 may suggest a partial photodimerization. This observation is an interesting hint deserving further investigation.

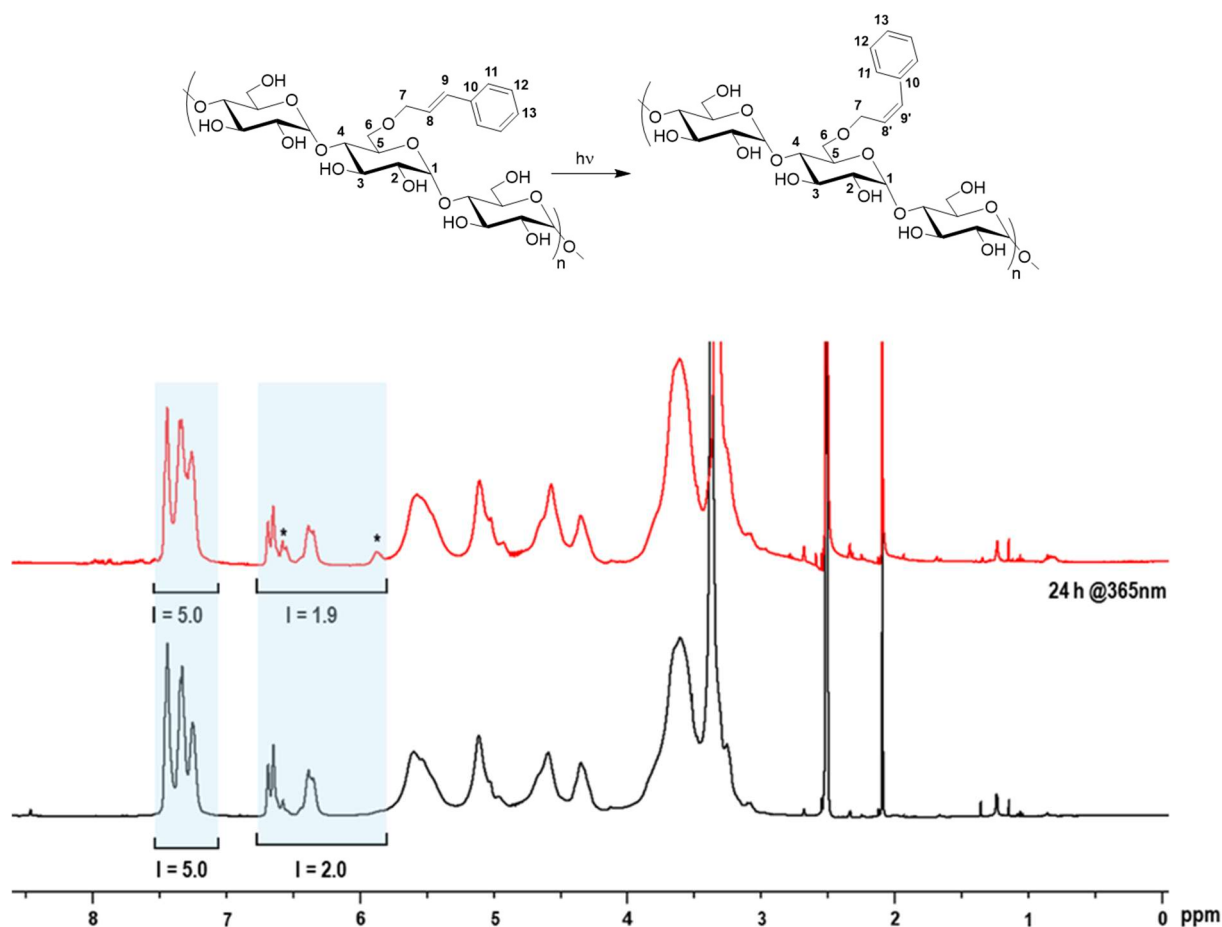


Figure 20.  $^1\text{H-NMR}$  spectra of the  $\text{CS}_2$  starch ether in  $\text{DMSO-d}_6$  before (solid black) and after 24 h UV exposure at  $\lambda \sim 365 \text{ nm}$  (solid red). Shaded areas highlight changes in the spectra and \* indicates new peak; relevant integrals are indicated (I).

$^1\text{H-NMR}$  (solid black) [ $\text{DMSO-d}_6$ ]:  $\delta$  (ppm) = 8.46 (s, H aldehyde hydrogen (Ziegler-Borowska et al. 2018)), 7.44-7.25 (m, H-11, 12, 13), 6.64 (m, H-9 vinyl trans), 6.38 (bs, H-8 vinyl trans), 5.60 (bs, -OH 3), 5.52 (bs, -OH 2), 5.10 (bs, H-1  $\alpha$ -1,4), 4.9 (bs, H-1  $\alpha$ -1,4 reducing end), 4.59

(bs, -OH 6), 4.35 (bs, H-7), 4.26 (d), 3.61 (bm, H-3, 5, 6, 6'), 3.33 (water), 3.0 (m, H-4 end group). Sample name: SF2-F-15UV.

$^1\text{H-NMR}$  (solid red) [ $\text{DMSO-d}_6$ ]:  $\delta$  (ppm) = 8.46 (s, H aldehyde hydrogen), 7.44-7.25 (m, H-11, 12, 13), 6.64 (m, H-9 vinylic proton trans), 6.57 (m, H-9' vinylic proton cis), 6.38 (bs, H-8 vinylic proton trans), 5.87 (m, H-8' vinylic proton cis), 5.60 (bs, -OH 3), 5.52 (bs, -OH 2), 5.10 (bs, H-1  $\alpha$ -1,4), 4.9 (bs, H-1  $\alpha$ -1,4 reducing end), 4.59 (bs, -OH 6), 4.35 (bs, H-7), 4.26 (d), 3.61 (bm, H-3, 5, 6, 6'), 3.33 (water), 3.0 (m, H-4 end group).

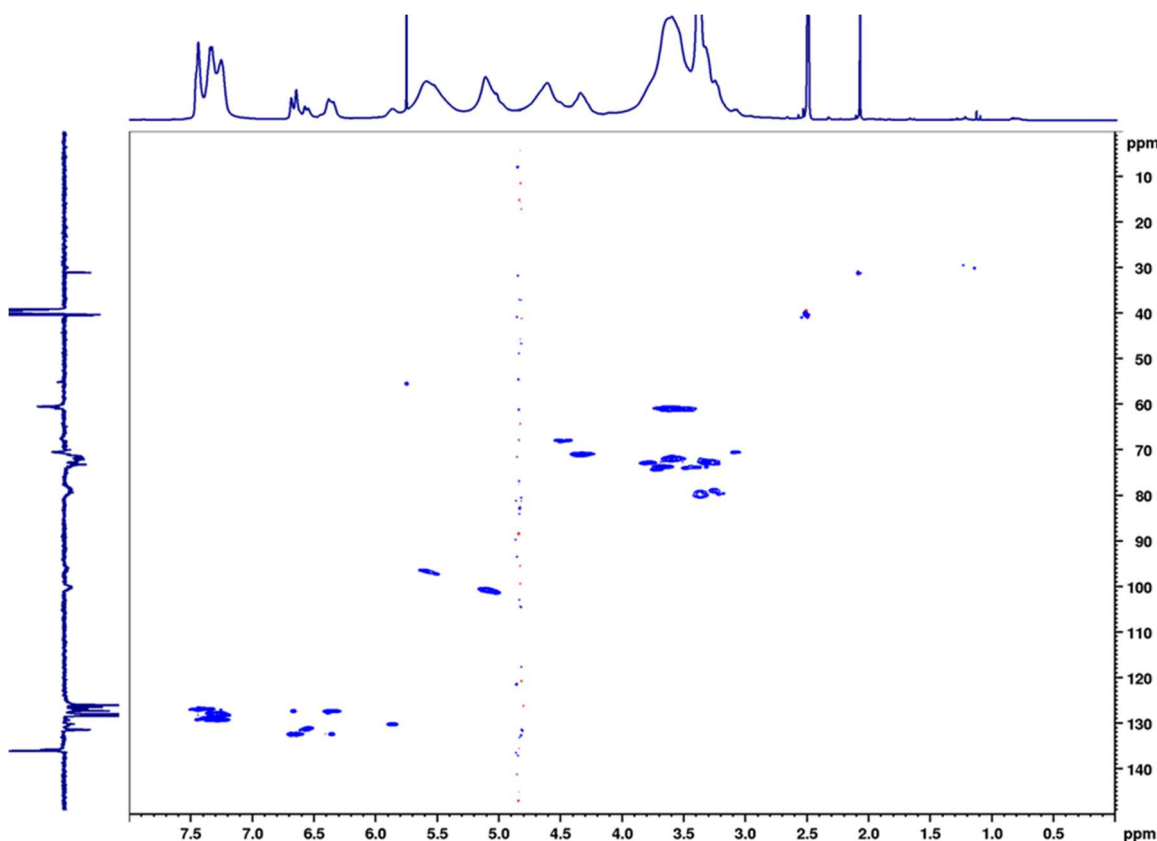


Figure 21.  $^1\text{H-}^{13}\text{C}$  HSQC spectrum of  $\text{CS}_2$  dissolved in  $\text{DMSO-d}_6$  after irradiation at 365 nm.

Taken together, these observations indicate that, under the used experimental conditions, a competition between the two processes occurs, as widely reported for cinnamyl derivatives in several literature studies (Egerton et al., 1981a) (“1963 - Topochemistry - The photochemistry of trans-cinnamic acid”).

In summary, UV-Vis and NMR investigations support a partial but successful cross-linking reaction through the [2+2] cycloaddition of the double bonds of the starch cinnamyl units.

### 3.3.4 Cinnamyl Starch thermoresponsive film

Owing to provide a proof of concept of the potential applicability of the novel bio-based bio-inspired polymer, films were produced by the solvent-casting technique. CS1 derivatives were used, due to their water solubility (a biocompatible solvent).

The obtained film appears homogeneous and transparent (Fig. 22a). The observation of the films under a TLC UV lamp at  $\lambda = 254$  nm or  $\sim 365$  nm shows emission in the Vis range as a qualitative confirmation of the surface exposure of the cinnamyl chromophoric units (Figure 22b and c). Control films made by pristine starch are used as control (Figure 22d-f).

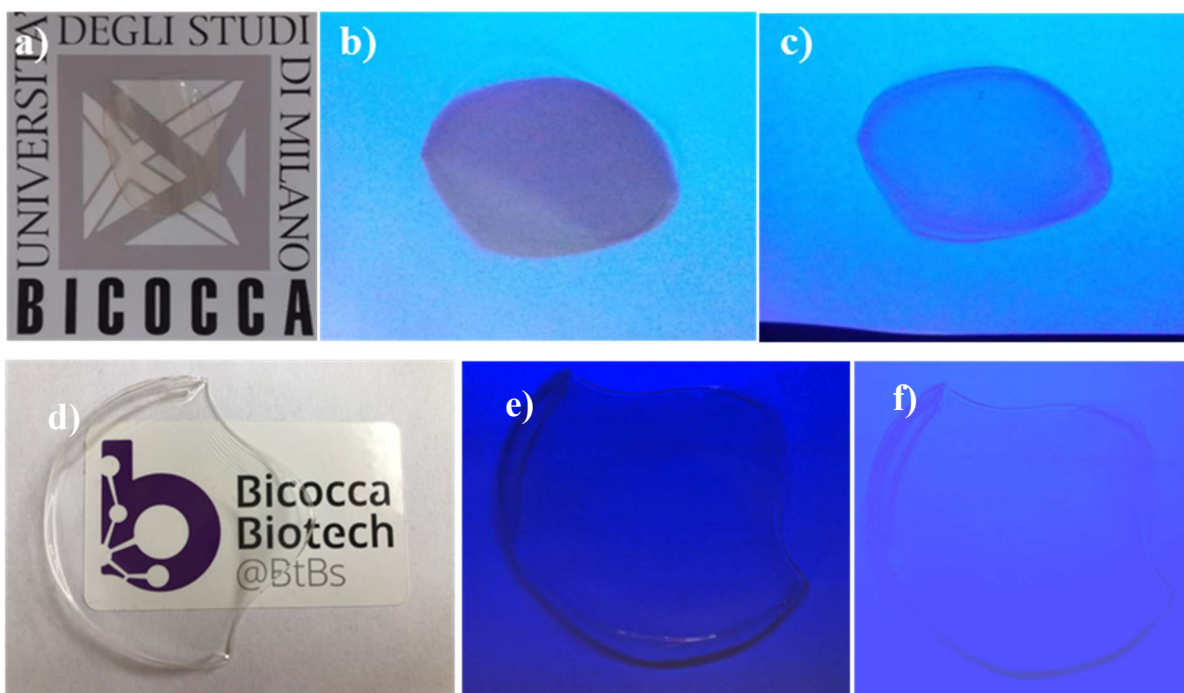


Figure 22. a) drop-casted film of cinnamyl ether CS1; film under UV lamp at b) 254 nm and c) at 365 nm wavelengths; d) drop-casted film of pristine starch; film under UV lamp at e) 254 nm and f) at 365 nm wavelengths.

Even though the crosslinking was a minor photo-reaction; the films of starch ether, produced by drop casting, showed the reversible ability to deform when touched by hand Fig. 23.

This interesting property deserves to be further investigated. In literature similar phenomena are observed for the hydrogels where the random presence of apolar groups create a discontinuity in polymer assembly and determine a volume transition at temperatures in the range of the human body 40-35°C.

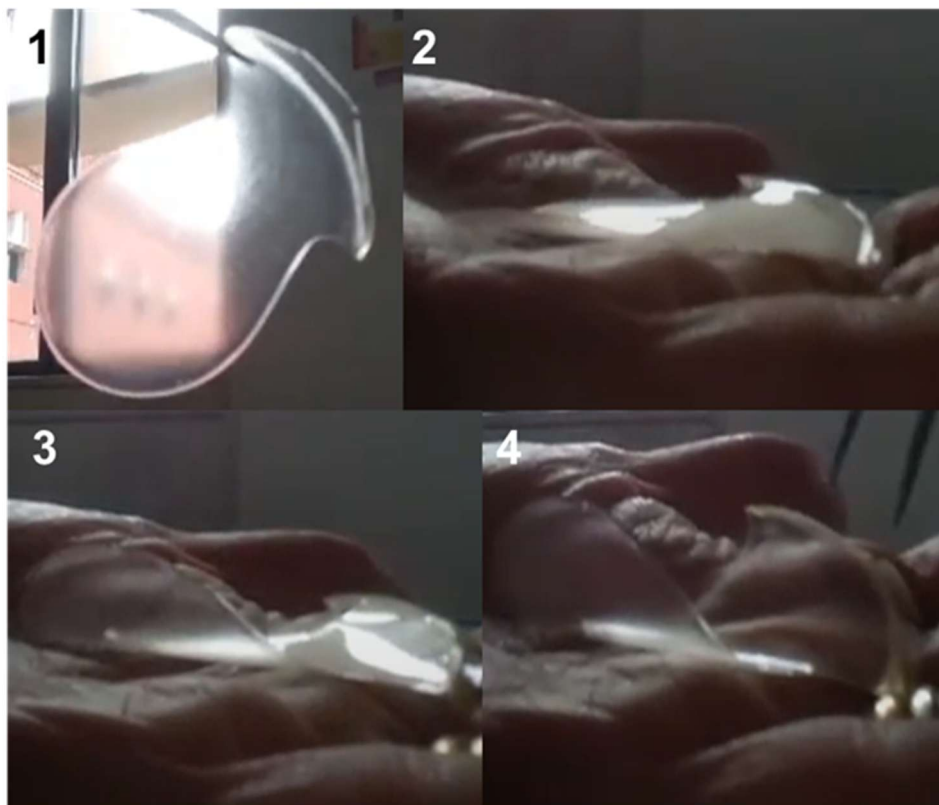


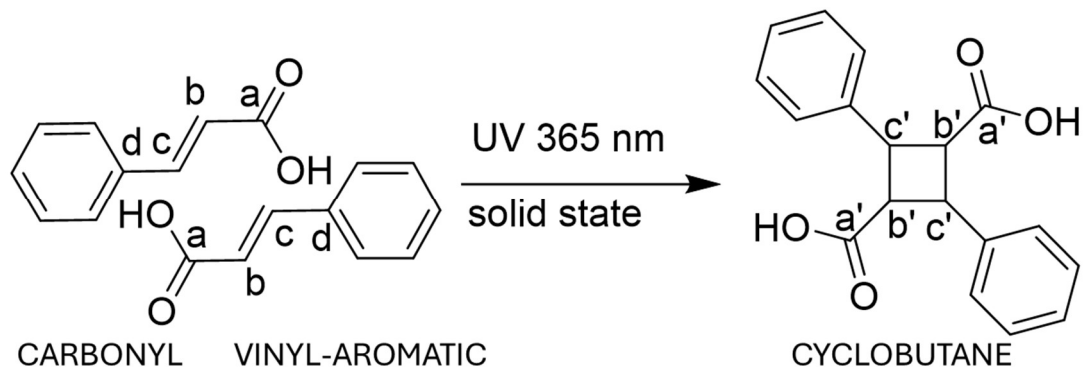
Figure 23. Frames of a video on the starch ether film deformation upon hand touch.

### 3.3.5 Starch Cinnamoyl Ester characterization and photodimerization

The study of the starch cinnamyl ethers photodimerization provided more insight on the characterization of photochemical reactions of the biopolymer and it motivated the in-depth analysis of starch cinnamoyl ester to better understand the drivers of photodimerization.

At first, the photodimerization of cinnamic acid as a model molecule was studied through  $^1\text{H}$ -NMR and  $^{13}\text{C}$  CPMAS NMR (Bertmer et al., 2006). The sample was irradiated with a UV lamp at 365 nm, 28-32  $\text{W}/\text{m}^2$  for 5 h and 16 h (Scheme 8). The so obtained powders were collected and characterised through solution and solid-state NMR and FTIR (ATR) spectroscopies.





Scheme 8. Photoinduced reaction of cinnamic acid in solid state.

The  $^{13}\text{C}$  CPMAS NMR spectra of cinnamic acid before (0 h) and after (5h and 16 h) the UV irradiation, together with carbon labelling and a sketch of the photo-reaction.

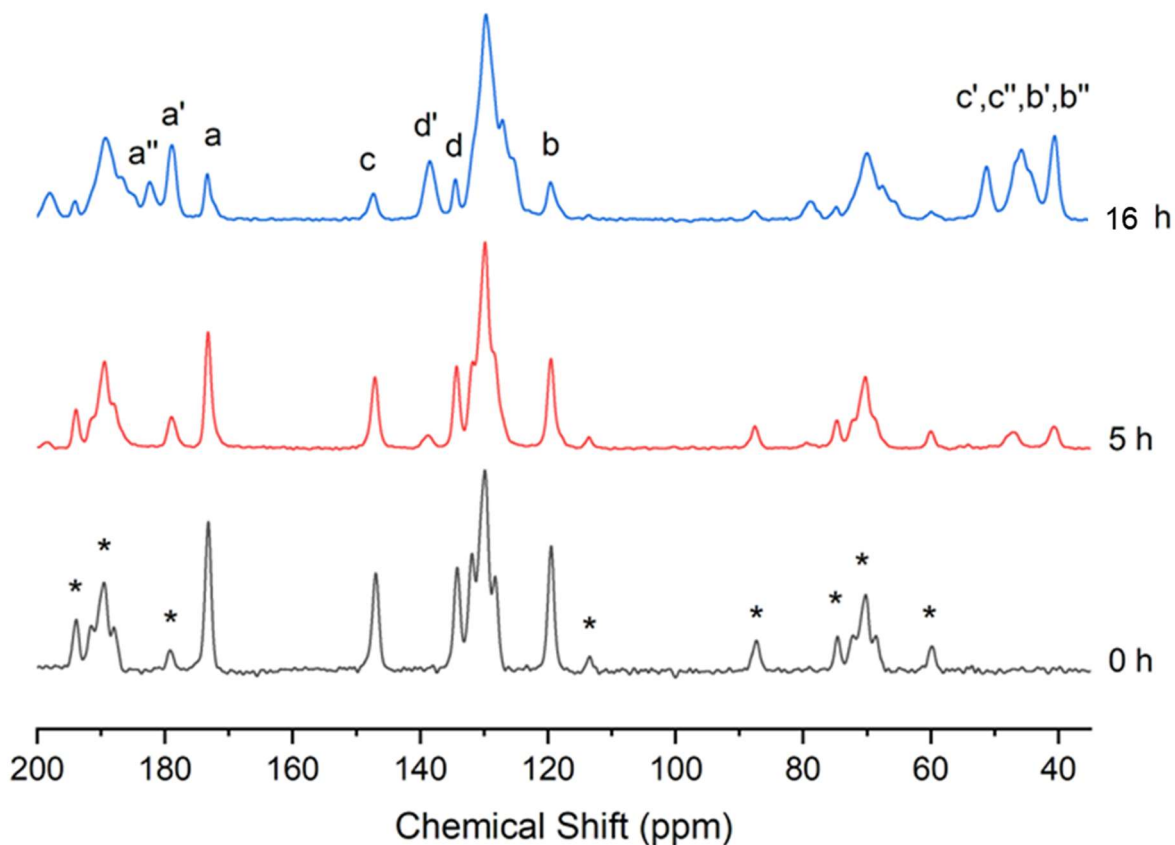


Figure 24.  $^{13}\text{C}$  CPMAS NMR spectra of cinnamic acid before and after UV irradiation at different times. \*=spinning sidebands, marked in the bottom spectrum only.

After 5 hours of irradiation the [2+2] cycloaddition reaction started, as shown by the butane ring carbons resonances at 47 and 41 ppm ( $c',b'$ ) and the carbonyl new signal ( $a'$ ) at 179 ppm

(Fonseca et al., 2008). In addition, the carbon atom in position d felt the effect of the cycloaddition giving rise to a new signal downfield shifted to 138 ppm (d'). These features are correlated with a decreased intensity of the vinyl peaks (b, c) at 147 and 119 ppm, and a broadening of the aromatic band (133-125 ppm), as expected. After 16 hours the decreased intensity of vinyl peaks was much more evident, together with the growth of the butane ring resonances. Among them new signals at 51 and 45 ppm appeared (c'', b''). Similar situation in the carbonyl region where a new carbonyl peak at 182 ppm (a'') is visible and the a peak reduces. Splitting signals of butane ring and carbonyl peaks can be explained by the nonsymmetric position of carbon atoms (due to distortions, phenyl twist ecc) as discussed in literature (Fonseca et al., 2012). In particular, the different conformations of  $\alpha$  and  $\beta$  cinnamic acid can give two different molecules after the photoreaction, namely  $\alpha$ -truxillic acid and  $\beta$ -truxinic acid, as reported in Fig. 25.

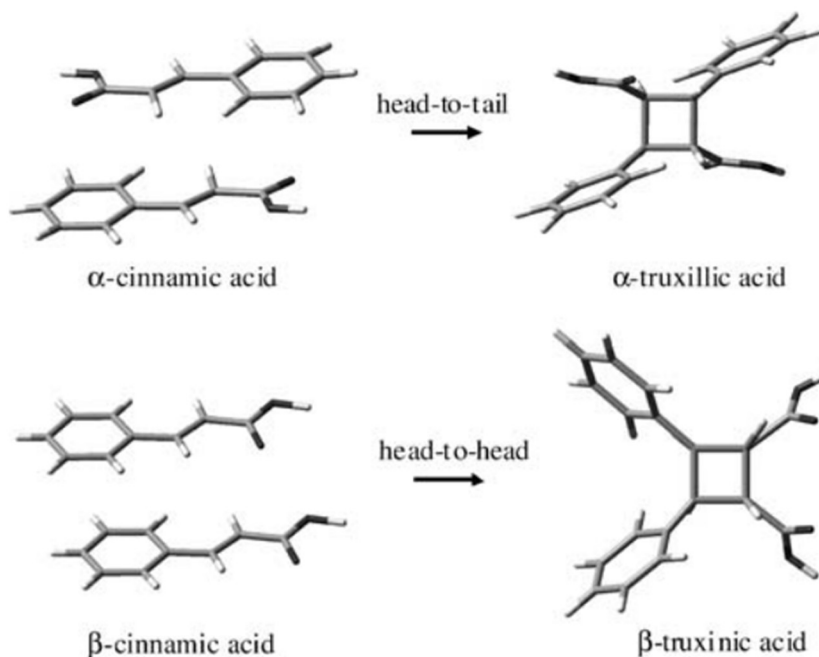


Figure 25. Suprafacial approaching of two molecules of cinnamic acid head to tail (top) head to head (bottom) (Fonseca et al. 2008).

After 5h of irradiation, two peaks in the butane ring region are present. This might suggest the formation of  $\beta$ -truxinic acid, as it is reported to show peaks at 41, 45 and 47 ppm (in present case the 45 and 47 ppm peaks could be merged together). With the increasing of the irradiation time, it seems to form  $\alpha$ -truxillic acid, due to the four resonances in the butane ring region. This could

be explained by the thermal conversion of beta to alpha cinnamic acid. The study shows a total conversion at about 77°C (Fonseca et al., 2008). The evolution of vibrations due to carbonyl group at 1670  $\text{cm}^{-1}$  and vinyl group at 1626  $\text{cm}^{-1}$  were followed during the photo-reaction in the FTIR ATR spectra of the samples. As shown in Fig. 26, the shifting of carbonyl peak to 1683  $\text{cm}^{-1}$  and the reduction in intensity of the vinyl signal (with respect to C=O intensity) are in agreement with the occurrence of the cycloaddition. For sake of clarity, the enlarged view of overlapped spectra is shown in Figure 27.

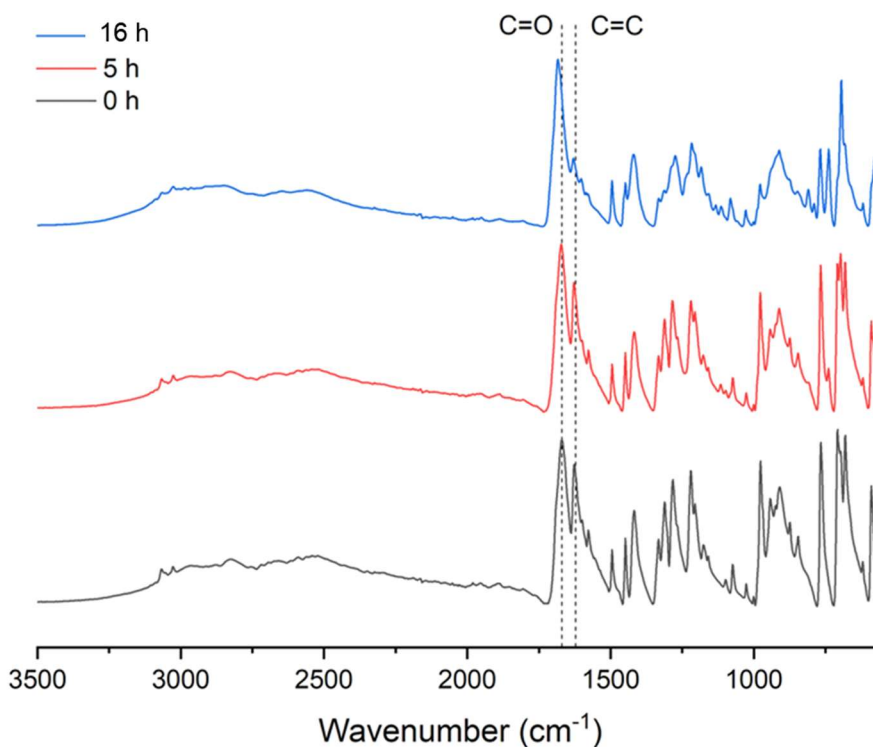


Figure 26. FTIR-ATR spectra of cinnamic acid irradiated at different time points.

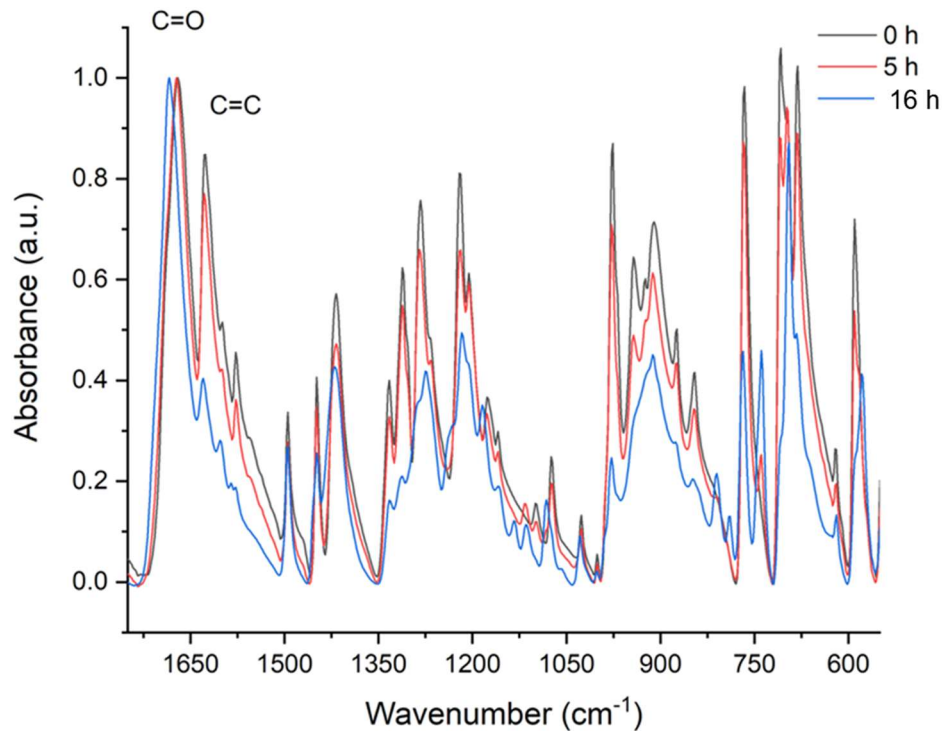


Figure 27. Enlarged view of the overlapped FTIR-ATR spectra of cinnamic acid samples.

In Fig. 28 the  $^1\text{H-NMR}$  of  $\alpha$ -trans cinnamic acid (black) and the same after UV exposure (red) @365 nm for 16h (Scheme 8) shows a reduction of the vinyl protons integrals (7.59 ppm and 6.53 ppm) and the occurrence of cyclobutane's protons at 4.3 ppm and 3.8 ppm; moreover, a shift to upfield of the aromatic protons due to the loss of the double bond is observed (Amjaour et al., 2019).

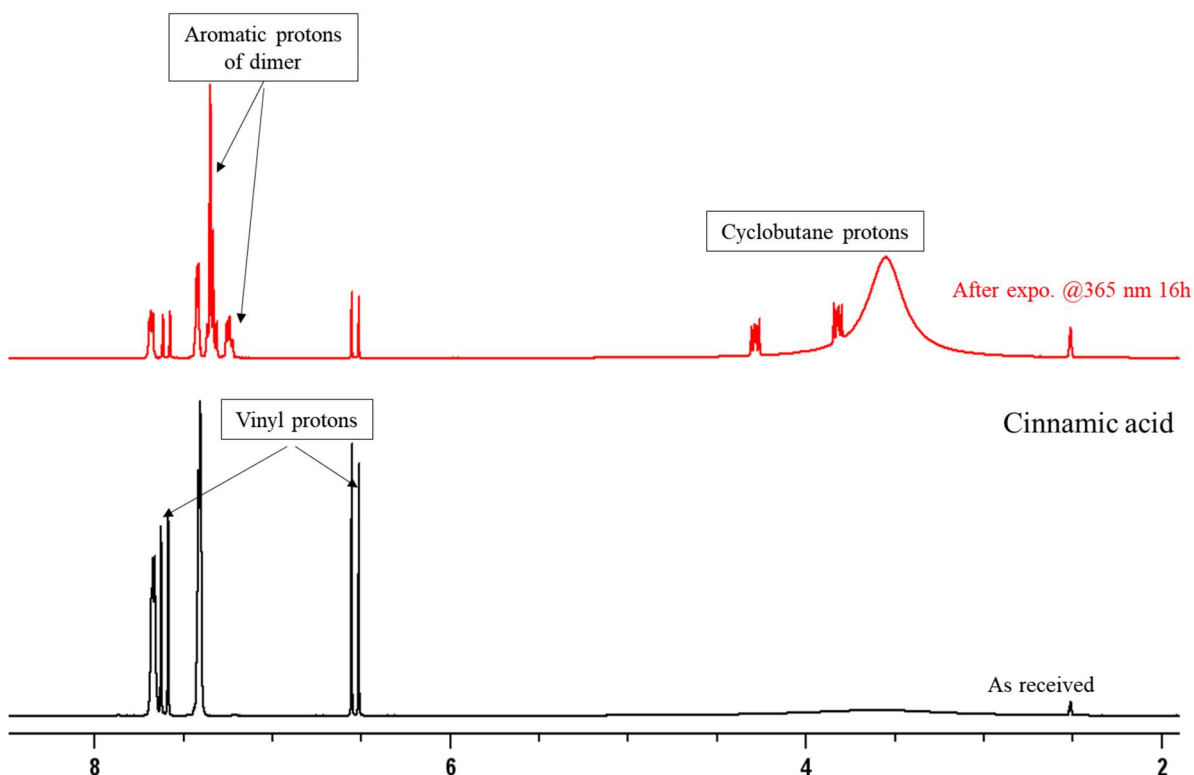
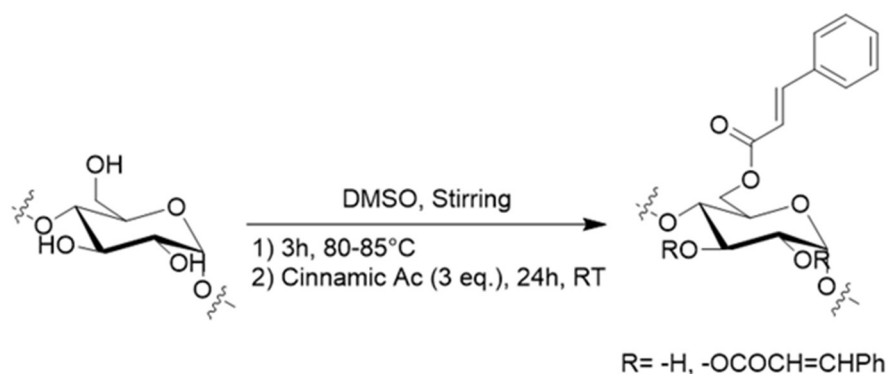


Figure 28.  $^1\text{H-NMR}$  in  $\text{DMSO-d}_6$  of cinnamic acid (black) and the same after UV exposure (red) on solid @365 nm for 16 h.

Starch esters obtained through an autocatalytic Fisher esterification (Scheme 9) were then submitted to photodimerization.



Scheme 9 Fisher esterification with cinnamic acid.

By comparing  $^1\text{H-NMR}$  spectra of cinnamic acid dimers (Fig. 28) with cinnamoyl starch esters (Fig. 29) it is possible to observe a similar shift of aromatic signals after UV exposure in solid state @365 nm for 8 hours (Fig. 29B) even at a DS = 0.01, while the signals of cyclobutane protons are not detected because they occur in the sugar region.

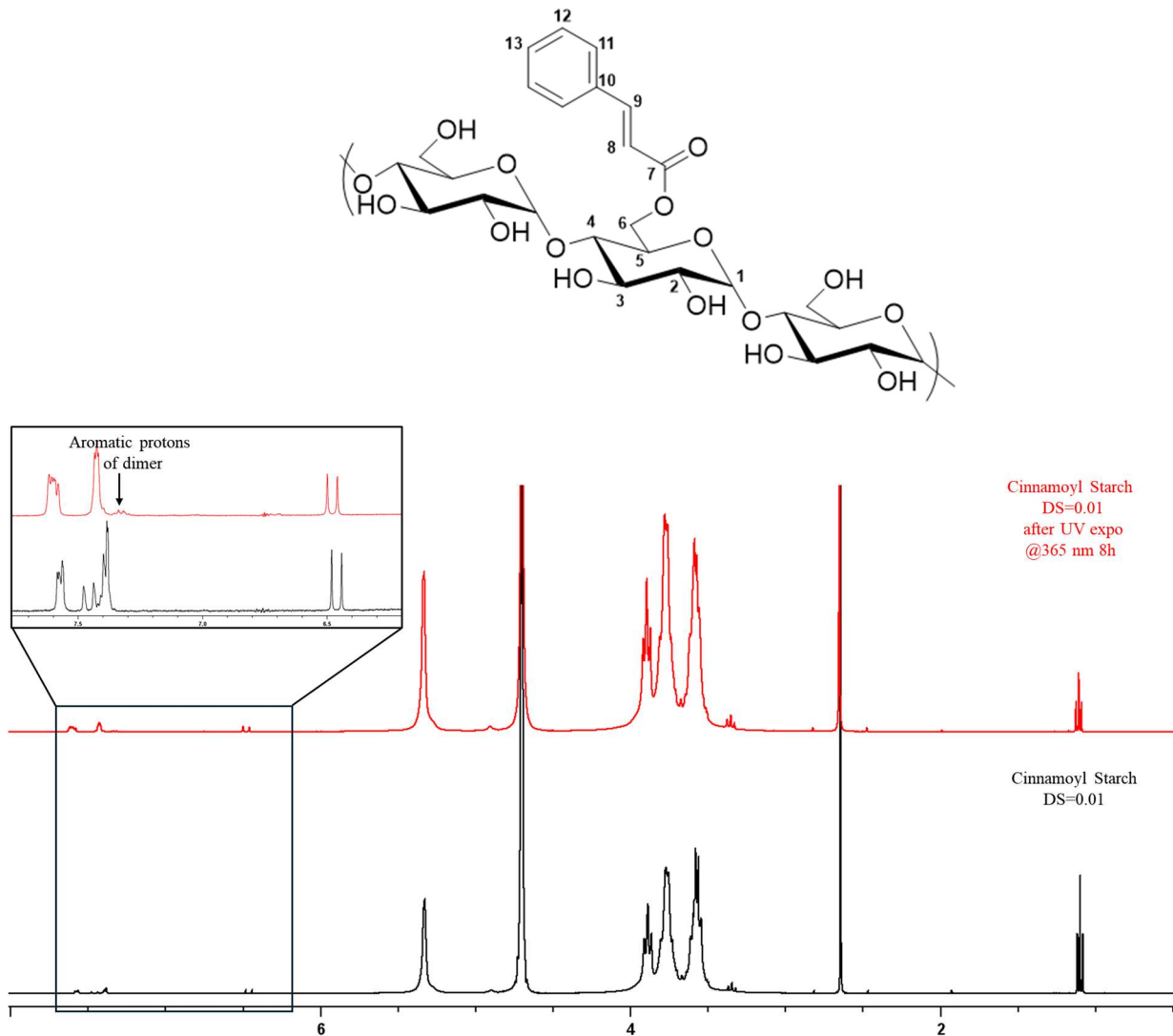


Figure 29.  $^1\text{H-NMR}$  in  $\text{D}_2\text{O}$  of starch cinnamoyl ester (black) and the same after UV exposure (red) on solid @365 nm for 8 h.

$^1\text{H-NMR}$  (solid black) [ $\text{D}_2\text{O}$ ]:  $\delta$  (ppm) = 8.35 (s, aldehydic proton), 7.58-7.56 (m, 2 H, H-11, 11' substituent), 7.46 (d, 1 H,  $J=16.08$  Hz, H-9), 7.40-7.38 (m, 3 H, H-12, 12' H-13 substituent), 6.46 (d, 1 H,  $J=16.02$  Hz, H-8), 5.33 (bs, H-1  $\alpha$ -1,4), 4.73 (water), 3.89 (t, H-3), 3.80-3.73 (m, H-6, 6', H-5), 3.63-3.49 (m, H-4, H-2), 3.34 (t, H-4 end group), 2.64 (s, Acetone), 1.09 (t, EtOH) (Ishizuca et al. 2004). Sample name: SPC-80-123.

$^1\text{H-NMR}$  (solid red) [ $\text{D}_2\text{O}$ ]:  $\delta$  (ppm) = 8.31 (s, aldehydic proton), 7.61-7.58 (m), 7.43 (t, H-Aromatic substituent), 7.39-7.29 (m, H-Aromatic dimer), 6.48 (d, 1 H,  $J=16.08$  Hz, H-8), 6.00 (d,  $J=12.52$  Hz, H-8'), 5.33 (bs, H-1  $\alpha$ -1,4), 4.73 (water), 3.89 (t, H-3), 3.81-3.74 (m, H-6, 6',

H-5), 3.61-3.50 (m, H-4, H-2), 3.34 (t, H-4 end group), 2.64 (s, Acetone ), 1.09 (t, EtOH )  
(Ishizuca et al. 2004). Sample name: SPC-80-124-365-8-S.

The occurrence of photodimerization in esters, even at low DS, could be ascribed to the extended conjugation system of the cinnamoyl moiety with the carbonyl group; these boundary conditions are not fulfilled in the starch cinnamyl ether.



## 4. CELLULOSE

### 4.1 Cellulose: Literature Review

As the most abundant biopolymer of the biosphere, cellulose is the fundamental component of a plant's skeleton; it is ubiquitous and inexhaustible; it is formed by the repeated D-glucose building block forms organised in stiff-chain. This biopolymer has interesting properties such as hydrophilicity, chirality, biodegradability and high density of functional groups. Due to these numerous properties, interest in this biopolymer across various disciplines is growing, and advancements in understanding its structure, reactivity, and applications have received significant attention in recent decades (Klemm et al., 2005).

In 1838 the French chemist Anselme Payen noticed a fibrous residue obtained from wood after treatment with acids and ammonia, and after extraction, by elemental analysis he determined the molecular formula  $C_6H_{10}O_5$  finding the isomerism with starch. In 1839 the French academy used for the first time the term cellulose in reference to Payen's work (Brogniart et al., 1839). However the polymer was already in use from thousands of years before the Payen discovery for building materials, clothings and heritage transmission, just think of the egyptian papyri importante for human history.

An interesting example of cellulose chemical modification as raw material for important goods is the reaction with nitric acid to produce the so called "celluloid" a thermoplastic material with chanfor as plasticizer by Hyatt Manufacturing for movies market. Hyatt Manufacturing demonstrated that materials derived from cellulose could be produced on an industrial large scale ("Celluloid Manufacturing Co. - Syracuse University Libraries Digital Collections," n.d.).

Cellulose represents  $1.5 \times 10^{12}$  tons of the biomass produced annually, it is considered an inexhaustible source of raw material for feeding the urgent demand of environment friendly and biocompatible goods. Wood pulp is the primary source for the production of cellulose which is mostly used in the market of paper and cardboard (Gilbert and Kadla, 1998).

The hierarchical architecture of cellulose is created by a network of hydrogen bonds among hydroxyl groups; it has been a research item for over a century. The advancements in understanding cellulose's structure are correlated with the evolution of analytical techniques, such as X-ray diffraction, electron microscopy, high-resolution  $^{13}C$  solid-state NMR spectroscopy, and neutron diffraction. The knowledge of cellulose's various structural levels is

important for the synthetic reactions and the tailored formation and characteristics of cellulose-based products.

As shown in Fig. 30, the hydroxyl groups of  $\beta$ -1,4-glucan cellulose are located at C2, C3 (secondary, equatorial), and C6 (primary) positions. Cellulose's supramolecular structure results in a solid state that exhibits both high-order (crystalline) and low-order (amorphous) regions.

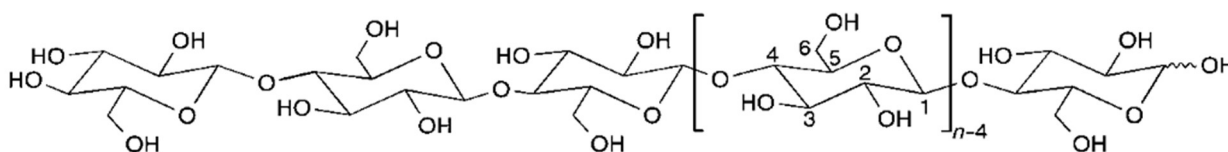


Figure 30. Molecular structure of cellulose (Klemm et al. 2005).

Initially, the crystal structure of native cellulose (cellulose I), as revealed by X-ray diffraction, can be approximated as a monoclinic unit cell (space group  $P2_1$ ) containing two cellulose chains arranged parallel with a twofold screw axis. In the 1980s,  $^{13}\text{C}$ -CP/MAS NMR spectroscopy led to the identification of two distinct crystalline forms of cellulose I ( $I_\alpha$  and  $I_\beta$ ), which coexist in varying ratios depending on the cellulose source (Atalla and VanderHart, 1984). Recent studies using electron microbeam diffraction and combined X-ray and neutron diffraction have identified the crystalline structures as having triclinic ( $I_\alpha$ ) and monoclinic ( $I_\beta$ ) unit cells (Zugenmaier, 2001). Figure 31 presents a schematic of the  $I_\beta$  crystal structure. The side view of the unit cell's central chains reveals two intramolecular, chain-stiffening hydrogen bonds. Recent findings on the  $I_\beta$  structure highlight variations in neighboring chain conformations and hydrogen bonding systems within adjacent molecular layers.

Besides the less stable cellulose I, other crystalline forms of cellulose (cellulose II, III, and IV) exist, with cellulose II being the most relevant for industrial applications. This structure can be generated from cellulose I through treatment with aqueous sodium hydroxide (mercerization) or by dissolving cellulose followed by precipitation/regeneration, as seen in fiber and film production. The monoclinic crystal structure of cellulose II shows two antiparallel chains per unit cell and is characterised by specific unit cell geometry and a modified hydrogen bonding system. The alkalization process is crucial for large-scale cellulose production, enhancing the reactivity of subsequent reactions and facilitating the mercerization of cotton. Depending on the concentration of lye, temperature, and mechanical force, cellulose I can be transformed into various alkali crystalline forms, each exhibiting different crystal structures and varying NaOH

and water contents. All forms will ultimately convert to crystalline “hydrated cellulose” during washing and to cellulose II upon drying. The mechanism by which the parallel chain arrangement of cellulose I turns to the antiparallel configuration of cellulose II, without an intermediate dispersion of cellulose molecules, remains unclear. Research on the structure of noncrystalline random cellulose chain segments is still limited, despite their significant impact on cellulose accessibility and reactivity, as well as the properties of synthetic cellulose fibers.

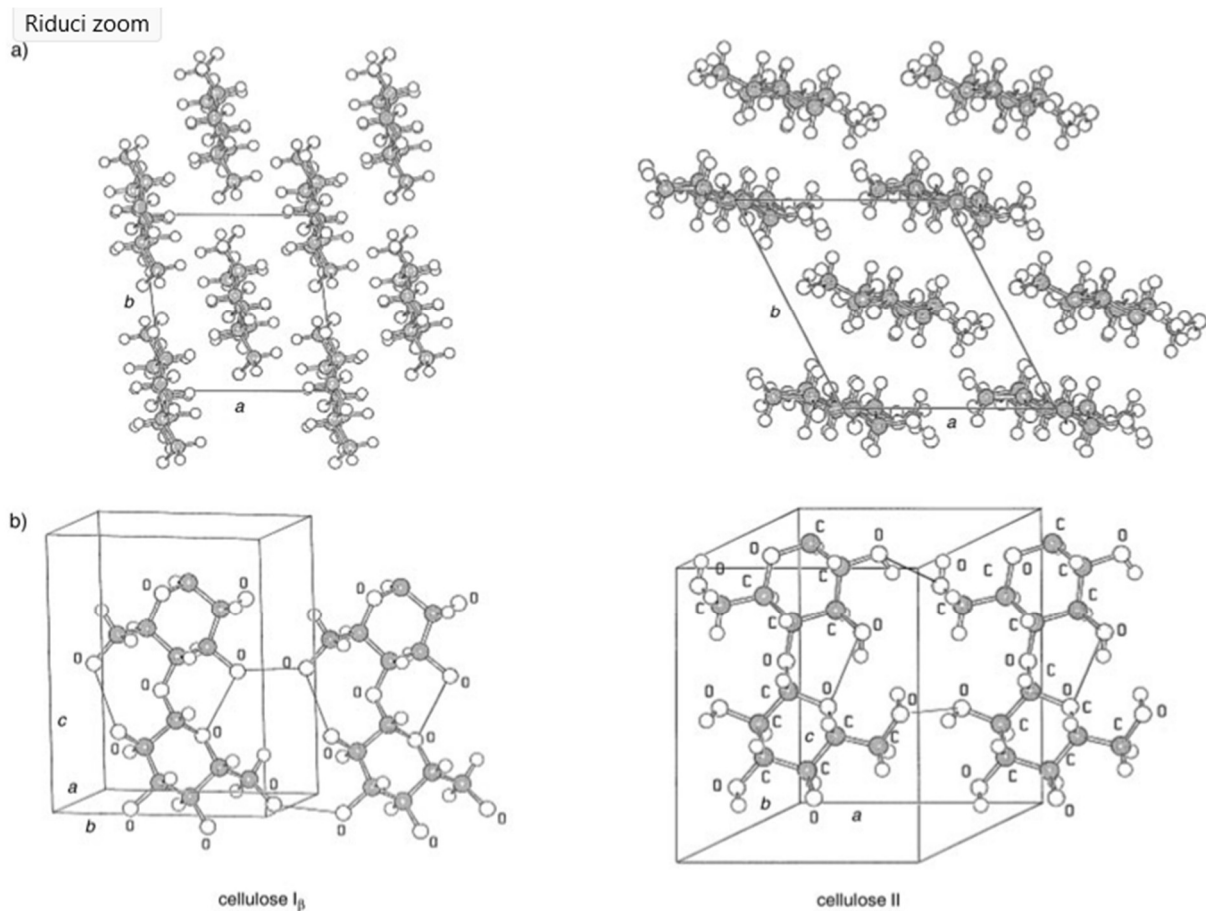


Figure 31. Crystal structure of cellulose I and II (Klemm et al. 2005).

Cellulose’s biological function and diverse applications are rooted in its unique fiber morphology as shown in Fig.32 (Channab et al., 2024) . This morphological hierarchy consists of elementary fibrils, microfibrils, and microfibrillar bands. The lateral dimensions of these structural units range from 1.5 to 3.5 nm for elementary fibrils, 10 to 30 nm for microfibrils, and approximately 100 nm for microfibrillar bands. Microfibrils typically measure several hundred nanometers in length.

The fringed fibrillar model, comprising crystalline regions of varying sizes (crystallites) alongside noncrystalline areas, has effectively described the structure of microfibrils and the partial crystalline nature of cellulose, particularly concerning the polymer's reactivity. The pore structure complements the fibril morphology of cellulose and is vital for chemical accessibility and enzymatic degradation.

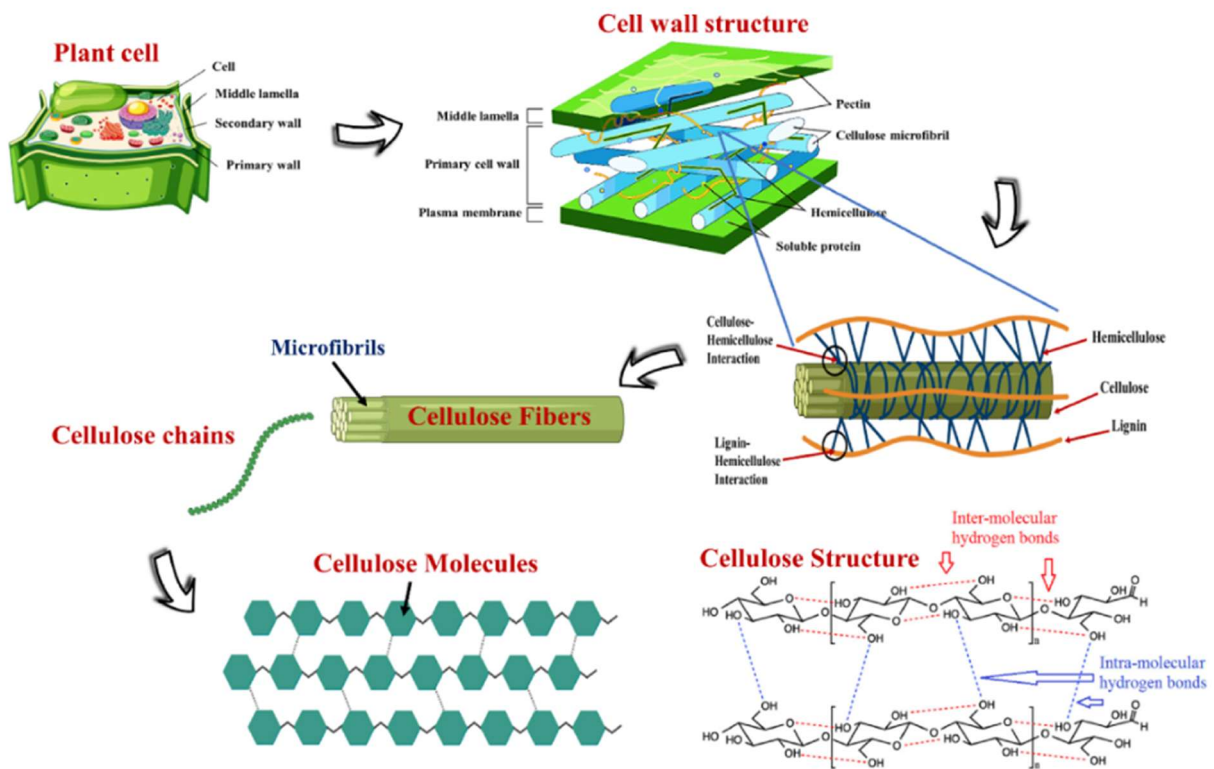


Figure 32. Hierarchy structure in natural fibers (Channab et al. 2024).

Controlled variations in pore structures enable cellulose products to cater to a wide array of applications, from specialised membrane materials to consumer goods like nonwovens with superior absorption properties (Široký et al., 2012).

As the primary structural component in plants, cellulose is organised into a hierarchical cellular structure. When combined with hemicelluloses, lignin, and pectin, this organisation contributes to the exceptional properties of natural composite materials such as wood, cotton, flax, and hemp. Figure 33 provides a schematic representation of cotton and wood cell walls with differently structured layers, where the secondary cell-wall layer S2 contains the majority of cellulose (Ioelovich, 2009).

Cellulose molecules arranged in microfibrils within cell walls exhibit characteristic orientations (helix angles) that vary by cell wall layer and plant type. Cotton fibers, with a lower microfibril orientation (helix angle of  $18^\circ$ ), show lower elasticity and higher elongation at break compared to bast fibers, which have a significantly higher microfibril orientation (helix angles of  $48\text{--}58^\circ$ ) and strength. The ability of wood to adapt its mechanical properties to environmental conditions through varying helix angles is remarkable and remains unmatched by synthetic composite materials. However, advancements allow for the customization of parameters in synthetic cellulose fibers to meet user specifications, enabling the development of low-orientation fibers akin to cotton (high elongation) and high-orientation, high-elasticity technical fibers similar to bast fibers.

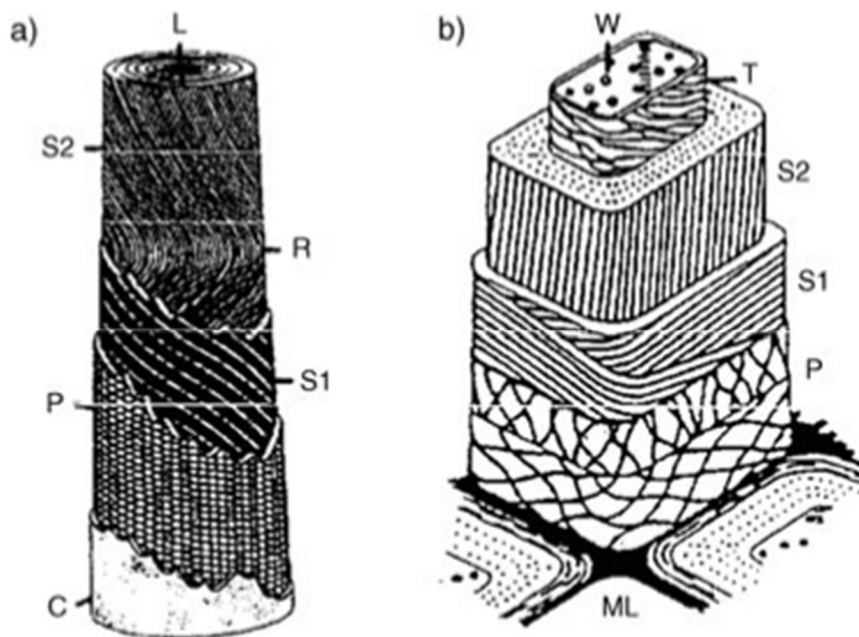


Figure 33. Structural design of plant cell walls exemplified by a) cotton and b) wood fibers: C = cuticula layer, L = lumen, ML = middle lamella, P = primary cell wall layer, R = reversing point, S1 = secondary cell wall layer 1, S2 = secondary cell wall layer 2, T = tertiary cell wall, W = wart layer (Heinze, 2016).

By the virtue of its structure cellulose exhibits convenient properties for important large-scale sectors such as textile and building, but also several more specific utilizations on a lower scale, such as drug delivery, wound care, tissue engineering, metal/dye removal and as a separation material for chiral high-performance liquid chromatography (HPLC) (Bui et al., 2021) (Dalei et al., 2022) (Hesse and Hagel, 1976). Indeed one of the key features of biopolymers and natural



resources in general is “chirality” (Fittolani et al., 2022), which is well understood as a result of covalent bonds (Noyori 2002) , but difficult to achieve through synthetic pathways.

Chirality refers to the property of molecules that are non-superimposable mirror images, similar to left and right hands. Chiral molecules can be categorised into enantiomers, which are mirror images with identical energy levels, and diastereomers, which differ in symmetry and energy. Enantiomers share physical properties except in their interaction with polarised light. A racemic mixture contains equal amounts of both enantiomers, resulting in no net optical rotation.

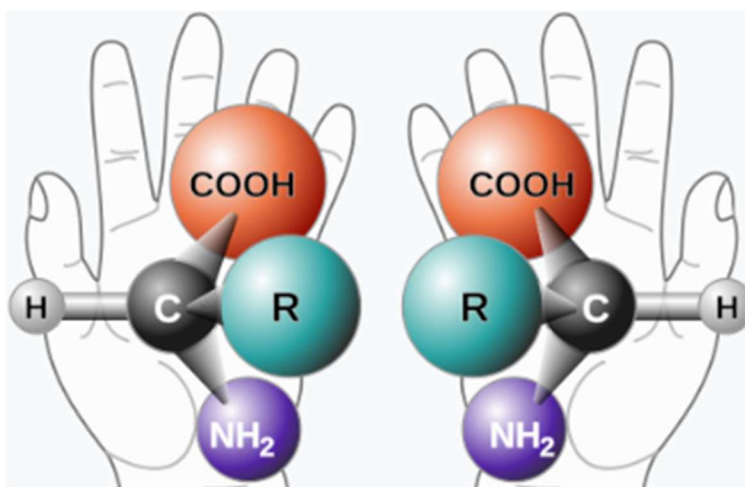


Figure 34 Chirality of amino acids.

Chirality is crucial in biology because most natural amino acids and sugars exist in only one enantiomeric form. This has implications for how living organisms metabolise chiral compounds, such as flavourings and drugs. For example, the enantiomers of limonene (Fig. 32) produce different odours; the R enantiomer is responsible for the pleasant orange scent, while the S enantiomer has a turpentine odour.

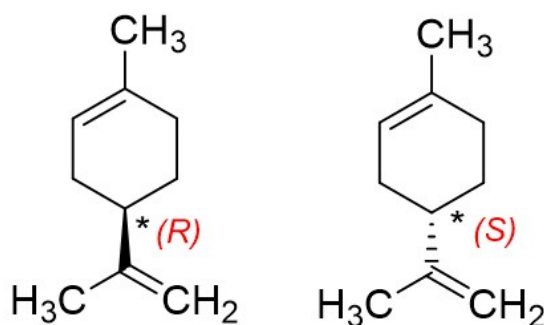


Figure 35. Limonene left R enantiomer, right S enantiomer.

Certain drugs have different therapeutic effects depending on their chirality. The sadly famous case of thalidomide illustrates the importance of chirality in medicine; one enantiomer was beneficial, while the other caused severe side effects in the foetus (Kim and Scialli, 2011).

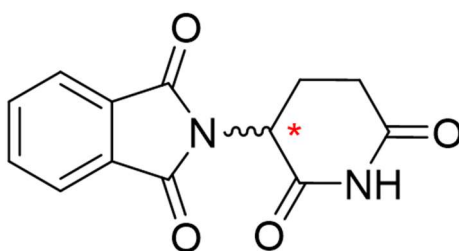
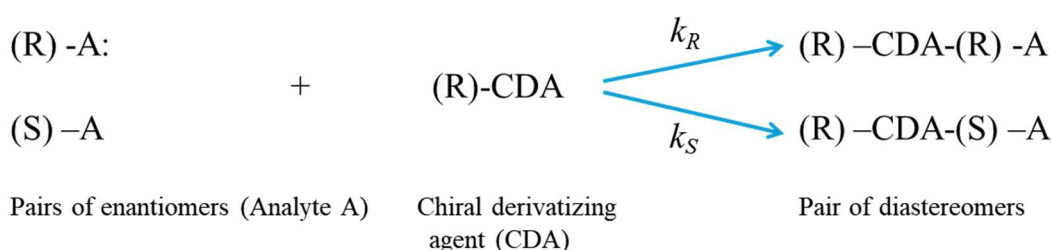


Figure 36. Structure of thalidomide.

Given this premise, the separation of enantiomers is a very important tool for monitoring life and health, especially in analytical, but also in preparative applications

Enantiomers separation can be achieved through two main strategies: indirect and direct methods (Fig. 37). The indirect approach involves forming diastereomers using a chiral derivatizing agent, while the direct approach uses non-covalent interactions with a chiral selector. In the present work direct approach has been studied because of the advantage to not create covalent bonds, resulting in a more versatile method.

### Indirect approach:



### Direct approach:

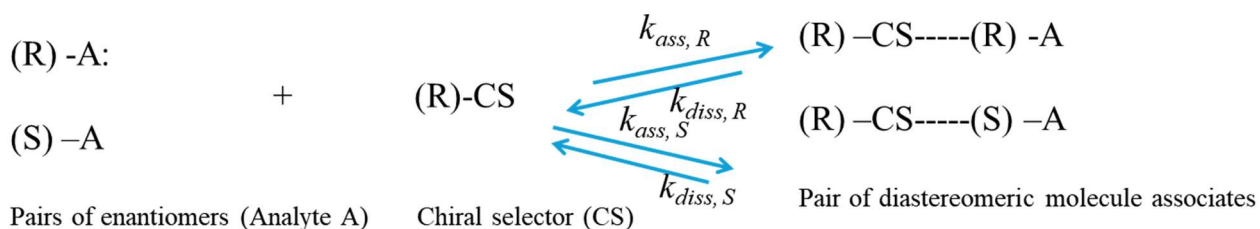


Figure 37. Two approaches to separate enantiomers by chromatography

The interaction of the chiral selector with the enantiomer to form a diastereomeric molecule associated with different physical properties, such as the solubility into elution solvent, can be described through the three-point interaction model. It explains the direct separation process, emphasizing the importance of complementary interactions between the chiral selector CS and the analyte A as shown in Fig. 38 (Berthod, 2006).

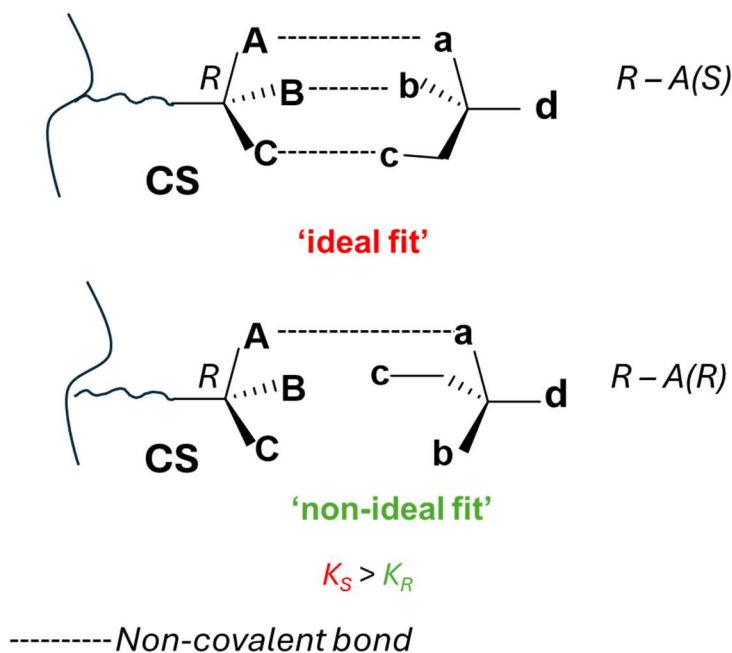


Figure 38. Three points interaction modelling: interaction of chiral selector CS with analyte S is stronger than interaction with enantiomer R.

As a chiral selector, cellulose is – by nature – a homochiral biopolymer and can separate enantiomers by selective, stronger interaction with one of the two enantiomers, thereby increasing its retention time during chromatography. To enhance the enantiomeric separation by creating additional interaction sites, native cellulose is derivatized. At first, cellulose acetate was used as a chiral selector (CS) (Hesse and Hagel, 1973) (Lüttringhaus and Dirksen, 1963), while nowadays phenyl carbamate derivatives of both, cellulose and amylose are mostly used (Bui et al., 2021). The latter represent standard selectors for the separation of small enantiomeric molecules in various fields of application, such as the food industry, the pharmaceutical industry and pesticide production (Bui et al., 2023a).



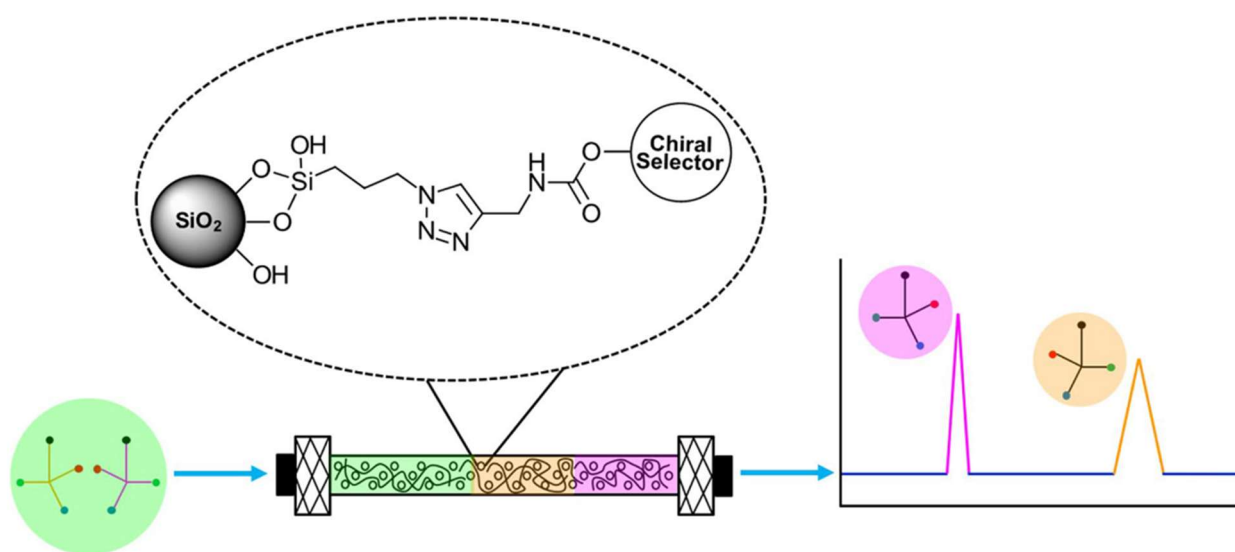


Figure 39. HPLC chiral separation cellulose on Silica gel illustration (Bui et al., 2023b).

For utilisation as separation materials in HPLC, the enantiopure CSs, *i.e.* the cellulose derivatives, are combined with inert, mechanically stable carrier materials, mostly (functionalized) silica, to obtain the chiral stationary phases (CSPs). Due to their facile preparation, CSPs obtained by physical coating of the CS onto the carrier material are traditionally the method of choice (Okamoto et al., 1984). However, the separation methods available for coated-type CSPs are often constrained by the comparably high solubility of the selector in organic solvents, such as THF, acetone, chloroform, *etc.*, and thus significantly limits the choice of mobile phase, as the latter might cause leaching of the CS or even destruction of the column material. To enhance the applicable solvents and facilitate method optimization, a chemically immobilised CS is thus frequently the more convenient option (Bui et al., 2021). To achieve immobilisation of the cellulose-derived selectors, several methods have been reported to date. Initially, cross-linking of cellulose 3,5-dimethylphenyl carbamate- and 3,5-dichlorophenyl carbamate selectors onto 3-aminopropyl-functionalized silica gel using diisocyanates was reported (Okamoto et al., 1987). However, a major drawback of these CSPs exhibiting a high degree of linkages was the diminished separation performance compared to their coated-type equivalents, which was attributed to the decreased flexibility of the polymeric selector (Chang et al., 2018). Following this pioneering work by Okamoto and co-workers, several new methods for covalent immobilisation of CSs have been developed to simultaneously maintain or even increase the separation performance. Cross-linking with diisocyanates was developed further

(Chen and Stewart, 2002), while also vinyl group polymerization (Minguillón et al., 1996) or alkoxysilyl groups condensation (Ikai et al., 2006) were reported as promising alternatives. However, these self-cross-linking functional groups are often hard to control and can thus result in highly cross-linked networks thereby diminishing the enantioseparation performance due to their stiffness. Thus, more controlled methods, such as amidation (Han et al., 2017), implementation of epoxide-modified silica (Chankvetadze et al., 2004), Staudinger ligation (Lin et al., 2018; Zhang et al., 2007) or thiol-ene click chemistry (Huang et al., 2014; Zhou et al., 2020), are generally preferred, as they allow precise optimization of the number of linkages. Recently, Hettegger reported the implementation of another click chemistry-type reaction, a Cu(I)-catalysed alkyne-azide *Huisgen* cycloaddition, to immobilise a cellulose 3,5-dimethylphenyl carbamate-type selector (Bui et al., 2023b). Azidopropyl-functionalized silica gel was reacted with the CS equipped with reactive propynyl groups at a low degree of substitution (DS = 0.1). However, structural considerations raised questions about the influence of the aliphatic nature of the linker. The propynyl carbamate linker, as a rather short and thus rigid structural element, might limit the flexibility of the attached CS and thus diminish the overall separation performance.

For a better understanding of structural and functional properties influence on performance the present work was performed during the PhD period abroad at BOKU University; the work focus on the synthesis of cellulose functionalized with 3,5-dichlorophenyl carbamate and 4-propargyloxy-3,5-dichlorophenyl carbamate groups at a low degree of substitution (DS = 0.17; **CS1**). As a reference material, cellulose *tris*(3,5-dichlorophenyl carbamate) (**CS2**) was synthesised. Both CSs were comprehensively characterised and, after either chemical immobilisation or physical coating, the resulting CSP were packed into standard HPLC columns 150 x 3 mm and tested using a representative set of chiral analytes to evaluate their separation performance.

## 4.2 Cellulose: Methods and Materials

### 4.2.1. Materials

Microcrystalline cellulose (MCC, Avicel® PH-101), *N,N*-diisopropylethylamine (> 99%), *p*-toluenesulfonic acid (98.5%), tetra-*n*-butylammonium iodide (99%), and *p*-cymene[s1] (99%), 3,5-dichloro-4-hydroxybenzoic acid (97%) were purchased from Sigma-Aldrich (Schnelldorf,

Germany) and used without further purification. MCC was dried at 40 °C in a vacuum oven for at least two days before use. 3,5-Dichlorophenyl isocyanate (> 98%), (3-chloropropyl)trimethoxysilane (> 97%), and NaN<sub>3</sub> (> 99%) were purchased from TCI Europe N.V. (Zwijndrecht, Belgium). Organic solvents, such as *N,N*-dimethylacetamide (DMAc), *N,N*-dimethylformamide (DMF), tetrahydrofuran (THF), acetonitrile (MeCN), and pyridine, were all reagent grade and dried over either 3 Å or 4 Å activated molecular sieves (Sigma-Aldrich) for at least five days before use. Acetone and methanol (MeOH) for precipitation and washing were of technical grade and obtained from Carl Roth GmbH + Co. KG (Karlsruhe, Germany) or Fisher Scientific (Vienna, Austria) and used as received. Silica gel (Daisogel, grade SP-300-5P, 5 µm, 300 Å, 115 m<sup>2</sup>/g by BET) was purchased from Osaka Soda Co. Ltd. (Awaza, Japan). Empty stainless steel HPLC columns (150 × 3 mm, i.d.) and column hardware were purchased from Bischoff Analysentechnik u. -geräte GmbH (Leonberg, Germany). The commercially available chiral analytes, 2-phenylcyclohexanone (> 98%, a), benzoin (> 98%, b), and Pirkle's alcohol (> 99%, d), were purchased from TCI Europe N.V. (Zwijndrecht, Belgium). Flavanone (98%, c), trans-stilbene oxide (98%, e), and Tröger's base (98%, f) were obtained from Sigma-Aldrich (Schnelldorf, Germany). Mandelic acid derivatives (g-j), 1-methoxy-2-(1-methoxy-3-phenylpropyl) benzene (k), and 1-(*o*-hydroxyphenyl)-3-phenyl-1-propanol (l) were synthesized according to standard procedures. The HPLC solvents *n*-hexane (95%, *n*-hex), 2-propanol (99.9%, *i*PrOH), tetrahydrofuran (> 99.9%, THF), and chloroform (99.8%, CHCl<sub>3</sub>) were obtained from Fisher Scientific.

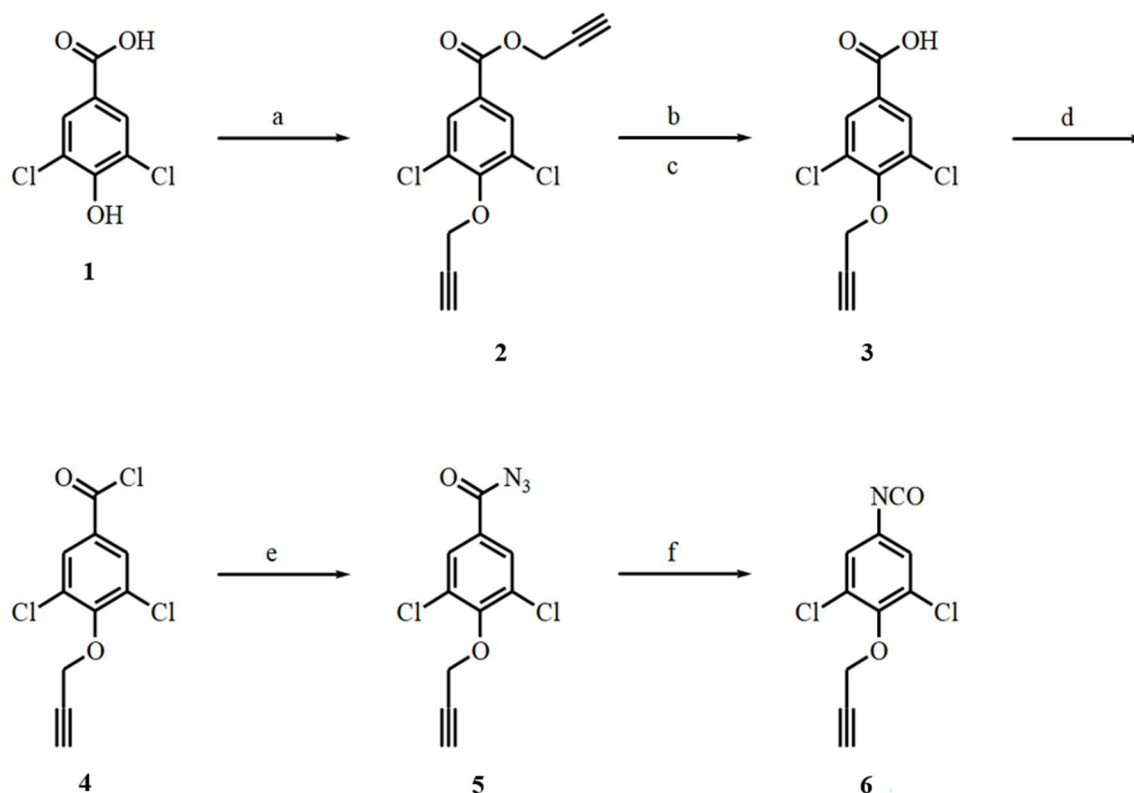
#### 4.2.2 Instrumentation

Elemental analyses were performed with a EURO EA 3000 CHNS-O instrument (HEKAtech, Wegberg, Germany), both at the microanalytical laboratory of the University of Vienna, Austria. Thermogravimetric analysis (TGA) was carried out with a TG 209 F1 Iris thermo-microbalance (Netzsch GmbH & Co. KG, Selb, Germany), with a dried sample mass of 10–15 mg, an oxidizing atmosphere (N<sub>2</sub>:O<sub>2</sub> = 4:1, v/v), a flow rate of 20 mL/min and a temperature gradient of 20 °C/min up to a maximum temperature of 1000 °C. Solution-state NMR spectra were recorded using a Bruker Avance II 400 spectrometer equipped with a cryogenically-cooled broadband observing (BBO) 5 mm probe-head (CryoProbe<sup>TM</sup> Prodigy, N<sub>2</sub>-cooled) (Bruker, Rheinstetten, Germany). The NMR experiments were performed with *z*-gradients at 303 K

(unless indicated otherwise) at resonance frequencies of 400.13 MHz for  $^1\text{H}$  and 100.61 MHz for  $^{13}\text{C}$  using standard Bruker pulse programs. Chemical shifts are given in parts per million (ppm) and were referenced to the respective residual solvent signal as internal reference (DMSO- $d_6$ : 2.50 ppm for  $^1\text{H}$ , 39.52 ppm for  $^{13}\text{C}$ ). For all experiments, the number of scans and spectral widths were adjusted individually depending on the nature and the concentration of the sample. All NMR data were acquired and processed using Bruker TopSpin 3.2.7, 3.6.5, and/or 4.3.0 software. ATR-FTIR spectra were recorded on a Frontier IR single-range spectrometer (PerkinElmer, Waltham, Massachusetts, US) equipped with a diamond/ZnSe crystal, LiTaO<sub>3</sub> detector, and KBr windows using PerkinElmer Spectrum software (version 10.03.02). An Agilent Technologies, Inc. (Santa Clara, CA, USA) 1100 HPLC apparatus equipped with a degasser (G1322A), quaternary pump (G1311A), autosampler (G1313A), thermostatted column compartment (G1316A), and DAD (G1315A) was used to evaluate the enantioseparation performance of the chiral columns. OpenLab CDS software (Agilent) was used for chromatography data processing and evaluation.

#### 4.2.3 Syntheses

**Synthesis of 3,5-dichloro-propargyloxybenzoic acid propargyl ester (2):** A suspension of 14.6 g of 3,5-dichloro-4-hydroxybenzoic acid (70.4 mmol, 1.0 equiv.), 36.6 mL of propargyl bromide (80% in toluene, 427 mmol, 6.1 equiv.) and 36.7 g of potassium carbonate (pH = 10) (266 mmol, 3.8 equiv.) in 80 mL of acetone was heated to 60°C and stirred at this temperature overnight. The brown suspension was cooled to RT and poured into 300 mL of water. After extraction with EtOAc (3 x 140 mL), the combined organic phases were washed with 100 mL of H<sub>2</sub>O and 60 mL of saturated aqueous NaCl solution, dried over MgSO<sub>4</sub>, filtered and concentrated *in vacuo*. The product was obtained as a colourless solid and dried under vacuum for 48 h (19.7 g, 69.8 mmol, 99%).



Scheme 10. Conditions: (a) propargyl bromide,  $K_2CO_3$ , acetone, reflux, 18h; (b) NaOH, ethanol, water, 1h, (c) HCl, 0°C, (d)  $(COCl)_2$ , DMF (catalyst), 1h, (e)  $NaN_3$ , acetone, water, 0°C, 1h, (f) toluene, reflux, 3h.

**Synthesis of 3,5-dichloro-propargyloxybenzoic acid (3):** Compound 2 (19.6 g, 69.5 mmol, 1.0 equiv.) was dissolved in 140 mL of EtOH and a solution of 5.18 g NaOH (129 mmol, 1.9 equiv.) in 40 ml of water was added. The reaction mixture was heated to refluxing temperature 1 h. Subsequently, the brown solution was diluted with 40 mL of EtOH and 40 mL of  $H_2O$  and cooled down to 0°C using an ice-bath. Upon acidification with concentrated HCl to pH~2, a colourless precipitate formed. The solid product was isolated by filtration washed with 2 x 100 mL of cold  $H_2O$  and lyophilized (15.9 g, 64.9 mmol, 93%).

**Synthesis of 3,5-dichloro-propargyloxybenzoic azide (5):**

(a) Compound 3 (6.11 g, 24.9 mmol, 1.0 equiv.) was slowly added to 40.5 mL of oxalyl chloride ( $(COCl)_2$ , 472 mmol, 19 equiv.) at 0 °C and four drops of dry DMF as a catalyst were carefully added. The suspension was stirred at 0 °C for 15 min and then heated up to 30 °C for 45 min whereupon the colourless solid dissolved and the colour changed from colourless to yellowish with little brown drops. Subsequently, the unreacted oxalyl chloride was distilled off and 90 mL of petrol ether were added to the reaction mixture together with a spatula tip of activated carbon

(approx. 200 mg) for purification. After refluxing for 3 min the reaction mixture was filtered hot and evaporated to dryness under reduced pressure. Due to the reduced stability of the acyl chloride, the product 3 was used without further purification or characterization and directly converted into the corresponding azide.

(b) A solution of 4.00 g of the acyl chloride 3a (15.2 mmol, 1.0 equiv.) in 40 mL of cold acetone was cooled to 0°C using an ice-bath and 3.06 g NaN<sub>3</sub> (47.1 mmol, 3.1 equiv.) dissolved in 16.7 mL of H<sub>2</sub>O was added dropwise to the acyl under vigorous stirring during 1 h at this temperature, whereupon a voluminous, colorless precipitate formed in the orange solution. The solid was filtered off and washed with cold H<sub>2</sub>O (2 x 50 mL). For an effective drying the resulting solid was dissolved in 150 mL of EtOAc, washed with 20 mL of H<sub>2</sub>O, 20 mL of saturated aqueous NaCl solution, and dried over anhydrous MgSO<sub>4</sub>. After concentration *in vacuo* at room temperature, the product was obtained as a colourless solid (2.9 g, 11.0 mmol, 71%). The compound was stored at -20 °C until further use.

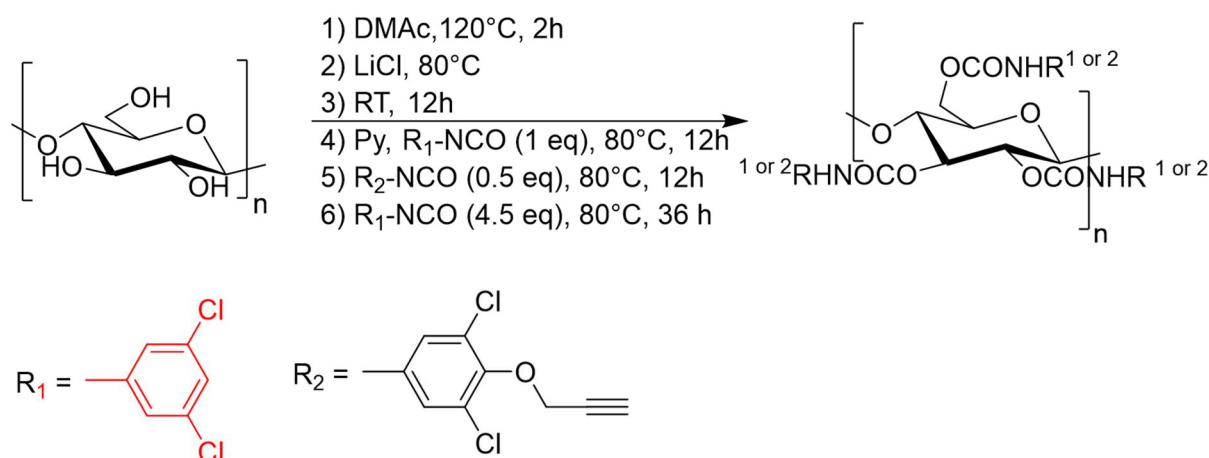
**Synthesis of 4-propargyloxy-3,5-dichlorophenyl isocyanate (6):** 4-Propargyloxy-3,5-dichlorophenyl azide (3, 0.416 g) was suspended in 20 mL toluene, dried by azeotropically distilling off 20 mL using a Dean-Stark trap, and heated to refluxing temperature for 3 h. The solution was subsequently evaporated to dryness *in vacuo* and the product was obtained as a colourless solid in quantitative yield. Due to the high reactivity and water sensitivity of the isocyanate, the compound was directly prepared before use to avoid prolonged storage and used without purification.

**Synthesis of cellulose 3,5-dichlorophenyl and 4-propargyloxy-3,5-dichlorophenyl-carbamate (CS1):** A two-necked round-bottom flask loaded with pre-dried MCC (0.300 g, 1.85 mmol, 1.0 equiv.) was flushed with N<sub>2</sub> for 1 h, before dry DMAc (9.0 mL, conc. 33 g cellulose/L) was added, heated to 120 °C and vigorously stirred under a dry nitrogen atmosphere. After 2 h, the suspension was cooled down to RT and anhydrous LiCl (0.547 g, 6.5% of DMAc w/w) was slowly added during cooling below 80 °C. The mixture was allowed to stir at RT until a clear solution had formed (approx. 3 h). The solution was heated at 80°C and 9.0 mL of anhydrous pyridine were added. Subsequently, a solution of 0.349 g of 3,5-dichlorophenyl isocyanate (1.86 mmol, 1.0 equiv./AGU) in 1.0 mL of DMAc was added dropwise, whereupon the solution turned slightly yellow and was stirred 8 h at 80 °C.

Subsequently, a yellow solution of freshly synthesised 4-propargyloxy-3,5-dichlorophenyl isocyanate (0.249 g, 0.92 mmol 0.5 equiv.) in 2.0 mL anhydrous pyridine was added dropwise under stirring to the reaction mixture, whereupon gas evolution and increased viscosity was observed. After 12 h the reaction mixture had turned brown and transparent and An inert, pink solution 3,5-dichlorophenyl isocyanate (1.567 g, 8.33 mmol, 4.5 equiv./AGU) in 5 mL of anhydrous DMAc was added dropwise to the reaction mixture, whereupon the viscosity decreased. After another 24 h at 80 °C, the brown solution was poured into 300 mL of methanol and the precipitate was collected by centrifugation. For purification, the solid was dissolved in 40 mL of acetone and reprecipitated in 200 mL of MeOH: H<sub>2</sub>O 1 : 1 (v/v). The solid product was collected by centrifugation, washed with diluted HCl (M=10<sup>-4</sup> mol/L, pH = 4), deionized water and subsequently freeze dried (m = 1.35 g, quant.).

**Synthesis of cellulose *tris*(3,5-dichlorophenyl carbamate) (CS2):** MCC (0.500 g, 3.08 mmol AGU) was immersed in anhydrous DMAc (15 mL) and heated at 120 °C for 2 h under nitrogen atmosphere during vigorous stirring. Cellulose degradation during that heating period was considered to be tolerable (Potthast et al., 2003). Anhydrous LiCl (0.91 g) was added slowly after cooling down to 86 °C. The mixture was further cooled to room temperature (RT) and stirred for 3 h until a clear solution had formed. The solution was heated up to 80 °C and then anhydrous pyridine (15 mL) was added slowly. Subsequently, 3.48 g of 3,5-dichlorophenyl isocyanate (18.5 mmol, corresponding to 6 molar equivalents/AGU) dissolved in 5.0 ml of DMAc were added dropwise to the solution, whereupon the solution turned slightly yellow. After stirring the reaction mixture at 80°C for 18 h, the brown solution was poured into 300 mL of methanol and the precipitate was collected by centrifugation. For purification, the solid was dissolved in 100 mL of acetone and reprecipitated in 200 mL MeOH : H<sub>2</sub>O 1 : 1 (v/v). The solid product was collected by centrifugation, washed with diluted HCl (M = 10<sup>-4</sup> mol/L, pH = 4), and deionized water and subsequently freeze dried (m = 1.3 g, 58%).





*Scheme 11. Synthesis of cellulose tris (3,5-dichlorophenyl carbamate).*

### Pre-modification of silica gel (AzPS)

**Synthesis of 3-chloropropyl functionalized silica (CIPS):** (a) Silica gel (10 g) and *p*-toluene sulfonic acid (20 mg) as a catalyst were suspended in toluene (200 mL) and mechanically stirred. The suspension was dried by azeotropic distillation using a Dean-Stark trap under inert N<sub>2</sub> atmosphere removing approx. 100 mL of solvent. The suspension was cooled to 80 °C, and (3-chloropropyl) trimethoxysilane (4.6 mL, 25.2 mmol) was added dropwise to the mixture over a period of 15 min. The reaction mixture was mechanically stirred at this temperature for 38 h. Subsequently, the suspension was cooled down to RT and the product was collected by filtration using a glass fritted funnel (DURAN®, porosity 4), and washed with toluene (2 x 100 mL) and MeOH (2 x 100 mL). The modified silica was subsequently re-suspended in toluene (100 mL), mechanically stirred at 80 °C for 2 h for washing and cooled down to RT again. Purified CIPS was collected by vacuum filtration, washed with toluene (100 mL), MeOH (100 mL), and distilled water (200 mL, two times each), and dried at 40 °C in a vacuum oven for two days (9.97 g).

**Synthesis of 3-azidopropyl functionalized silica (AzPS):** (b) 3-Chloropropyl functionalized silica (9.97 g) was suspended in a 250 mL three-necked flask and 4.950 g of sodium azide (75.08 mmol) and 60 mg of *n*-tetrabutylammonium iodide in 100 mL of dimethyl sulfoxide (DMSO). The reaction mixture was stirred for 3 days at 80 °C. The solid was filtered on a frit porosity 4 and washed with 500 ml of DI water on frit, 250 ml of MeOH put in the plastic bottle and left in the vacuum oven at 40° for two days. The loading of propylazide on silica was 288.8 μmol/g determined by elemental analysis (calculated based on the N-content).



#### 4.2.4 Preparation of immobilised CS (CSP1)

CS1 (0.60 g) was dissolved and stirred in THF (60 mL) in a Schott DURAN® bottle. AzPS (2.5 g) was added and the suspension was shaken on a laboratory shaker at RT for 24 h. A catalyst solution was prepared by dissolving CuI (17 mg) in MeCN (10 mL). *N,N*-Diisopropylethylamine (1 mL) was added to the CS / AzPS mixture in THF, followed by the CuI solution. The mixture was degassed by purging with N<sub>2</sub> through a syringe needle for 30 min. The vessel was closed, sealed with Parafilm®, and allowed to slowly rotate for 24 h on an overhead shaker at RT. **CSP1** was collected by vacuum filtration through a sintered glass frit (DURAN®, porosity 4), washed with THF (200 mL), MeCN (100 mL), MeOH (100 mL), and distilled water (200 mL, two times each), and dried at 40 °C in a vacuum oven for two days (2.61 g, 84%).

#### 4.2.5 Preparation of coated CS (CSP2-CSP5)

A solution of the chiral selector (CS1 or CS2) in THF (40 mL, HPLC grade, unstabilized) was added to a flask loaded with AzPS in the desired weight ratio to obtain either 9% or 20% selector loading (see Table 6 below). The suspension was sonicated for 20 min, slowly evaporated to dryness at 40 °C / 357 mbar and further dried in the vacuum oven. The coated silica particles were sieved through an analytical sieve (40 µm mesh) before column packing. The loading was determined by TGA and EA analysis.

Table 6. Amount of stationary phase by the adsorption of CS on the functionalized silica gel AzSP.

	CS	CS	AzPS	Yield
<b>CSP2</b>	CS1 9%	0.270 g	2.73 g	2.73 g (91%)
<b>CSP3</b>	CS1 20%	0.600 g	2.40g	2.34 g (78%)
<b>CSP4</b>	CS2 9%	0.270 g	2.73 g	2.65 g (88%)
<b>CSP5</b>	CS2 20%	0.600 g	2.40g	2.54 g (84%)

## 4.3 Cellulose : Results and Discussion

### 4.3.1 Synthesis of CS

The synthesis of the chiral selector CS was based on the isocyanate chemistry that allowed an efficient reaction between cellulose hydroxyl groups and phenyl isocyanate in homogeneous phase (Chen et al., 2015). Therefore the 3,5-dichlorophenyl isocyanate being commercially available was exploited in the reaction to fully substitute the cellulose was fully substituted with a large excess of six molar equivalents. On the other hand the synthesis of the chiral selector cellulose 3,5-dichlorophenyl carbamate equipped with 4-propargyloxy-3,5-dichlorophenyl carbamate group at a low degree of substitution of the propynyl anchor (**CS1**) required the a priori synthesis of the 4-propargyloxy-3,5-dichlorophenyl isocyanate.

The commercially available 3,5-dichloro-4-hydroxybenzoic acid was transformed into its 4-propargyloxy-3,5 dichlorobenzoic acid propargyl ester by reaction with propargyl bromide. The ester group of the purified intermediate was then hydrolyzed with sodium hydroxide. Acidification with hydrochloric acid led to the carboxylic acid form 3 of Scheme 10. This intermediate was then treated with oxalyl chloride and dry DMF as a catalyst providing the respective acyl halide 4, which was subsequently converted into acyl azide 5 by reaction with sodium azide, which could be easily isolated by precipitation and extraction. By heating up the fully dry acyl azide led to the isocyanate via Curtius Rearrangement, the test on the in situ rearrangement of the azide was unsuccessful, so the isocyanate was produced about five hours before the addition; by refluxing in dry toluene for 3 hours. The two compounds were compared by FTIR as shown in Fig. 40.

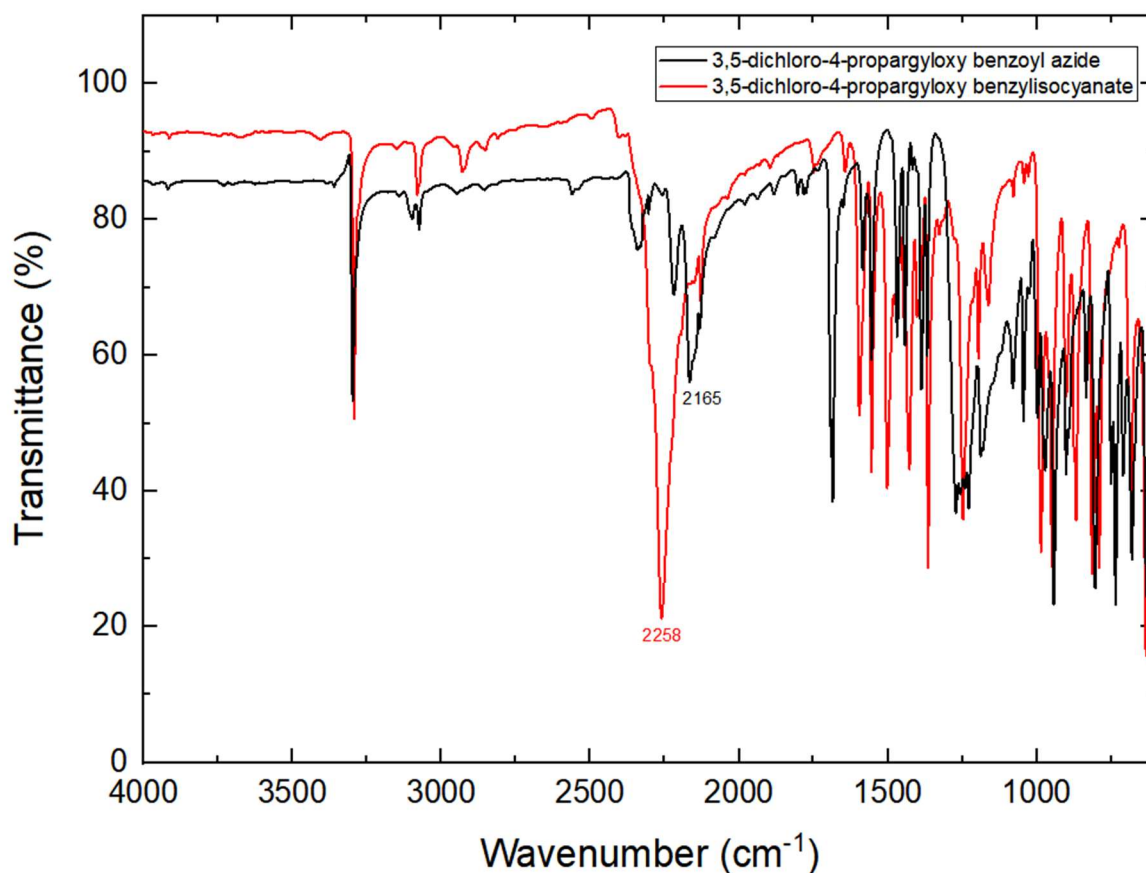


Figure 40. FTIR spectra of 3,5-dichloro-4-propargyloxy benzoylazide:  $\nu = 2165$  ( $-N=N=N$ ); 3,5-dichloro-4-propargyloxy benzylisocyanate:  $\nu = 2258$  ( $-N=C=O$ )  $\text{cm}^{-1}$ .

Dry toluene was azeotropically distilled just before using too. These functional anchor groups were attached for immobilisation on the azido propyl-functionalized silica as a chromatographic support by a *Huisgen*-type click reaction and to compare the separation performances of enantiomers by HPLC. As an analogous reference material, cellulose *tris*(3,5-dichlorophenyl carbamate) (**CS2**) was synthesised to allow evaluation of the influence of the covalent linkage on the separation performances.

Functionalization of the well-characterised starting material, Avicel<sup>®</sup> PH-101 cellulose, was carried out in a homogeneous reaction for both, **CS1** and **CS2**, to allow homogeneous distribution of the linker groups along the cellulose chain in the first. Understanding the structure of cellulose and its derivatives in solution is not only scientifically intriguing but also practically significant (Medronho et al., 2012). The structural behavior of cellulose in solution has been a topic of considerable research and discussion in recent decades. Typically, cellulose derivatives with free

hydroxyl groups are not molecularly dispersible. However, studies on partially substituted cellulose carbamates and benzoates (Pourjavadi et al., 2011) have shown that aggregate-free solutions can be achieved through specific polymer-solvent interactions. In the present work the cellulose was homogeneously dissolved in DMAc/LiCl according to the protocol by Heinze et al. (Ganske and Heinze, 2018), subsequent addition of pyridine in ratio 1:1 was preliminary tested in terms of solubility and then successfully applied as reaction medium. Fully 3,5-dichlorophenyl carbamate-functionalized **CS2** was obtained from a carbamoylation using the homogeneous DMAc/LiCl/pyridine (1/0.065/1) (v/w/v) medium. The pre-dried MCC was activated in anhydrous DMAc at 120 °C for 2 h, during which cellulose degradation was considered to be tolerable due to the absence of LiCl (Potthast et al., 2003). Before the addition of the latter for dissolution, the suspension was cooled to 80 °C or lower, which was left under stirring at room temperature for about three hours, until transparent. To allow full functionalization, a significant excess of 3,5-dichlorophenyl isocyanate was used due to its high reactivity toward residual water. The resulting by-products were efficiently removed by re-precipitation from acetone into a 1:1 mixture of MeOH : H<sub>2</sub>O (v/v) and through washing with diluted HCl and water. Mixed-type **CS1** was obtained using an analogous procedure: after full dissolution of the MCC, 1.0 equivalent of 3,5-dichlorophenyl isocyanate was added, before 0.5 equivalents of freshly synthesised 4-propargyloxy-3,5-dichlorophenyl isocyanate (**6**) to avoid complete loss of the linker to water hydrolysis. Subsequently, residual free OH groups were fully functionalized by an excess of 3,5-dichlorophenyl isocyanate.

The derivatization of cellulose with 3,5-dichlorophenyl isocyanate or 4-propargyloxy-3,5-dichlorophenyl isocyanate was confirmed by FTIR that shows a significant depletion of -OH band at 3000 cm<sup>-1</sup> and the intense signal at 1721 cm<sup>-1</sup> corresponding to carbonyl group of carbamates (Fig. 41).

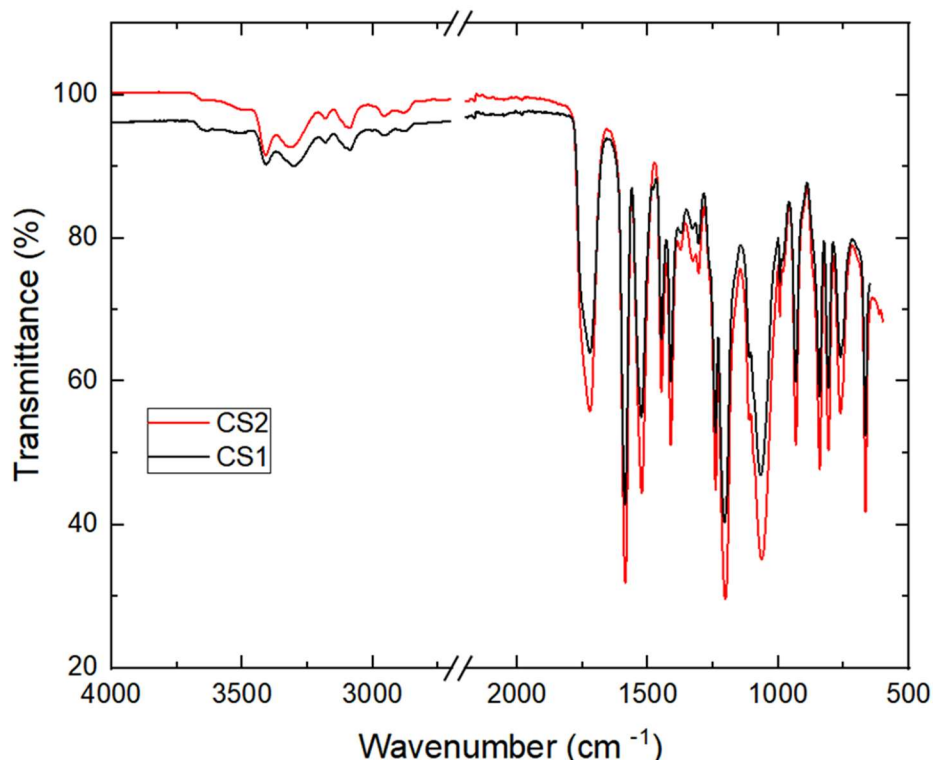


Figure 41. FTIR spectra of CS1 (black) vs. CS2 (red); CS2:  $\nu = 3408, 3179, 3105$  (N-H), 2960, 2870 (C-H), 1718 (C=O), 1584, 1242, 1071, 934 (aromatic rings), 1205  $\text{cm}^{-1}$  (C-O-C); CS1:  $\nu = 2137 \text{ cm}^{-1}$  (C≡C-H).

The degree of substitution of cellulose 3,5-chlorophenyl carbamate was estimated by quantitative  $^1\text{H}$  NMR in  $\text{DMSO-}d_6$  at 70 °C. Elevated temperature measurements resulted in higher-quality spectra with well-resolved signals allowing integration, especially the separation of the sugar region from the residual water signal (Qu et al., 2011). The integral of the protons corresponding to the saturated CH/CH<sub>2</sub> groups of the glucose repeating unit (3.5 – 5.5 ppm) was set to 7.0 resulting in an integral of 3.0 of the broad singlet at 9.44 ppm corresponding to the carbamate N-H protons (Fig. 42 , top). Thus, NMR analysis suggests full derivatization (DS = 3.0) of the selector CS2. Assuming also full derivatization of cellulose during synthesis of CS1, the DS of the linker-containing group 4-propargyloxy-3,5-dichlorophenyl carbamate was estimated by integration of the signals originating from the alkin protons (at  $\delta_H = 3.37, 3.42$  and 3.45 ppm; three triplets; see Fig. 42 bottom). By referencing the latter to the carbamate N-H protons, a DS of 0.17 was calculated for the linker carbamate.

Figure  $^1\text{H}$  NMR in  $\text{DMSO-}d_6$  at 80°C of cellulose 3,5-dichlorophenyl carbamate (top, red) and cellulose 4-propargyloxy-3,5-dichlorophenyl (DS = 0.17) 3,5-dichlorophenyl carbamate (DS = 2.83) carbamate (bottom, black), inset of integrated signals.

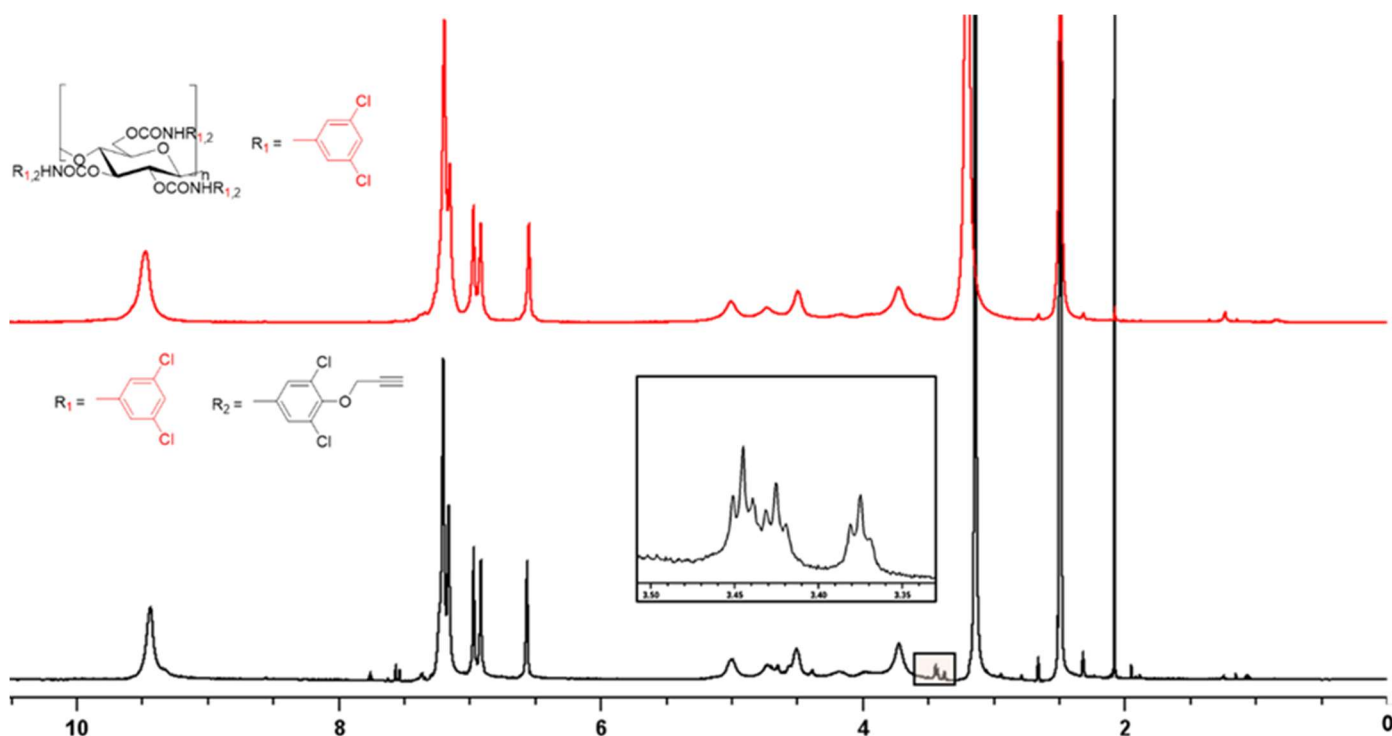


Figure 42.  $^1\text{H}$  NMR in  $\text{DMSO-}d_6$  at  $80^\circ\text{C}$  of cellulose 3,5-dichlorophenyl carbamate (top, red) and cellulose 4-propargiloxy-3,5-dichlorophenyl (DS = 0.17) 3,5-dichlorophenyl carbamate (DS = 2.83) carbamate (bottom, black), inset of integrated signals.

The DS of the linker was further investigated by the elemental analysis, in Table \$ the percentages of carbon C, hydrogen H, oxygen O, nitrogen N and chloride Cl are compared to the ones calculated assuming the cellulose fully substituted in CS2 and fully substituted with the linker DS 0.17. The comparison shows a good agreement and the analysis conducted on the two CS.

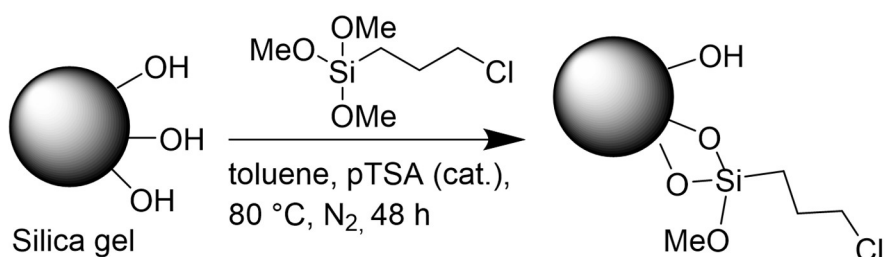
Table 7. Elemental analysis data of the chiral selectors *CS1* and *CS2*; overall DS calculated based on the N- content.

<i>Sample</i>	C [%] Calc. (found)	H [%] Calc. (found)	N [%] Calc. (found)	O [%] Calc. (found)	Cl [%] Calc. (found)	DS1 based on N- content	DS2 based on N- content
<i>CS1</i>	44,72 (44,67)	2,65 (2,88)	5,76 (5,04)	17,68 (19,92)	29,17 (27,49)	2,49	0,17
<i>CS2</i>	44,66 (43,89)	2,63 (2,71)	5,78 (5,41)	17,62 (18,65)	29,29 (29,31)	3	

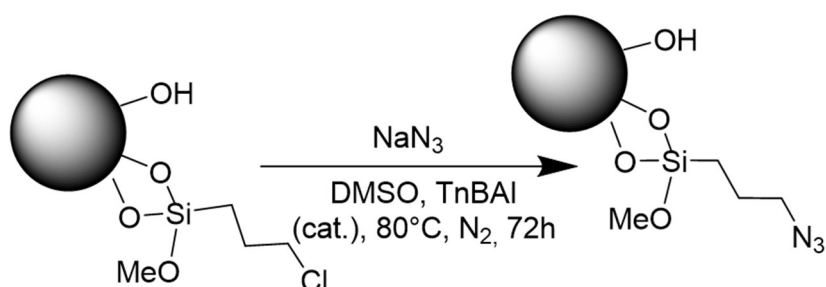
### 4.3.2 Preparation of CSPs

#### 4.3.2.1 3-Chloropropyl-functionalized silica gel

Silica gel was derivatized in a two-step process, firstly the condensation of (3-chloropropyl)trimethoxy silane with neat silica gel in toluene, then the (3-chloropropyl)modified silica was converted to azide through a nucleophilic substitution in DMSO (Bui et al., 2023).



Scheme 12. Silica gel 3-Chloropropyl-methoxy silane condensation.



Scheme 13. S<sub>N</sub> with Sodium azide.

The loading of the silica gel was determined by means of EA and TGA (Table 7). For the Az-PS, the loading based on the residual dry mass was found to be 3.64 % (TGA) and 4.69 % (EA). Based on the found N wt%, a total N<sub>3</sub>-group-content 288.8 μmol/g available for further functionalization was calculated by the following equations:

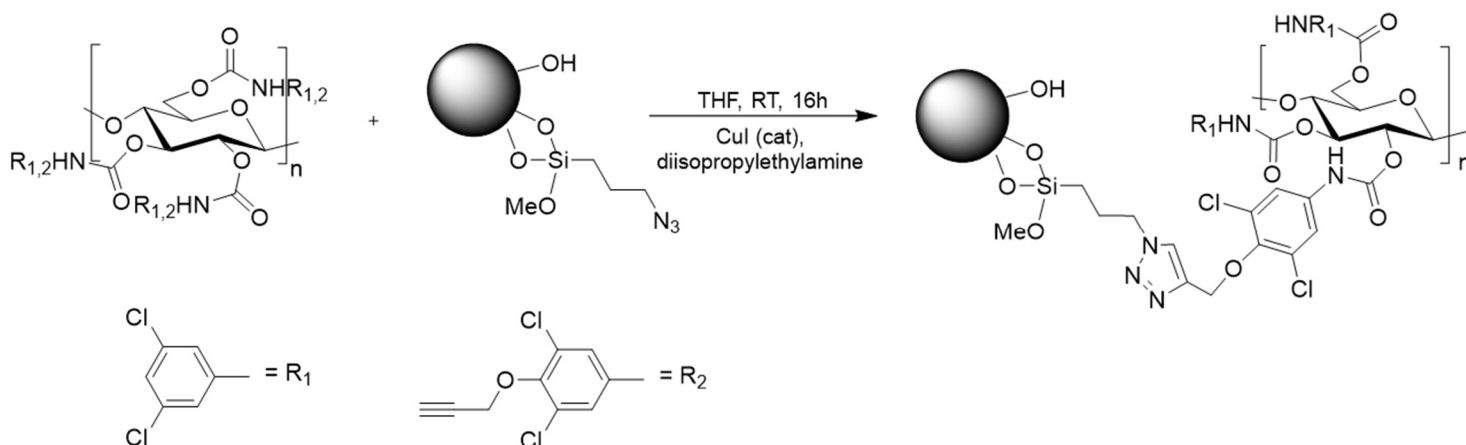
$$m_N = \frac{w\%N * m_{tot}}{100}$$

$$n_{N_3} = \frac{m_N}{14,007 * 3}$$

$$loading \left( \frac{\mu mol}{g} \right) = \frac{n_{N_3}}{m_{tot}} * 10^6$$

*Equation 3*

The synthesised chiral selector CS1 at low degree of substitution (DS = 0.17) was chemically bonded to the pre-modified silica gel through the Cu(I)-catalysed Huisgen alkyne-azide cycloaddition in mild condition.



*Scheme 14 Cu(I)-catalyzed alkyne-azide Huisgen cycloaddition.*

The amount of CS1 linked to AzSP, determined by TGA, was about 9 % (CSP1) and this was related to the number of anchor points present on cellulose carbamates (Fig. 42).

In order to provide a comprehensive study of the determining factors in enantiomeric separation two different percentages in weight of chiral selector were adsorbed onto silica: 9% , which is the loading achieved through covalent bonding of CSP1, and 20% which is the typical loading of commercially available stationary phases .

The chiral selector with cellulose fully substituted by 3,5-dichlorophenyl carbamate (CS2) was adsorbed onto silica by coating at 9% (CSP4) and 20%, (CSP5) similarly the chiral selector with the linker CS1 was applied by coating at 9% (CSP2) and 20% (CSP3) for comparison, with five samples in total to test at HPLC, including the first covalently immobilised (CSP1).

The organic components added to silica gel by adsorption were quantified by TGA, in Fig. 43 the grey solid is referred to prefunctionalized silica with azido group (SPAz).



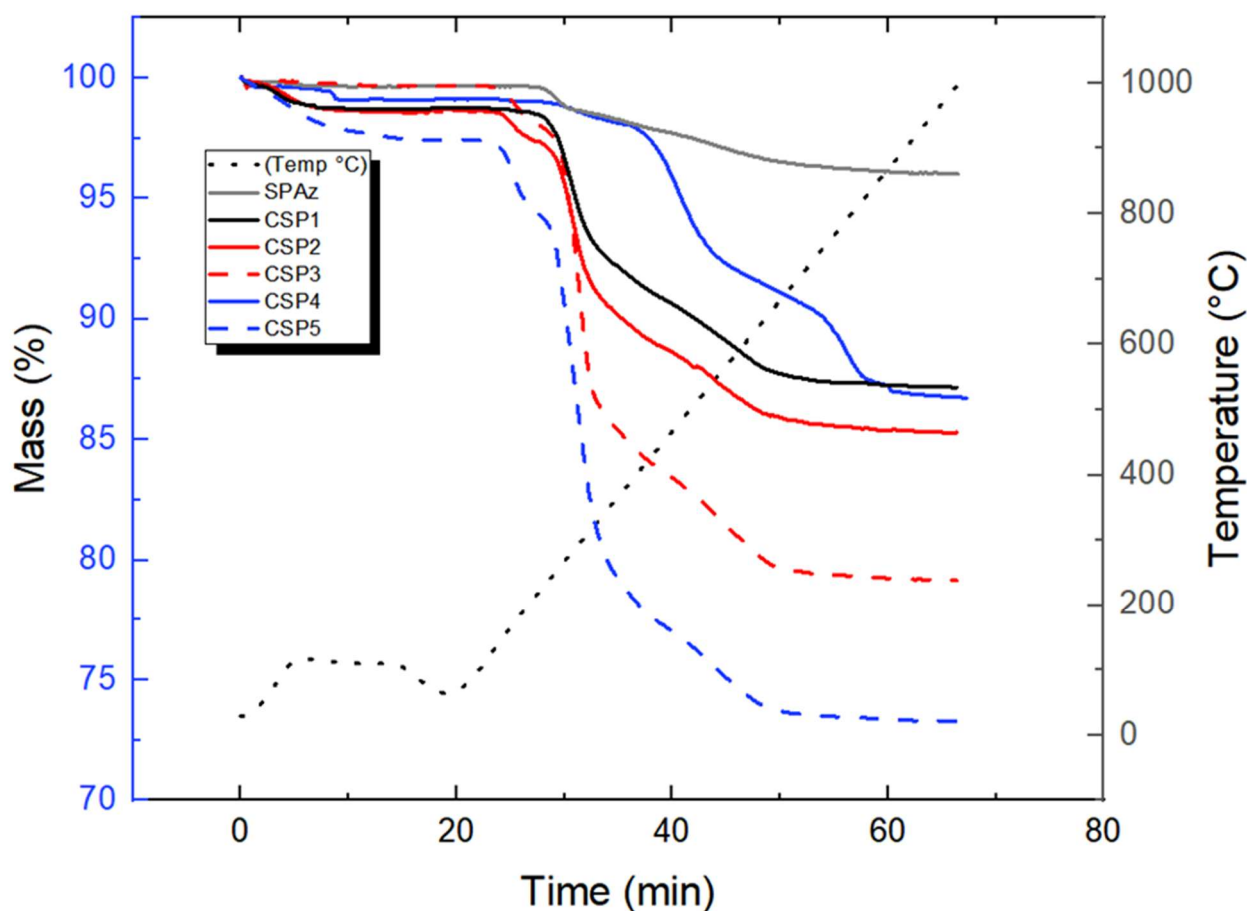


Figure 43. Thermogravimetric analysis of the 5 chiral stationary phases compared to the propyl azido silica stationary phase (solid grey).

The loading of the stationary phase (SP) was determined by EA and showed  $\mu\text{mol/g}$ ; moreover the combination of the chiral selector with the linker and without it nominally loaded at 9 % and 20 % was studied by EA the results are reported in Table 8.

Table 8. Loading of CS on **CSP1-CSP5** calculated based on TGA and EA measurements; elemental analysis data of chiral stationary phases, mmol of functionalized anhydroglucose unit per gram of CSP.

Sample	Loading [%]		C [%] (mmol/g)	H [%] (mmol/g)	N [%] (mmol/g)	Cl [%] (mmol/g)	fAGU (mmol/g)	N <sub>3</sub> -groups ( $\mu\text{mol/g}$ )
	TGA	EA						
<b>Cl-PS</b>	-	<b>4.62</b>	<b>1.38</b>	<b>0.45</b>	<b>n.d.</b>	<b>0.96</b>	-	-

<i>Az-PS</i>	–	<b>3.64</b>	<b>4.69</b>	<b>1.46</b>	<b>0.41</b>	<b>1.21</b>	<b>0.05</b>	–	288.8	
<i>CSP1</i>	CS1 clicked (9%)	–	<b>8.01</b>	<b>7.65</b>	<b>4.94</b> (4.11)	<b>0.54</b> (5.44)	<b>1.46</b> (1.04)	<b>2.21</b> (0.63)	(0.10)	–
<i>CSP2</i>	CS1 coated (9%)	–	<b>9.83</b>	<b>10.33</b>	<b>6.44</b> (5.36)	<b>0.75</b> (7.42)	<b>1.56</b> (1.11)	<b>2.37</b> (0.66)	(0.11)	–
<i>CSP3</i>	CS1 coated (20%)	–	<b>16.93</b>	<b>18.72</b>	<b>10.05</b> (8.36)	<b>0.97</b> (9.62)	<b>1.88</b> (1.34)	<b>4.56</b> (1.28)	(0.21)	–
<i>CSP4</i>	CS2 coated (9%)	–	<b>8.76</b>	<b>8.51</b>	<b>6.11</b> (5.08)	<b>0.72</b> (7.11)	<b>1.53</b> (1.09)	<b>2.29</b> (0.64)	(0.11)	–
<i>CSP5</i>	CS2 coated (20%)	–	<b>21.04</b>	<b>22.17</b>	<b>12.23</b> (10.18)	<b>1.21</b> (11.97)	<b>1.89</b> (1.34)	<b>4.89</b> (1.37)	(0.23)	–

The amount of chiral selector loaded on silica gel by coating procedure, as described in section 4.2.5, was calculated according to the linked chiral selector obtained by click chemistry. In particular the elemental analysis of Table 8 shows a comparable amount mmol/g of stationary phase for both commercial CS2 and designed CS1.

### 4.3.3. Enantioseparation evaluation

Subsequent work at the IMC Krems University of Applied Sciences (Austria) will test the immobilised selector CSP1 and the coated-only alternatives CSP2-5 on the same pre-modified silica gel to ensure a good comparison. The HPLC performance tests are in progress at the time of writing and the methods used to evaluate the performance will be based on the analysis of the twelve racemates. The chiral analytes are shown in Fig. 44: 2-phenylcyclohexanone (a), benzoin (b), flavanone (c), Pirkle's alcohol (d), trans-stilbene oxide (e), Tröger's base (f), four mandelic acid derivatives (g-j), 1-methoxy 2-(1-methoxy-3-phenylpropyl) benzene (k), and 1-(o-hydroxyphenyl)-3-phenyl-1-propanol (l).

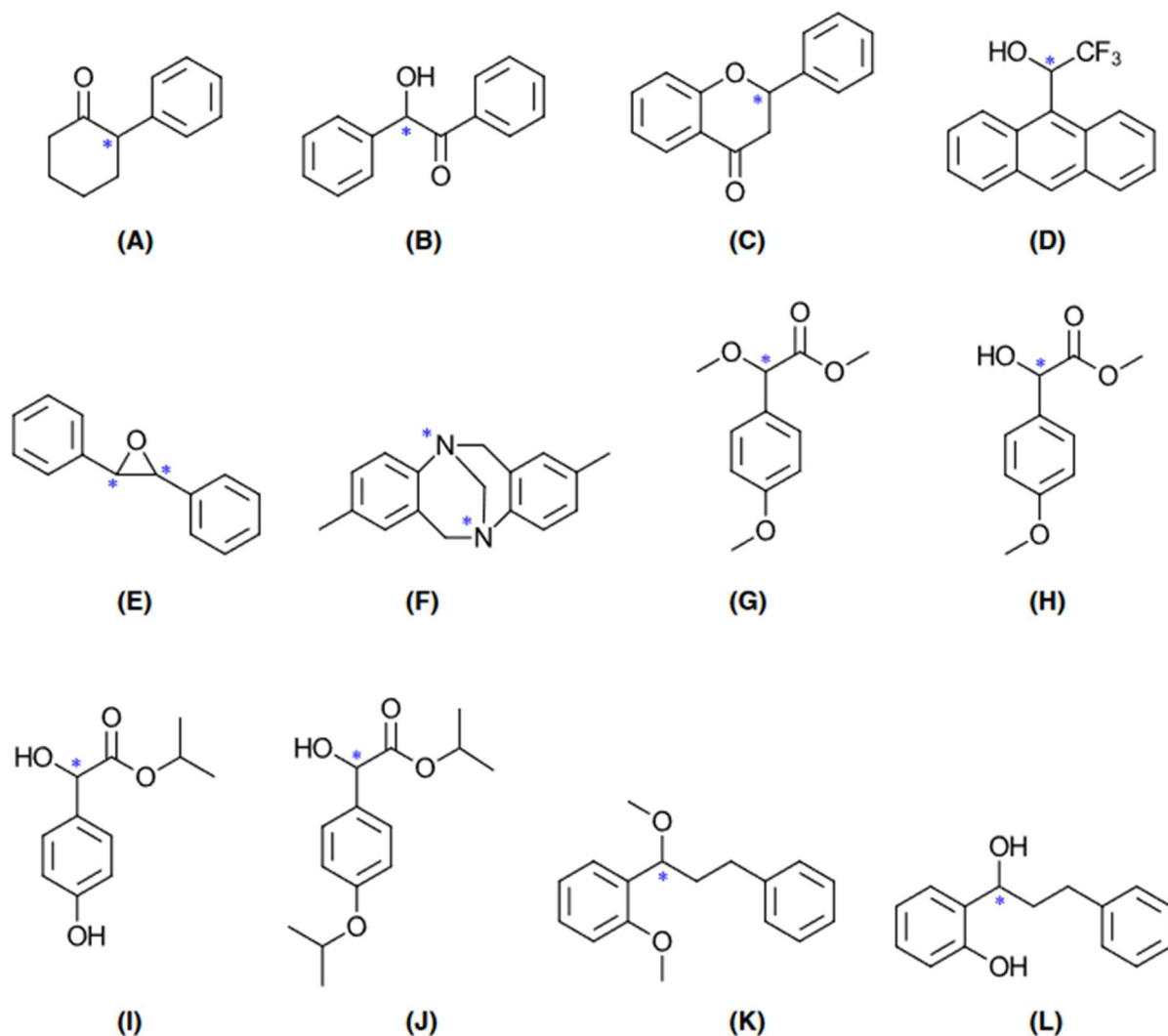


Figure 44. Chiral analytes used to evaluate HPLC separation performances.

The chromatographic parameters used to quantify the separation performances are the retention factor ( $k_1$ ), the selectivity ( $\alpha$ ) and the resolution ( $R_s$ ).

Chromatographic retention factor  $k_1$  is:

$$k_1 = \frac{t_1 - t_0}{t_0}$$

Equation 4

The retention factor is calculated by the difference between the retention time of the analyte and the void time, divided by the void time. It represents the binding strength between the single enantiomer A and the chiral selector CS. The larger the  $k_1$  value, the stronger the interaction.

Selectivity coefficient  $\alpha$  is:

$$\alpha = \frac{k_2}{k_1}$$

*Equation 5*

Selectivity coefficient, or separation factor  $\alpha$ , reflects the selectivity of the CS towards the single enantiomer. It is defined by the ratio of the retention factor of the first eluted  $k_1$  and the second eluted  $k_2$ , in order to have a separation  $\alpha$  must be higher than 1.

Resolution R:

$$R = \frac{\sqrt{N_{av}}}{4} \cdot \frac{\alpha - 1}{\alpha} \cdot \frac{k_2}{1 + k_{av}}$$

*Equation 6*

The resolution represents the quality of separation, and it depends on three terms the efficiency, the selectivity and the retention. In the first term includes the square root of  $N_{av}$ , which is the the average number of theoretical plates of separation, it describes the separation performances. The higher the number of plates, the higher the resolution. The second term accounts for selectivity  $\alpha$ . In the third term the retention factor of the second eluted and the average retention factor for both enantiomers.

The  $N_i$  number of theoretical plates is calculated by the formula:

$$N_i = 5.54 \cdot \left( \frac{t_i}{w_{i_{1/2}}} \right)$$

*Equation 7*

The number of theoretical plates  $N_i$  represents the separation performances according to the equilibrium of analyte enantiomer between mobile phase and stationary phase; it depends on the the stationary phase quality; it is calculated by dividing the retention time of the eluted by the full width at half maximum of the peak.

## 5 CONCLUSIONS

The modification of starch and cellulose polysaccharides shed light on the numerous opportunities to obtain innovative materials from biomasses.

The biopolymer based on starch was grafted with cinnamyl moieties; FTIR, solution and solid-state NMR definitively demonstrated the effectiveness of the grafting process through a covalent ether bond. The degree of substitution can be tuned, varying the reagents ratio. Interestingly, starch is converted into a water soluble bio-inspired polymer when the degree of substitution is low, allowing film formation in biocompatible conditions.

NMR studies allowed to better detail the photochemical process, revealing a double bond isomerization competing with the cycloaddition and cyclobutane ring formation which is the minor product.

These outcomes appear encouraging and demonstrate the efficacy of the methodological approach adopted in supplying a bio-based light responsive system potentially applicable to packaging products. Furthermore the film showed an interesting response to temperature change in the range of 35-40°C that makes it suitable as sensor and actuator in medical applications.

The second synthetic strategy provides a cinnamoyl ester of starch synthesised in a very simple and greenway showed even at low degree of substitution DS=0.01 a clue of photodimerization, caught by analogy with the photoinduced cycloaddition of the model molecule: the cinnamic acid. A possible explanation of this phenomena could be the tendency of cinnamoyl pendants to place, within the polymer matrix, in suprafacial relative position the carbonyl group over aromatic ring being electron poor and electron rich entities respectively; thus achieving the required distance of 4 Å. This result deserves to be further investigated with modelling support. Moreover, the chemical strategies used to valorise cellulose as chiral selector in HPLC further reinforces the circular economy model that proposes biomasses as sources of valuable raw materials. The chiral selectors were successfully synthesized starting from microcrystalline cellulose: one almost fully substituted 3,5-dichlorophenyl carbamate and a second similar except for the grafting with 3,5-dichloro-4-propargyloxy phenyl carbamate, the linker. The last was designed with a propargyl group for bonding covalently through the click reaction to silica gel the chiral selector.

The covalent bonding represents an important advancement in the reliability of HPLC stationary phases especially when they are washed out by strong solvents such as THF, acetone or chloroform (Bezhitashvili et al., 2018).

From separation study more insight on the influence of anchoring and structural variation of carbamate substituents is expected, indeed the rigidity of stationary phase related to immobilisation and the presence of the alkin substituent could be not negligible in separation mechanism.

## 6 BIBLIOGRAPHY

«Laudato si' (24 maggio 2015) | Francesco».

[https://www.vatican.va/content/francesco/it/encyclicals/documents/papa-francesco\\_20150524\\_enciclica-laudato-si.html](https://www.vatican.va/content/francesco/it/encyclicals/documents/papa-francesco_20150524_enciclica-laudato-si.html).

Chen, X., Stewart, P.S., 2002. Role of electrostatic interactions in cohesion of bacterial biofilms.

*Appl Microbiol Biotechnol* 59, 718–720. <https://doi.org/10.1007/s00253-002-1044-2>

Dona, A., Yuen, C.-W.W., Peate, J., Gilbert, R.G., Castignolles, P., Gaborieau, M., 2007. A new NMR method for directly monitoring and quantifying the dissolution kinetics of starch in DMSO. *Carbohydr Res* 342, 2604–2610. <https://doi.org/10.1016/j.carres.2007.08.010>

Garg, S., Jana, A.K., 2011. Characterization and evaluation of acylated starch with different acyl groups and degrees of substitution. *Carbohydrate Polymers* 83, 1623–1630. <https://doi.org/10.1016/j.carbpol.2010.10.015>

Ikai, T., Yamamoto, C., Kamigaito, M., Okamoto, Y., 2006. Immobilized Polysaccharide-Based Chiral Stationary Phases for HPLC. *Polym J* 38, 91–108. <https://doi.org/10.1295/polymj.38.91>

Kim, J.H., Scialli, A.R., 2011. Thalidomide: The Tragedy of Birth Defects and the Effective Treatment of Disease. *Toxicological Sciences* 122, 1–6. <https://doi.org/10.1093/toxsci/kfr088>

Minguillón, C., Franco, P., Oliveros, L., 1996. Bonded cellulose-derived high-performance liquid chromatography chiral stationary phases II. Influence of the porosity of the silica gel matrix on performance. *Journal of Chromatography A, 19th International Symposium on Column Liquid Chromatography and Related Techniques* 728, 415–422. [https://doi.org/10.1016/0021-9673\(95\)01203-6](https://doi.org/10.1016/0021-9673(95)01203-6)

Santayanan, R., Wootthikanokkhan, J., 2003. Modification of cassava starch by using propionic anhydride and properties of the starch-blended polyester polyurethane. *Carbohydrate Polymers* 51, 17–24. [https://doi.org/10.1016/S0144-8617\(02\)00109-1](https://doi.org/10.1016/S0144-8617(02)00109-1)

Schmidt, G.M.J., 1971. Photodimerization in the solid state. *Pure and Applied Chemistry* 27, 647–678. <https://doi.org/10.1351/pac197127040647>

1963 - Topochemistry - The photochemistry of trans-cinnamic acid.pdf, n.d.

A new Circular Economy Action Plan, n.d.

- Abdallah, M., Yoshikawa, C., Hearn, M.T.W., Simon, G.P., Saito, K., 2019. Photoreversible Smart Polymers Based on  $2\pi + 2\pi$  Cycloaddition Reactions: Nanofilms to Self-Healing Films. *Macromolecules* 52, 2446–2455. <https://doi.org/10.1021/acs.macromol.8b01729>
- Adamowicz, M., 2017. BIOECONOMY – CONCEPT, APPLICATION AND PERSPECTIVES. *Probl. Agric. Econ.* 350, 29–49. <https://doi.org/10.30858/zer/82998>
- Adams, D.J., Chappellet, S., Lincker, F., Ibn-Elhaj, M., Watts, B., Iannuzzi, M., Šišak Jung, D., Pignedoli, C.A., Passerone, D., 2014. Identifying Photoreaction Products in Cinnamate-Based Photoalignment Materials. *J. Phys. Chem. C* 118, 15422–15433. <https://doi.org/10.1021/jp504765f>
- Agenda 2030 Archivi [WWW Document], 2024. . ONU Ital. URL <https://unric.org/it/category/agenda-2030-sviluppo-sostenibile/> (accessed 8.22.24).
- Amato-Lourenço, L.F., Carvalho-Oliveira, R., Júnior, G.R., dos Santos Galvão, L., Ando, R.A., Mauad, T., 2021. Presence of airborne microplastics in human lung tissue. *J. Hazard. Mater.* 416, 126124. <https://doi.org/10.1016/j.jhazmat.2021.126124>
- Amjaour, H., Wang, Z., Mabin, M., Puttkammer, J., Busch, S., Chu, Q.R., 2019. Scalable preparation and property investigation of a *cis* -cyclobutane-1,2-dicarboxylic acid from  $\beta$ - *trans* -cinnamic acid. *Chem. Commun.* 55, 214–217. <https://doi.org/10.1039/C8CC08017H>
- Atalla, R.H., VanderHart, D.L., 1984. Native Cellulose: A Composite of Two Distinct Crystalline Forms. *Science* 223, 283–285. <https://doi.org/10.1126/science.223.4633.283>
- Bazin, A., Duval, A., Avérous, L., Pollet, E., 2022. Synthesis of Bio-Based Photo-Cross-Linkable Polyesters Based on Caffeic Acid through Selective Lipase-Catalyzed Polymerization. *Macromolecules* 55, 4256–4267. <https://doi.org/10.1021/acs.macromol.2c00499>
- Bergel, B.F., Dias Osorio, S., da Luz, L.M., Santana, R.M.C., 2018. Effects of hydrophobized starches on thermoplastic starch foams made from potato starch. *Carbohydr. Polym.* 200, 106–114. <https://doi.org/10.1016/j.carbpol.2018.07.047>
- Berthod, A., 2006. Chiral Recognition Mechanisms. *Anal. Chem.* 78, 2093–2099. <https://doi.org/10.1021/ac0693823>
- Bertoft, E., 2017. Understanding Starch Structure: Recent Progress. *Agronomy* 7, 56. <https://doi.org/10.3390/agronomy7030056>



- Bezhitashvili, L., Bardavelidze, A., Mskhiladze, A., Gumustas, M., Ozkan, S.A., Volonterio, A., Farkas, T., Chankvetadze, B., 2018. Application of cellulose 3,5-dichlorophenylcarbamate covalently immobilized on superficially porous silica for the separation of enantiomers in high-performance liquid chromatography. *J. Chromatogr. A* 1571, 132–139. <https://doi.org/10.1016/j.chroma.2018.08.011>
- Bongiovanni, R., Vacche, S.D., Vitale, A., 2021. Photoinduced Processes as a Way to Sustainable Polymers and Innovation in Polymeric Materials. *Polymers* 13, 2293. <https://doi.org/10.3390/polym13142293>
- Bugnotti, D., Dalle Vacche, S., Esposito, L.H., Callone, E., Orsini, S.F., Ceccato, R., D'Arienzo, M., Bongiovanni, R., Dirè, S., Vitale, A., 2023. Structure of Starch–Sepiolite Bio-Nanocomposites: Effect of Processing and Matrix–Filler Interactions. *Polymers* 15, 1207. <https://doi.org/10.3390/polym15051207>
- Bui, C.V., Rosenau, T., Hettegger, H., 2023a. Synthesis by carbonate aminolysis and chiral recognition ability of cellulose 2,3-bis(3,5-dimethylphenyl carbamate)-6-( $\alpha$ -phenylethyl carbamate) selectors. *Cellulose* 30, 153–168. <https://doi.org/10.1007/s10570-022-04898-8>
- Bui, C.V., Rosenau, T., Hettegger, H., 2023b. Immobilization of a cellulose carbamate-type chiral selector onto silica gel by alkyne-azide click chemistry for the preparation of chiral stationary chromatography phases. *Cellulose* 30, 915–932. <https://doi.org/10.1007/s10570-022-04932-9>
- Bui, C.V., Rosenau, T., Hettegger, H., 2021. Polysaccharide- and  $\beta$ -Cyclodextrin-Based Chiral Selectors for Enantiomer Resolution: Recent Developments and Applications. *Molecules* 26, 4322. <https://doi.org/10.3390/molecules26144322>
- Celluloid Manufacturing Co. - Syracuse University Libraries Digital Collections [WWW Document], n.d. URL <https://digitalcollections.syr.edu/Documents/Detail/celluloid-manufacturing-co./287752> (accessed 10.24.24).
- Chang, L., Zhang, Jinming, Chen, W., Zhang, M., Yin, C., Tian, W., Luo, Z., Liu, W., He, J., Zhang, Jun, 2018. Controllable synthesis of cellulose benzoates for understanding of chiral recognition mechanism and fabrication of highly efficient chiral stationary phases. *Anal. Methods* 10, 2844–2853. <https://doi.org/10.1039/C8AY00162F>
- Channab, B.-E., El Idrissi, A., Essamlali, Y., Zahouily, M., 2024. Nanocellulose: Structure,

- modification, biodegradation and applications in agriculture as slow/controlled release fertilizer, superabsorbent, and crop protection: A review. *J. Environ. Manage.* 352, 119928. <https://doi.org/10.1016/j.jenvman.2023.119928>
- Charoenkul, N., Uttapap, D., Pathipanawat, W., Takeda, Y., 2006. Simultaneous determination of amylose content & unit chain distribution of amylopectins of cassava starches by fluorescent labeling/HPSEC. *Carbohydr. Polym.* 65, 102–108. <https://doi.org/10.1016/j.carbpol.2005.12.030>
- Chen, W., Zhang, M., Feng, Y., Wu, J., Gao, X., Zhang, Jinming, He, J., Zhang, Jun, 2015. Homogeneous synthesis of partially substituted cellulose phenylcarbamates aiming at chiral recognition. *Polym. Int.* 64, 1037–1044. <https://doi.org/10.1002/pi.4884>
- Chi, H., Xu, K., Wu, X., Chen, Q., Xue, D., Song, C., Zhang, W., Wang, P., 2008. Effect of acetylation on the properties of corn starch. *Food Chem.* 106, 923–928. <https://doi.org/10.1016/j.foodchem.2007.07.002>
- Cohen, M.D., Schmidt, G.M.J., 1964. 383. Topochemistry. Part I. A survey. *J. Chem. Soc.* Resumed 1996–2000. <https://doi.org/10.1039/JR9640001996>
- Crutzen, P.J., 2002. Geology of mankind. *Nature* 415, 23–23. <https://doi.org/10.1038/415023a>
- Dalei, G., Das, S., Pradhan, M., 2022. Dialdehyde cellulose as a niche material for versatile applications: an overview. *Cellulose* 29, 1–33. <https://doi.org/10.1007/s10570-022-04619-1>
- Delville, J., Joly, C., Dole, P., Bliard, C., 2002. Solid state photocrosslinked starch based films: a new family of homogeneous modified starches. *Carbohydr. Polym.* 49, 71–81. [https://doi.org/10.1016/S0144-8617\(01\)00302-2](https://doi.org/10.1016/S0144-8617(01)00302-2)
- Directorate-General for Research and Innovation (European Commission), 2018. Review of the 2012 European Bioeconomy Strategy. Publications Office of the European Union.
- Do, D.T., Singh, J., Oey, I., Singh, H., 2020. Isolated potato parenchyma cells: Physico-chemical characteristics and gastro-small intestinal digestion *in vitro*. *Food Hydrocoll.* 108, 105972. <https://doi.org/10.1016/j.foodhyd.2020.105972>
- Du, L., Xu, Z.-Y., Huang, C.-L., Zhao, F.-Y., Fan, C.-J., Dai, J., Yang, K.-K., Wang, Y.-Z., 2020. From a body temperature-triggered reversible shape-memory material to high-sensitive bionic soft actuators. *Appl. Mater. Today* 18, 100463.

- <https://doi.org/10.1016/j.apmt.2019.100463>
- Egerton, P.L., Hyde, E.M., Trigg, J., Payne, A., Beynon, P., Mijovic, M.V., Reiser, A., 1981a. Photocycloaddition in liquid ethyl cinnamate and in ethyl cinnamate glasses. The photoreaction as a probe into the micromorphology of the solid. *J. Am. Chem. Soc.* 103, 3859–3863. <https://doi.org/10.1021/ja00403a039>
- Egerton, P.L., Pitts, E., Reiser, A., 1981b. Photocycloaddition in solid poly(vinyl cinnamate). The photoreactive polymer matrix as an ensemble of chromophore sites. *Macromolecules* 14, 95–100. <https://doi.org/10.1021/ma50002a019>
- Falua, K.J., Pokharel, A., Babaei-Ghazvini, A., Ai, Y., Acharya, B., 2022. Valorization of Starch to Biobased Materials: A Review. *Polymers* 14, 2215. <https://doi.org/10.3390/polym14112215>
- Fittolani, G., Vargová, D., Seeberger, P.H., Ogawa, Y., Delbianco, M., 2022. Bottom-Up Approach to Understand Chirality Transfer across Scales in Cellulose Assemblies. *J. Am. Chem. Soc.* 144, 12469–12475. <https://doi.org/10.1021/jacs.2c04522>
- Fonseca, I., Baias, M., Hayes, S.E., Pickard, C.J., Bertmer, M., 2012. Effects of Aromatic Substitution on the Photodimerization Kinetics of  $\beta$ -trans Cinnamic Acid Derivatives Studied with  $^{13}\text{C}$  Solid-State NMR. *J. Phys. Chem. C* 116, 12212–12218. <https://doi.org/10.1021/jp301703d>
- Fonseca, I., Hayes, S.E., Blümich, B., Bertmer, M., 2008. Temperature stability and photodimerization kinetics of  $\beta$ -cinnamic acid and comparison to its  $\alpha$ -polymorph as studied by solid-state NMR spectroscopy techniques and DFT calculations. *Phys. Chem. Chem. Phys.* 10, 5898. <https://doi.org/10.1039/b806861e>
- Ganske, K., Heinze, T., 2018. Evaluation of the Synthesis of Soluble Aromatic Cellulose Carbonates of Low Degree of Substitution. *Macromol. Chem. Phys.* 219, 1800152. <https://doi.org/10.1002/macp.201800152>
- Garavand, F., Rouhi, M., Razavi, S.H., Cacciotti, I., Mohammadi, R., 2017. Improving the integrity of natural biopolymer films used in food packaging by crosslinking approach: A review. *Int. J. Biol. Macromol.* 104, 687–707. <https://doi.org/10.1016/j.ijbiomac.2017.06.093>
- Geyer, R., Jambeck, J.R., Law, K.L., 2017. Production, use, and fate of all plastics ever made. *Sci. Adv.* 3, e1700782. <https://doi.org/10.1126/sciadv.1700782>

- Gilbert, R.D., Kadla, J.F., 1998. Polysaccharides — Cellulose, in: Kaplan, D.L. (Ed.), *Biopolymers from Renewable Resources*. Springer, Berlin, Heidelberg, pp. 47–95.  
[https://doi.org/10.1007/978-3-662-03680-8\\_3](https://doi.org/10.1007/978-3-662-03680-8_3)
- Guillard, V., Gaucel, S., Fornaciari, C., Angellier-Coussy, H., Buche, P., Gontard, N., 2018. The Next Generation of Sustainable Food Packaging to Preserve Our Environment in a Circular Economy Context. *Front. Nutr.* 5, 121.  
<https://doi.org/10.3389/fnut.2018.00121>
- Guzman, J.D., 2014. Natural Cinnamic Acids, Synthetic Derivatives and Hybrids with Antimicrobial Activity. *Molecules* 19, 19292–19349.  
<https://doi.org/10.3390/molecules191219292>
- Heinze, T., 2016. Cellulose: Structure and Properties, in: Rojas, O.J. (Ed.), *Cellulose Chemistry and Properties: Fibers, Nanocelluloses and Advanced Materials*. Springer International Publishing, Cham, pp. 1–52. [https://doi.org/10.1007/12\\_2015\\_319](https://doi.org/10.1007/12_2015_319)
- Hesse, G., Hagel, R., 1976. Die chromatographische Racemattrennung. *Justus Liebigs Ann. Chem.* 1976, 996–1008. <https://doi.org/10.1002/jlac.197619760604>
- Hesse, G., Hagel, R., 1973. Eine vollständige Recemattennung durch elutionschromatographie an cellulose-tri-acetat. *Chromatographia* 6, 277–280.  
<https://doi.org/10.1007/BF02282825>
- Hoover, R., 2001. Composition, molecular structure, and physicochemical properties of tuber and root starches: a review. *Carbohydr. Polym.* 45, 253–267.  
[https://doi.org/10.1016/S0144-8617\(00\)00260-5](https://doi.org/10.1016/S0144-8617(00)00260-5)
- Hu, Q., Zhang, Y., Wang, T., Sun, W., Tong, Z., 2021. pH Responsive Strong Polyion Complex Shape Memory Hydrogel with Spontaneous Shape Changing and Information Encryption. *Macromol. Rapid Commun.* 42, 2000747.  
<https://doi.org/10.1002/marc.202000747>
- Il regolamento. Sugli imballaggi l'Italia resta isolata: il Consiglio Ue tira dritto [WWW Document], 2023. URL <https://www.avvenire.it/economia/pagine/sugli-imballaggi-l-italia-resta-isolata-a-bruxelle> (accessed 10.22.24).
- Infrazioni, aggiornamento del 23 maggio 2024 [WWW Document], n.d. . Dipartimento Gli Aff. Eur. URL <http://www.affarieuropei.gov.it/it/attivita/procedure-dinfrazione/stato-delle-infrazioni/23-mag-24/> (accessed 10.22.24).

- Ioelovich, M., 2009. Accessibility and crystallinity of cellulose. *BioResources* 4, 1168–1177.  
<https://doi.org/10.15376/biores.4.3.1168-1177>
- Ishizuka, Yasuko, Tadashi Nemoto, Kenji Kanazawa, e Hiroshi Nakanishi. «<sup>1</sup>H NMR Spectra of Branched-Chain Cyclomaltohexaoses ( $\alpha$ -Cyclodextrins)». *Carbohydrate Research* 339, fasc. 4 (marzo 2004): 777–85.
- Kasashima, Y., Uzawa, A., Hashimoto, K., Nishida, T., Murakami, K., Mino, T., Sakamoto, M., Fujita, T., 2010. Synthesis of Cinnamyl Ethers from  $\alpha$ -Vinylbenzyl Alcohol Using Iodine as Catalyst. *J Oleo Sci.*
- Katoh, E., Murata, K., Fujita, N., 2020. <sup>13</sup>C CP/MAS NMR Can Discriminate Genetic Backgrounds of Rice Starch. *ACS Omega* 5, 24592–24600.  
<https://doi.org/10.1021/acsomega.0c03113>
- Kaur, G., Johnston, P., Saito, K., 2014. Photo-reversible dimerisation reactions and their applications in polymeric systems. *Polym Chem* 5, 2171–2186.  
<https://doi.org/10.1039/C3PY01234D>
- Klemm, D., Heublein, B., Fink, H.-P., Bohn, A., 2005. Cellulose: Fascinating Biopolymer and Sustainable Raw Material. *Angew. Chem. Int. Ed.* 44, 3358–3393.  
<https://doi.org/10.1002/anie.200460587>
- Kovacs, B. (Ed.), 2015. Sustainable agriculture, forestry and fisheries in the bioeconomy: a challenge for Europe : 4th SCAR foresight report. Publications Office, Luxembourg.
- Krauze-Baranowska, M., 2002. Truxillic and truxinic acids--occurrence in plant kingdom. *Acta Pol. Pharm.* 59, 403–410.
- Laudato si' (24 maggio 2015) | Francesco [WWW Document], n.d. URL  
[https://www.vatican.va/content/francesco/it/encyclicals/documents/papa-francesco\\_20150524\\_enciclica-laudato-si.html](https://www.vatican.va/content/francesco/it/encyclicals/documents/papa-francesco_20150524_enciclica-laudato-si.html) (accessed 8.22.24).
- Law, K.L., Thompson, R.C., 2014. Microplastics in the seas. *Science* 345, 144–145.  
<https://doi.org/10.1126/science.1254065>
- Li, H., Ma, Y., Gao, X., Chen, G., Wang, Z., 2021. Probing the structure-antioxidant activity relationships of four cinnamic acids porous starch esters. *Carbohydr. Polym.* 256, 117428. <https://doi.org/10.1016/j.carbpol.2020.117428>
- Lüttringhaus, A., Dirksen, H.-W., 1963. Tetramethylharnstoff als Lösungsmittel und Reaktionspartner. *Angew. Chem.* 75, 1059–1068.

- <https://doi.org/10.1002/ange.19630752204>
- McCormick, K., Kautto, N., 2013. The Bioeconomy in Europe: An Overview. *Sustainability* 5, 2589–2608. <https://doi.org/10.3390/su5062589>
- Medronho, B., Romano, A., Miguel, M.G., Stigsson, L., Lindman, B., 2012. Rationalizing cellulose (in)solubility: reviewing basic physicochemical aspects and role of hydrophobic interactions. *Cellulose* 19, 581–587. <https://doi.org/10.1007/s10570-011-9644-6>
- Mirabella, N., Castellani, V., Sala, S., 2014. Current options for the valorization of food manufacturing waste: a review. *J. Clean. Prod.* 65, 28–41. <https://doi.org/10.1016/j.jclepro.2013.10.051>
- OECD, 2009. OECD Factbook 2009: Economic, Environmental and Social Statistics. Organisation for Economic Co-operation and Development, Paris.
- Okamoto, Y., Aburatani, R., Hatada, K., 1987. Chromatographic chiral resolution: XIV. Cellulose tribenzoate derivatives as chiral stationary phases for high-performance liquid chromatography. *J. Chromatogr. A* 389, 95–102. [https://doi.org/10.1016/S0021-9673\(01\)94414-0](https://doi.org/10.1016/S0021-9673(01)94414-0)
- Okamoto, Y., Kawashima, M., Hatada, K., 1986a. Chromatographic resolution: XI. Controlled chiral recognition of cellulose triphenylcarbamate derivatives supported on silica gel. *J. Chromatogr. A* 363, 173–186. [https://doi.org/10.1016/S0021-9673\(01\)83736-5](https://doi.org/10.1016/S0021-9673(01)83736-5)
- Okamoto, Y., Kawashima, M., Hatada, K., 1986b. Chromatographic resolution: XI. Controlled chiral recognition of cellulose triphenylcarbamate derivatives supported on silica gel. *J. Chromatogr. A* 363, 173–186. [https://doi.org/10.1016/S0021-9673\(01\)83736-5](https://doi.org/10.1016/S0021-9673(01)83736-5)
- Okamoto, Y., Kawashima, M., Yamamoto, K., Hatada, K., 1984. USEFUL CHIRAL PACKING MATERIALS FOR HIGH-PERFORMANCE LIQUID CHROMATOGRAPHIC RESOLUTION. CELLULOSE TRIACETATE AND TRIBENZOATE COATED ON MACROPOROUS SILICA GEL. *Chem. Lett.* 13, 739–742. <https://doi.org/10.1246/cl.1984.739>
- Okkerse, C., Bekkum, H. van, 1999. From fossil to green. *Green Chem.* 1, 107–114. <https://doi.org/10.1039/A809539F>
- Packaging waste statistics [WWW Document], n.d. URL <https://ec.europa.eu/eurostat/statistics->

- explained/index.php?title=Packaging\_waste\_statistics (accessed 10.22.24).
- Pérez, S., Bertoft, E., 2010a. The molecular structures of starch components and their contribution to the architecture of starch granules: A comprehensive review. *Starch - Stärke* 62, 389–420. <https://doi.org/10.1002/star.201000013>
- Pérez, S., Bertoft, E., 2010b. The molecular structures of starch components and their contribution to the architecture of starch granules: A comprehensive review. *Starch - Stärke* 62, 389–420. <https://doi.org/10.1002/star.201000013>
- Persson, L., Carney Almroth, B.M., Collins, C.D., Cornell, S., de Wit, C.A., Diamond, M.L., Fantke, P., Hassellöv, M., MacLeod, M., Ryberg, M.W., Søgaaard Jørgensen, P., Villarrubia-Gómez, P., Wang, Z., Hauschild, M.Z., 2022. Outside the Safe Operating Space of the Planetary Boundary for Novel Entities. *Environ. Sci. Technol.* 56, 1510–1521. <https://doi.org/10.1021/acs.est.1c04158>
- Piotrowski, S., Carus, M., Essel, R., 2015. Global Bioeconomy in the Conflict Between Biomass Supply and Demand. *Ind. Biotechnol.* 11, 308–315. <https://doi.org/10.1089/ind.2015.29021.stp>
- Potthast, A., Rosenau, T., Sartori, J., Sixta, H., Kosma, P., 2003. Hydrolytic processes and condensation reactions in the cellulose solvent system N,N-dimethylacetamide/lithium chloride. Part 2: degradation of celluloseq.
- Pourjavadi, A., Seidi, F., Afjeh, S.S., Nikoseresht, N., Salimi, H., Nemati, N., 2011. Synthesis of soluble N-functionalized polysaccharide derivatives using phenyl carbonate precursor and their application as catalysts. *Starch - Stärke* 63, 780–791. <https://doi.org/10.1002/star.201100064>
- Qu, H., Li, J., Wu, G., Shen, J., Shen, X., Okamoto, Y., 2011. Preparation and chiral recognition in HPLC of cellulose 3,5-dichlorophenylcarbamates immobilized onto silica gel. *J. Sep. Sci.* 34, 536–541. <https://doi.org/10.1002/jssc.201000800>
- Richardson, K., Steffen, W., Lucht, W., Bendtsen, J., Cornell, S.E., Donges, J.F., Drüke, M., Fetzer, I., Bala, G., Von Bloh, W., Feulner, G., Fiedler, S., Gerten, D., Gleeson, T., Hofmann, M., Huiskamp, W., Kummu, M., Mohan, C., Nogués-Bravo, D., Petri, S., Porkka, M., Rahmstorf, S., Schaphoff, S., Thonicke, K., Tobian, A., Virkki, V., Wang-Erlandsson, L., Weber, L., Rockström, J., 2023. Earth beyond six of nine planetary boundaries. *Sci. Adv.* 9, eadh2458. <https://doi.org/10.1126/sciadv.adh2458>



- Rockström, J., Steffen, W., Noone, K., Persson, Å., Chapin, F.S., Lambin, E.F., Lenton, T.M., Scheffer, M., Folke, C., Schellnhuber, H.J., Nykvist, B., de Wit, C.A., Hughes, T., van der Leeuw, S., Rodhe, H., Sörlin, S., Snyder, P.K., Costanza, R., Svedin, U., Falkenmark, M., Karlberg, L., Corell, R.W., Fabry, V.J., Hansen, J., Walker, B., Liverman, D., Richardson, K., Crutzen, P., Foley, J.A., 2009a. A safe operating space for humanity. *Nature* 461, 472–475. <https://doi.org/10.1038/461472a>
- Rockström, J., Steffen, W., Noone, K., Persson, Å., Chapin, F.S.I., Lambin, E., Lenton, T.M., Scheffer, M., Folke, C., Schellnhuber, H.J., Nykvist, B., De Wit, C.A., Hughes, T., Van Der Leeuw, S., Rodhe, H., Sörlin, S., Snyder, P.K., Costanza, R., Svedin, U., Falkenmark, M., Karlberg, L., Corell, R.W., Fabry, V.J., Hansen, J., Walker, B., Liverman, D., Richardson, K., Crutzen, P., Foley, J., 2009b. Planetary Boundaries: Exploring the Safe Operating Space for Humanity. *Ecol. Soc.* 14, art32. <https://doi.org/10.5751/ES-03180-140232>
- Salanti, A., Zoia, L., Tolppa, E.-L., Orlandi, M., 2012. Chromatographic Detection of Lignin–Carbohydrate Complexes in Annual Plants by Derivatization in Ionic Liquid. *Biomacromolecules* 13, 445–454. <https://doi.org/10.1021/bm2014763>
- Sánchez, J., Curt, M.D., Robert, N., Fernández, J., 2019. Chapter Two - Biomass Resources, in: Lago, C., Caldés, N., Lechón, Y. (Eds.), *The Role of Bioenergy in the Bioeconomy*. Academic Press, pp. 25–111. <https://doi.org/10.1016/B978-0-12-813056-8.00002-9>
- Sangermano, M., Razza, N., Crivello, J.V., 2014. Cationic UV-Curing: Technology and Applications. *Macromol. Mater. Eng.* 299, 775–793. <https://doi.org/10.1002/mame.201300349>
- Sangermano, M., Roppolo, I., Chiappone, A., 2018. New Horizons in Cationic Photopolymerization. *Polymers* 10, 136. <https://doi.org/10.3390/polym10020136>
- Santayanan, R., Wootthikanokkhan, J., 2003a. Modification of cassava starch by using propionic anhydride and properties of the starch-blended polyester polyurethane. *Carbohydr. Polym.* 51, 17–24. [https://doi.org/10.1016/S0144-8617\(02\)00109-1](https://doi.org/10.1016/S0144-8617(02)00109-1)
- Santayanan, R., Wootthikanokkhan, J., 2003b. Modification of cassava starch by using propionic anhydride and properties of the starch-blended polyester polyurethane. *Carbohydr. Polym.* 51, 17–24. [https://doi.org/10.1016/S0144-8617\(02\)00109-1](https://doi.org/10.1016/S0144-8617(02)00109-1)
- Schmidt, G.M.J., 1971. Photodimerization in the solid state. *Pure Appl. Chem.* 27, 647–678.

<https://doi.org/10.1351/pac197127040647>

- Schmitz, S., Dona, A.C., Castignolles, P., Gilbert, R.G., Gaborieau, M., 2009. Assessment of the extent of starch dissolution in dimethyl sulfoxide by <sup>1</sup>H NMR spectroscopy. *Macromol. Biosci.* 9, 506–514. <https://doi.org/10.1002/mabi.200800244>
- Sepehrifar, R., Boysen, R.I., Danylec, B., Yang, Y., Saito, K., Hearn, M.T.W., 2017. Design, synthesis and application of a new class of stimuli-responsive separation materials. *Anal. Chim. Acta* 963, 153–163. <https://doi.org/10.1016/j.aca.2017.01.061>
- Shi, Y.-C., Capitani, T., Trzasko, P., Jeffcoat, R., 1998. Molecular Structure of a Low-Amylopectin Starch and Other High-Amylose Maize Starches. *J. Cereal Sci.* 27, 289–299. <https://doi.org/10.1006/jcrs.1997.9998>
- Silent Spring | Rachel Carson's Environmental Classic | Britannica [WWW Document], 2024. URL <https://www.britannica.com/topic/Silent-Spring> (accessed 8.24.24).
- Široký, J., Benians, T.A.S., Russell, S.J., Bechtold, T., Paul Knox, J., Blackburn, R.S., 2012. Analysis of crystallinity changes in cellulose II polymers using carbohydrate-binding modules. *Carbohydr. Polym.* 89, 213–221. <https://doi.org/10.1016/j.carbpol.2012.02.073>
- Soetaert, W., Vandamme, E., 2006. The impact of industrial biotechnology. *Biotechnol. J.* 1, 756–769. <https://doi.org/10.1002/biot.200600066>
- Spinozzi, F., Ferrero, C., Perez, S., 2020. The architecture of starch blocklets follows phyllotaxic rules. *Sci. Rep.* 10, 20093. <https://doi.org/10.1038/s41598-020-72218-w>
- Sriroth, K., Chollakup, R., Chotineeranat, S., Piyachomkwan, K., Oates, C.G., 2000. Processing of cassava waste for improved biomass utilization. *Bioresour. Technol.* 71, 63–69. [https://doi.org/10.1016/S0960-8524\(99\)00051-6](https://doi.org/10.1016/S0960-8524(99)00051-6)
- Steffen, W., Richardson, K., Rockström, J., Cornell, S.E., Fetzer, I., Bennett, E.M., Biggs, R., Carpenter, S.R., De Vries, W., De Wit, C.A., Folke, C., Gerten, D., Heinke, J., Mace, G.M., Persson, L.M., Ramanathan, V., Reyers, B., Sörlin, S., 2015. Planetary boundaries: Guiding human development on a changing planet. *Science* 347, 1259855. <https://doi.org/10.1126/science.1259855>
- Tabaglio, V., Fiorini, A., Ndayisenga, V., Ndereyimana, A., Minuti, A., Nyembo Nyembo, R., Nyembo Ngoy, D., Bertoni, G., 2023. Sustainable Intensification of Cassava Production towards Food Security in the Lomami Province (DR Congo): Role of Planting Method

- and Landrace. *Agronomy* 13, 228. <https://doi.org/10.3390/agronomy13010228>
- Tester, R.F., Karkalas, J., Qi, X., 2004a. Starch—composition, fine structure and architecture. *J. Cereal Sci.* 39, 151–165. <https://doi.org/10.1016/j.jcs.2003.12.001>
- Tester, R.F., Karkalas, J., Qi, X., 2004b. Starch—composition, fine structure and architecture. *J. Cereal Sci.* 39, 151–165. <https://doi.org/10.1016/j.jcs.2003.12.001>
- The European Green Deal [WWW Document], n.d. . Eur. Comm. - Eur. Comm. URL [https://ec.europa.eu/commission/presscorner/detail/en/fs\\_24\\_1391](https://ec.europa.eu/commission/presscorner/detail/en/fs_24_1391) (accessed 10.22.24).
- The Role of Bioenergy in the Bioeconomy, 2019. . Elsevier. <https://doi.org/10.1016/C2016-0-03740-3>
- Tizzotti, M.J., Sweedman, M.C., Tang, D., Schaefer, C., Gilbert, R.G., 2011. New <sup>1</sup>H NMR Procedure for the Characterization of Native and Modified Food-Grade Starches. *J. Agric. Food Chem.* 59, 6913–6919. <https://doi.org/10.1021/jf201209z>
- Wang, J., Liu, X., Li, Y., Powell, T., Wang, X., Wang, G., Zhang, P., 2019. Microplastics as contaminants in the soil environment: A mini-review. *Sci. Total Environ.* 691, 848–857. <https://doi.org/10.1016/j.scitotenv.2019.07.209>
- Wang, Y., Okochi, H., Tani, Y., Hayami, H., Minami, Y., Katsumi, N., Takeuchi, M., Sorimachi, A., Fujii, Y., Kajino, M., Adachi, K., Ishihara, Y., Iwamoto, Y., Niida, Y., 2023. Airborne hydrophilic microplastics in cloud water at high altitudes and their role in cloud formation. *Environ. Chem. Lett.* 21, 3055–3062. <https://doi.org/10.1007/s10311-023-01626-x>
- Wang, Z., Zhuang, X., Chen, Y., Wang, B., Yu, J., Huang, W., Marks, T.J., Facchetti, A., 2019. Cinnamate-Functionalized Natural Carbohydrates as Photopatternable Gate Dielectrics for Organic Transistors. *Chem. Mater.* 31, 7608–7617. <https://doi.org/10.1021/acs.chemmater.9b02413>
- Weligama Thuppahige, V.T., Moghaddam, L., Welsh, Z.G., Wang, T., Karim, A., 2023. Investigation of critical properties of Cassava (*Manihot esculenta*) peel and bagasse as starch-rich fibrous agro-industrial wastes for biodegradable food packaging. *Food Chem.* 422, 136200. <https://doi.org/10.1016/j.foodchem.2023.136200>
- Wu, X.L., Zilm, K.W., 1993. Complete Spectral Editing in CPMAS NMR. *J. Magn. Reson. A* 102, 205–213. <https://doi.org/10.1006/jmra.1993.1092>
- Yang, Y., Xie, E., Du, Z., Peng, Z., Han, Z., Li, L., Zhao, R., Qin, Y., Xue, M., Li, F., Hua, K.,

- Yang, X., 2023. Detection of Various Microplastics in Patients Undergoing Cardiac Surgery. *Environ. Sci. Technol.* 57, 10911–10918.  
<https://doi.org/10.1021/acs.est.2c07179>
- Yudhistira, B., Husnayain, N., Punthi, F., Gavahian, M., Chang, C.-K., Hsieh, C.-W., 2024. Progress in the Application of Emerging Technology for the Improvement of Starch-Based Active Packaging Properties: A Review. *ACS Food Sci. Technol.* 4, 1997–2012.  
<https://doi.org/10.1021/acsfoodscitech.4c00260>
- Zhang, R., Chu, F., Hu, Yunqin, Hu, H., Hu, Yulong, Liu, H., Huo, C., Wang, H., 2020. Preparation of Photo-Crosslinking Starch Colloidal Particles. *Starch - Stärke* 72, 1900175. <https://doi.org/10.1002/star.201900175>
- Zhang, Z.-W., Li, H.-B., Li, J., Wang, C.-C., Feng, J., Yang, Y.-H., Liu, S., 2020. Synthesis of Epoxides from Alkyl Bromides and Alcohols with in Situ Generation of Dimethyl Sulfonium Ylide in DMSO Oxidations. *J. Org. Chem.* 85, 537–547.  
<https://doi.org/10.1021/acs.joc.9b02621>
- Zhou, Z., Topping, D.L., Morell, M.K., Bird, A.R., 2010. Changes in starch physical characteristics following digestion of foods in the human small intestine. *Br. J. Nutr.* 104, 573–581. <https://doi.org/10.1017/S0007114510000875>
- Ziegler-Borowska, Marta, Katarzyna Wegrzynowska-Drzymalska, Dorota Chelminiak-Dudkiewicz, Jolanta Kowalonek, e Halina Kaczmarek. «Photochemical Reactions in Dialdehyde Starch». *Molecules* 23, fasc. 12 (18 dicembre 2018): 3358.  
<https://doi.org/10.3390/molecules23123358>.
- Zoia, L., King, A.W.T., Argyropoulos, D.S., 2011. Molecular Weight Distributions and Linkages in Lignocellulosic Materials Derivatized from Ionic Liquid Media. *J. Agric. Food Chem.* 59, 829–838. <https://doi.org/10.1021/jf103615e>
- Zugenmaier, P., 2001. Conformation and packing of various crystalline cellulose fibers. *Prog. Polym. Sci.* 26, 1341–1417. [https://doi.org/10.1016/S0079-6700\(01\)00019-3](https://doi.org/10.1016/S0079-6700(01)00019-3)